Materials Horizons

ROYAL SOCIETY OF CHEMISTRY

REVIEW

View Article Online
View Journal | View Issue

Cite this: *Mater. Horiz.*, 2026, 13, 2173

Evolving electrocatalytic nitrate-to-ammonia conversion on Cu- and Co-based catalyst engineering with paired electrolysis approaches

Nabilah Saafie,[ab] Noor Ashikin Mohamad,[ab] Wei Shan Koh,[ab] Xianhai Zeng,[c] Soo Young Kim *[d] and Wee-Jun Ong *[abefgh]

The electrocatalytic nitrate (NO_3^-) reduction reaction to ammonia (NH_3) offers a sustainable pathway for wastewater remediation and distributed NH_3 synthesis, presenting a capable alternative to the energy-intensive Haber–Bosch process. Copper (Cu)- and cobalt (Co)-based catalysts are among the most promising for this reaction due to their favourable electronic structure for NO_3^- activation and cost-effectiveness. However, their propensity for rapid deactivation caused by the strong adsorption of intermediates like *NO that poison active sites remains a primary impediment to high selectivity and stability. This review comprehensively investigates recent breakthroughs in overcoming this limitation through advanced catalyst design strategies specifically for Cu- and Co-based systems. In detail, the protocols were critically examined to regulate intermediate adsorption strength *via* facet engineering, oxidation state modulation, single-atom dispersion and construction of bimetallic catalysts that provide synergistic *H species to enhance hydrogenation kinetics through optimization of the d band center of Cu and Co. Furthermore, innovative tandem catalysis systems and paired electrolysis configurations are also explored to couple the NO_3^- reduction reaction with alternative oxidation reactions (AORs) to drastically improve energy efficiency and economic viability. Therefore, by synthesizing these design principles this review aims to guide the development of next-generation, high-performance and durable Cu- and Co-based electrocatalysts for scalable sustainable nitrogen management.

Received 22nd October 2025,
Accepted 24th November 2025

DOI: 10.1039/d5mh02001h

rsc.li/materials-horizons

Wider impact

The escalating disruption of the global nitrogen cycle driven by anthropogenic nitrate pollution and the carbon-intensive Haber–Bosch process represents a critical planetary boundary challenge. This review transcends the conventional scope of electrocatalyst design by articulating a transformative vision for sustainable nitrogen management. We critically synthesize pioneering advances in Cu- and Co-based electrocatalysts as the foundational enablers of a paradigm shift: paired electrolysis. By strategically replacing the energy-profligate oxygen evolution reaction with thermodynamically favorable alternative oxidation reactions, we demonstrate a pathway to slash the energy consumption of ammonia synthesis by up to 50% while simultaneously valorizing wastewater contaminants (sulfides, nitrates) and renewable organic feedstocks (glycerol, plastics) into value-added commodities. This integrated approach moves beyond mere environmental remediation, positioning electrochemical reactors as distributed, energy-smart refineries. The insights and design principles delineated herein provide a critical roadmap for decoupling ammonia production from fossil fuels, mitigating aquatic eutrophication, and establishing a circular nitrogen economy, thereby addressing urgent challenges in clean energy, water security, and sustainable chemical manufacturing.

[a] *School of Energy and Chemical Engineering, Xiamen University Malaysia, Sepang, Selangor Darul Ehsan 43900, Malaysia. E-mail: weejun.ong@xmu.edu.my*
[b] *Center of Excellence for NaNo Energy & Catalysis Technology (CONNECT), Xiamen University Malaysia, Sepang, Selangor Darul Ehsan 43900, Malaysia*
[c] *College of Energy, State Key Laboratory of Physical Chemistry of Solid Surfaces, Xiamen University, Xiamen 361102, China*
[d] *Department of Materials Science and Engineering, Korea University, Seoul 02841, Republic of Korea. E-mail: sooyoungkim@korea.ac.kr*
[e] *State Key Laboratory of Physical Chemistry of Solid Surfaces, College of Chemistry and Chemical Engineering, Xiamen University, Xiamen 361005, China*
[f] *Gulei Innovation Institute, Xiamen University, Zhangzhou 363200, China*
[g] *Shenzhen Research Institute of Xiamen University, Shenzhen 518057, China*
[h] *Department of Chemical and Biological Engineering, College of Engineering, Korea University, 145 Anam-ro, Seongbuk-gu, Seoul, 02841, Republic of Korea*

1. Introduction

The global nitrogen cycle, a cornerstone of ecological stability, involves the continuous transformation of nitrogen among various oxidation states including nitrate (NO_3^-) and ammonia (NH_3).[1] However, anthropogenic activities such as the disposal of nitrogenous waste, fossil fuel combustion, industrial agriculture and the widespread use of synthetic fertilizers have profoundly disrupted this natural balance, leading to alarming levels of nitrate contamination in water bodies worldwide.[2] Elevated nitrate concentrations trigger eutrophication, severely depleting dissolved oxygen and jeopardizing aquatic biodiversity.[3] Moreover, nitrate pollution poses direct risks to human health including endocrine disruption and potential carcinogenic effects through its conversion to nitrite (NO_2^-). Conventional nitrate removal techniques such as ion exchange, reverse osmosis and biological denitrification are hampered by significant drawbacks including secondary pollution, high energy consumption and excessive sludge production.[4–7] Thus, the development of innovative sustainable technologies for nitrate remediation is urgently needed.

Parallel to the environmental challenge of nitrate pollution, the conventional Haber–Bosch process known as the dominant method for global ammonia synthesis imposes a substantial energy and environmental burden.[8] Operating under extreme conditions of high pressures (150–300 atm) and temperatures (400–500 °C), this process consumes approximately 1–2% of the world's fossil energy and is a major contributor to greenhouse gas emissions.[9] In this context, the electrocatalytic nitrate reduction to ammonia has emerged as a promising alternative.[10,11] This process not only offers a sustainable pathway for nitrate removal from wastewater but also enables distributed ammonia synthesis under ambient conditions using renewable electricity. The conversion of nitrate, a harmful pollutant, into valuable ammonia, a key fertilizer and emerging carbon-free energy carrier, is a critical process.

The field of electrocatalytic nitrate reduction reaction has witnessed explosive growth and rapid conceptual advancement from 2017 to the present: 2017,[12] 2018,[13] 2019,[14] 2020,[15] 2021,[16] 2022,[17] 2023,[18] 2024,[19] 2025,[20] and 2026,[21] as illustrated in Fig. 1. This period has been marked by a series of foundational discoveries in catalyst design, mechanistic understanding and reactor engineering collectively driving improvements in activity, selectivity and stability. Referring to Fig. 2, the accelerating pace of innovation is further underscored by the dramatic increase in annual publication numbers and citations for the research concerning "electrocatalytic nitrate reduction" and "coupling electrocatalytic". Despite its promise, the electrocatalytic nitrate

Nabilah Saafie

Nabilah Saafie is a Post-Doctoral Research Fellow under the supervision of Prof. Dr. Wee-Jun Ong at the Center of Excellence for NaNo Energy & Catalysis Technology (CONNECT), Xiamen University Malaysia. Holding a BEng from Universiti Sains Malaysia and an MSc and PhD in Chemical Engineering from Universiti Teknologi PETRONAS, her research pioneers the interfacial engineering of heterostructure electrocatalysts for urea oxidation and nitrate valorization into ammonia. Her work in sustainable nanomaterial design extends to wastewater remediation and plastic upcycling, underpinning a research portfolio dedicated to advancing net-zero energy technologies.

Soo Young Kim

Soo Young Kim received his BS, MS and PhD degrees in materials science and engineering from Pohang University of Science and Technology (POSTECH) in South Korea. His laboratory is composed of two groups. One group is focusing on organic-based semiconductors, including organic light-emitting diodes, perovskite light-emitting diodes, perovskite solar cells, and perovskite memories. The other group is focusing on the synthesis of two-dimensional materials and its application to the hydrogen evolution reaction and CO_2 reduction. He has produced more than 400 publications and H-index is 84 (google scholar).

Wee-Jun Ong

*Wee-Jun Ong is a Full Professor and Director of the Center of Excellence for NaNo Energy & Catalysis Technology (CONNECT) at Xiamen University Malaysia. He earned his BEng and PhD in chemical engineering from Monash University. Since September 2024, he has been an Adjunct Professor at Korea University. His career includes a role as a Staff Scientist at A*STAR, Singapore, and a visiting professorship at Lawrence Berkeley National Laboratory. His research focuses on developing organic and inorganic hybrid nanostructures for photocatalytic, photoelectrocatalytic, and electrocatalytic applications, with specific interests in hydrogen evolution, carbon dioxide reduction, plastic reforming and nitrate-to-ammonia conversion. For more details, refer to https://sites.google.com/site/wjongresearch/.*

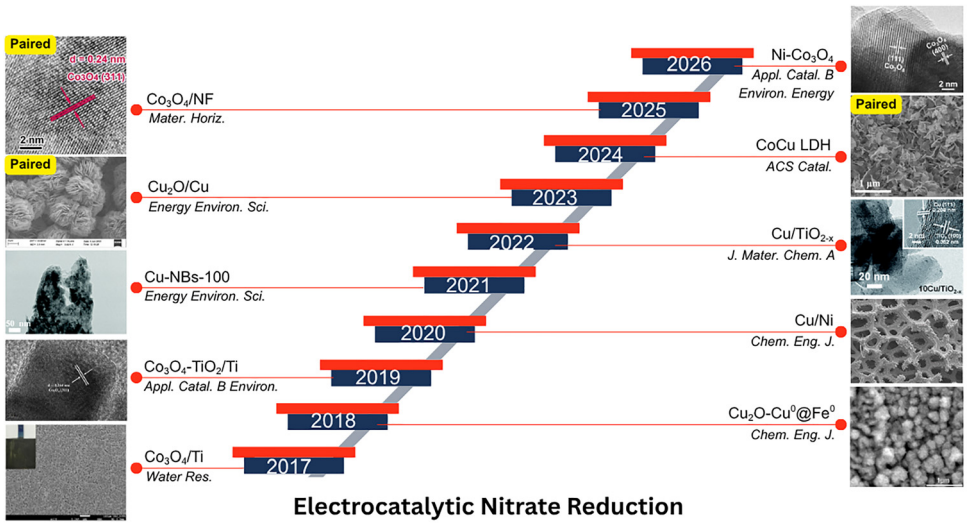

Fig. 1 Milestones of paired electrocatalytic nitrate reduction to ammonia on Cu- and Co-based catalyst research development from 2017 to the present: 2017[12] (reproduced from ref. 12, with permission from Elsevier, Copyright [2017].), 2018[13] (reproduced from ref. 13, with permission from Elsevier, Copyright [2018].), 2019[14] (reproduced from ref. 14, with permission from Elsevier, Copyright [2019].), 2020[15] (reproduced from ref. 15, with permission from Elsevier, Copyright [2020].), 2021[16] (reproduced from ref. 16, with permission from The Royal Society of Chemistry, Copyright [2021].), 2022[17] (reproduced from ref. 17, with permission from The Royal Society of Chemistry, Copyright [2022].), 2023[18] (reproduced from ref. 18, with permission from The Royal Society of Chemistry, Copyright [2023].), 2024[19] (reproduced from ref. 19, with permission from American Chemical Society, Copyright [2024].), 2025[20] (reproduced from ref. 20, with permission from The Royal Society of Chemistry, Copyright [2025].) and 2026[21] (reproduced from ref. 21, with permission from Elsevier, Copyright [2026]).

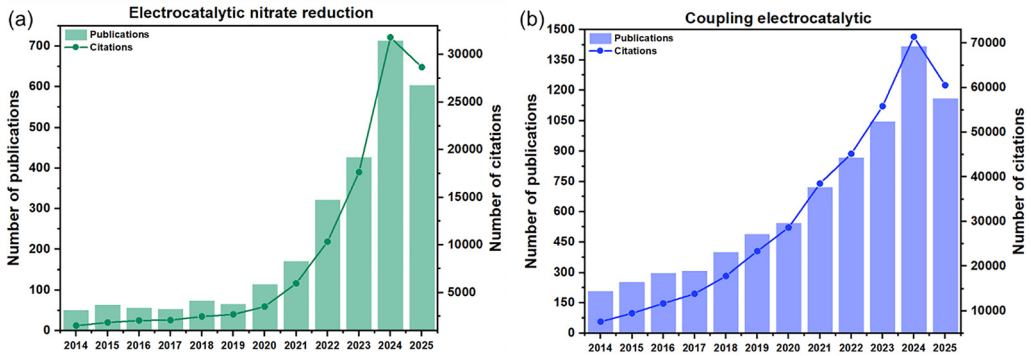

Fig. 2 Number of citations and yearly publications from 2014 to 2025 with the topic keywords (a) "electrocatalytic nitrate reduction" and (b) "coupling electrocatalytic" in the Clarivate database (2 October 2025).

reduction reaction involves a complex multi-step mechanism encompassing eight electrons and nine protons (NO_3^- + $9H^+$ + $8e^-$ → $3H_2O$ + NH_3) leading to a plethora of nitrogen-containing intermediates such as NO_2^-, nitric oxide (NO), nitrous oxide (N_2O) and hydroxylamine (NH_2OH).[22,23] This complexity often results in sluggish reaction kinetics and poor selectivity towards ammonia, and competition with the hydrogen evolution reaction (HER), which collectively hinder achieving a high faradaic efficiency (FE) and ammonia yield. Overcoming these limitations necessitates the rational design of advanced electrocatalysts capable of selectively promoting the N–O bond cleavage and N–H bond formation while suppressing undesired side reactions.[24]

Among the diverse array of electrocatalytic materials, copper (Cu)- and cobalt (Co)-based systems have emerged as particularly promising candidates for nitrate reduction, a status earned through their distinctive and complementary electronic structures that govern nitrate activation and pathway selectivity. Cu possesses a unique affinity for N–O bonds facilitating the critical initial adsorption of NO_3^- and its facile dissociation to NO_2^-. Its partially filled d orbitals' electronic structure provides an optimal energetic landscape for the stabilization of *NO key intermediates and their subsequent hydrogenation, steering the reaction pathway toward NH_3 instead of N_2.[25,26] Co conversely exhibits a pronounced efficacy in activating water and promoting proton-coupled electron transfer processes which are pivotal for the later stages of the reduction sequence where N–H bond formation is paramount.[27,28] This synergistic interplay, where Cu sites often excel at initial N–O bond scission

and Co sites facilitate efficient hydrogenation, underpins the high performance of catalysts based on these elements.[29] Their natural abundance and economic viability further solidify their position as frontrunners for scalable environmental and energy applications.[21,30] While iron (Fe) is indeed an earth-abundant alternative, its performance in nitrate reduction is often hampered by a stronger competitive HER and tendency to favor complete denitrification to N_2 over the selective formation of NH_3, resulting in lower NH_3 FE.[31] Precious metals like Ru or Pt demonstrate intrinsic activity; they are cost-prohibitive and scarce rendering them impractical for large-scale wastewater remediation or ammonia synthesis.[32]

Despite these advantages, conventional Cu and Co catalysts frequently exhibit limited operational stability due to the strong chemisorption of reaction intermediates such as *NO species which leads to active site poisoning and subsequent performance degradation.[33] This fundamental challenge is compounded by several knotted limitations that collectively hinder their transition from laboratory benchmarks to industrial-scale implementation. Firstly, the multi-step proton-coupled electron transfer mechanism necessities precise binding energies for a cascade of nitrogenous intermediates (*NO_2, *NO, and *NHO).[34,35] However, the monometallic sites of conventional Cu or Co catalysts often fail to optimally stabilize this entire sequence, leading to kinetic bottlenecks and the premature release of undesirable by-products like NO_2^- and N_2O. Secondly, the ubiquitous HER presents a fierce competitive drain on cathodic efficiency particularly in neutral or alkaline media and at the high negative potentials required for deep nitrate reduction.[36] Finally, these materials often suffer from structural and chemical instability under operational conditions, for example, Cu-based catalysts are prone to oxidation or leaching, while Co-based systems may undergo phase transformation or dissolution especially in fluctuating pH environments or during long-term electrolysis.[35] It is the concerted effort to surmount these formidable challenges encompassing selectivity, stability and scalability that drives the advanced catalyst engineering paradigms explored in Section 2.3 where atomic-level design and heterostructure strategies are leveraged to tailor the electronic properties and interfacial environments of Cu and Co active sites, thereby paving the way for practical electrochemical ammonia synthesis.

Addressing these limitations, sophisticated catalyst engineering approaches have been developed including precise facet control, single atom dispersion, vacancy engineering, heteroatom doping and fabrication of bimetallic architectures. Moreover, the implementation of these advanced catalysts within paired electrolysis configurations of nitrate reduction is coupled with thermodynamically favourable oxidation reactions such as sulfion or glycerol oxidation represents a paradigm shift that simultaneously enhances energy efficiency and enables the co-production of the value-added chemicals.[37–39] This integrated approach offers a transformative pathway toward sustainable electrochemical ammonia synthesis while addressing the economic and environmental constraints of conventional processes. The implementation of these catalysts within paired electrolysis configurations introduces a critical design paradigm which is the functional duality of the electrocatalyst. Systems can be architected using either a monofunctional catalyst where distinct Cu- or Co-based materials are specifically optimized for the cathode and anode, respectively, or bifunctional catalysts where a single material is engineered to catalyse both half-reactions simultaneously.[34,40] The pursuit of bifunctional systems represents a particularly compelling frontier as it simplifies reactor design and can unlock synergistic electronic effects that enhance overall process efficiency. However, this demands a precise orchestration of active sites to manage two distinct reaction pathways without cross-interference.[41] This review critically examines both design philosophies, with a dedicated focus on the sophisticated strategies being employed to develop robust bifunctional catalysts that enable the co-production of ammonia and value-added chemicals in a single, integrated electrochemical process. Up to the present time, several insightful reviews have summarized progress in electrocatalytic nitrate reduction highlighting advances in catalyst design and mechanistic understanding.[37,42–44] However, many of these studies lack a dedicated focus on the synergistic integration of Cu- and Co-based electrocatalysts with paired electrolysis systems. This is the critical gap that limits their applicability toward energy efficient and economically viable ammonia production.

Herein, this review aims to bridge that divide by offering a comprehensive examination of the latest advancements in Cu- and Co-based catalyst engineering strategies coupled with innovative anodic reactions for electrocatalytic nitrate to ammonia conversion. The review structure starts with elucidating the fundamental mechanisms and performance metrics of the nitrate reduction reaction followed by a critical analysis of state-of-the-art catalyst design paradigms from structural and defect engineering to single-atom and bimetallic architectures. The integration of density functional theory (DFT) and *in situ* characterization techniques is highlighted to provide deeper insights into reaction mechanisms, guiding the rational design of advanced catalysts. The synergistic benefits of paired electrolysis configurations in enhancing process sustainability are further explored. Thus, by synthesizing these cutting-edge developments, this review aims to provide foundational insights and guide the future design of high-performance, durable and scalable electrocatalytic systems for sustainable nitrogen management and green ammonia synthesis.

2. Fundamentals of electrocatalytic nitrate to ammonia conversion

The electrocatalytic reduction of nitrate to ammonia represents a paradigm shift in sustainable nitrogen management simultaneously addressing the pressing issues of environmental nitrate pollution and the carbon-intensive nature of the Haber–Bosch process. This transformation is a complex multi-electron/proton transfer process ($NO_3^- + 9H^+ + 8e^- \rightarrow 3H_2O + NH_3$) fraught with kinetic and selectivity challenges.[45]

A deep understanding of the underlying mechanisms, performance metrics and catalyst design principles is paramount for advancing this field. This section delves into the fundamental aspects that govern the nitrate reduction reaction establishing a critical foundation for evaluating and designing next generation electrocatalytic systems. The intricate pathways and key intermediates were first elucidated that dictate selectivity then further to define the essential performance indicators used to benchmark catalytic efficacy. Finally, a comprehensive correlation of key performance metrics (overpotential,[46] current density,[47] ammonia yield rate, FE, Tafel slope, selectivity) and critical analysis of state-of-the-art modifications (structure,[48] vacancy,[49] doping,[50] single atom,[51] bimetallic and alloying[52]) in Cu- and Co-based electrocatalysts for the nitrate reduction reaction with highlights for AOR (sulfion oxidation,[53] glycerol oxidation,[39] formaldehyde oxidation,[18] poly(ethylene) terephthalate oxidation[54] and hydrazine oxidation[55]) that replace the energy-intensive oxygen evolution reaction (OER) to enhance overall process efficiency and value are systematically correlated in Fig. 3. This strategy is pivotal for enhancing the overall energy efficiency and economic viability of electrochemical ammonia synthesis moving beyond the limitations of the traditional OER.

2.1. Mechanism of nitrate to ammonia reduction and oxidation reaction

The selective conversion of nitrate to ammonia proceeds through a complex network of elementary steps, in which the

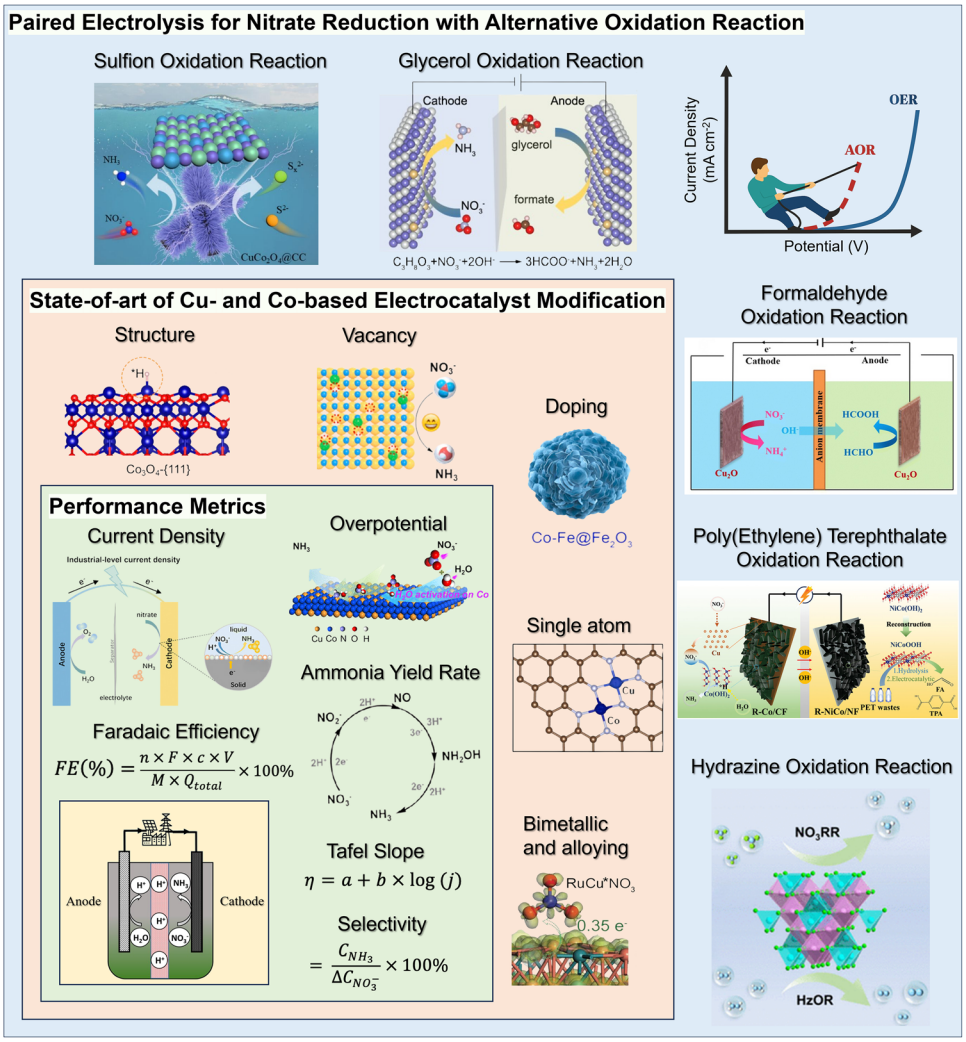

Fig. 3 An overview correlating to performance metrics and Cu- and Co-based catalyst design strategies for paired electrolysis facilitating nitrate to ammonia conversion.[18,39,46–55] (Reproduced from ref. 46 with permission from American Chemical Society, Copyright [2023], reproduced from ref. 47, with permission from John Wiley & Sons, Copyright [2024], reproduced from ref. 48, with permission from American Chemical Society, Copyright [2024], reproduced from ref. 49, with permission from Elsevier, Copyright [2022], reproduced from ref. 50, with permission from Elsevier, Copyright [2022], reproduced from ref. 51, with permission from Elsevier, Copyright [2025], reproduced from ref. 52, with permission from John Wiley & Sons, Copyright [2023], reproduced from ref. 53, with permission from Elsevier, Copyright [2025], reproduced from ref. 39, with permission from John Wiley & Sons, Copyright [2024], reproduced from ref. 18, with permission from The Royal Society of Chemistry, Copyright [2023], reproduced from ref. 54, with permission from John Wiley & Sons, Copyright [2025], reproduced from ref. 55, with permission from American Chemical Society, Copyright [2025]).

adsorption geometry and hydrogenation of nitrogen–oxygen intermediates direct the final product selectivity and FE. The reaction mechanism typically initiates with the adsorption of nitrate onto the catalyst surface followed by its sequential reduction through various nitrogen-containing intermediates such as NO_2^-, NO, N_2O, NH_2OH and ultimately NH_3.[56] Two primary pathways are recognized for the critical NO_2^- transformation which are the direct and indirect pathways as shown in Fig. 4.[57] The direct pathway as described by mechanisms from Vooys–Kooper and Duca–Feliu–Koper, involves the surface-bound reduction of $*NO_2^-$ to either N_2 or NH_3. In contrast, the indirect reduction pathway involves the desorption of NO_2^- into the electrolyte. Subsequent protonation or conversion to nitrogen dioxide (NO_2) or nitrous acid (HNO_2) *via* Vetter and Schmid mechanisms occurs prior to its re-adsorption and subsequent reduction.[58]

Niu *et al.*[59] further refined this understanding by proposing the adsorption configuration of key *NO intermediates as revealed in Fig. 5. The adsorption pathway includes O-end, NO-side with N-side or O-side and N-end. The large surface area and porosity of catalysts can promote the adsorption of nitrate.[4] In the O-end adsorption pathway, *NO is converted to ammonia through 3 proton-electron pairs targeting the nitrogen atoms, forming *O species. These *O species are further reduced to H_2O by adding 2 protons.[60] The N-end pathway is strongly dependent on N–N bonds.[61] If no N–N bond forms with adjacent *NO molecules, the reduction proceeds to *NOH, then *N, which undergoes further hydrogenation steps to yield ammonia. However, if N–N bonds form, the intermediate $*HN_2O_2$ can lead to the generation of $*N_2O$, which can either desorb as $*N_2O^-$ or further reduce to N_2, depending on its adsorption strength on the catalyst. In the NO-side pathway, *NO adsorbs parallel to the catalyst, allowing both nitrogen and oxygen atoms to engage in protonation. If nitrogen is protonated first, the reduction follows the O-end mechanism, leading to intermediates like *NOH. This can

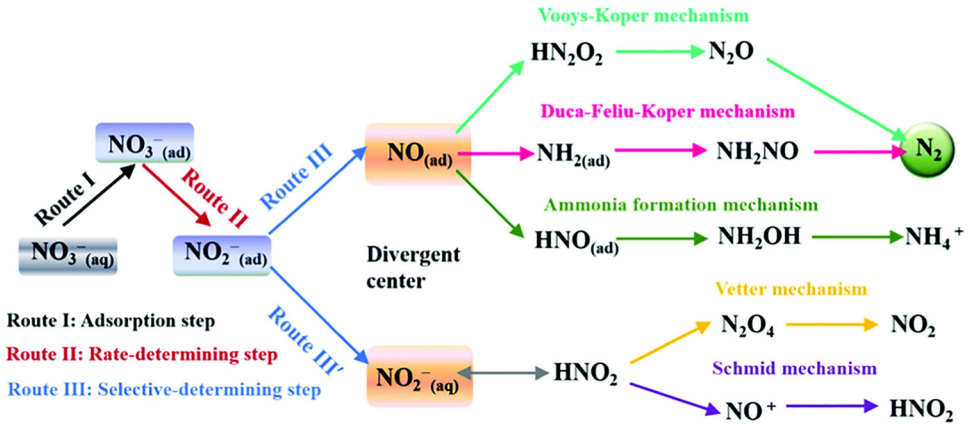

Fig. 4 Macroscopic roadmap of electrochemical nitrate reduction to ammonia, delineating the direct (surface-bound) and indirect (desorption-mediated) mechanistic routes.[57] Reproduced from ref. 57, with permission from The Royal Society of Chemistry, Copyright [2023].

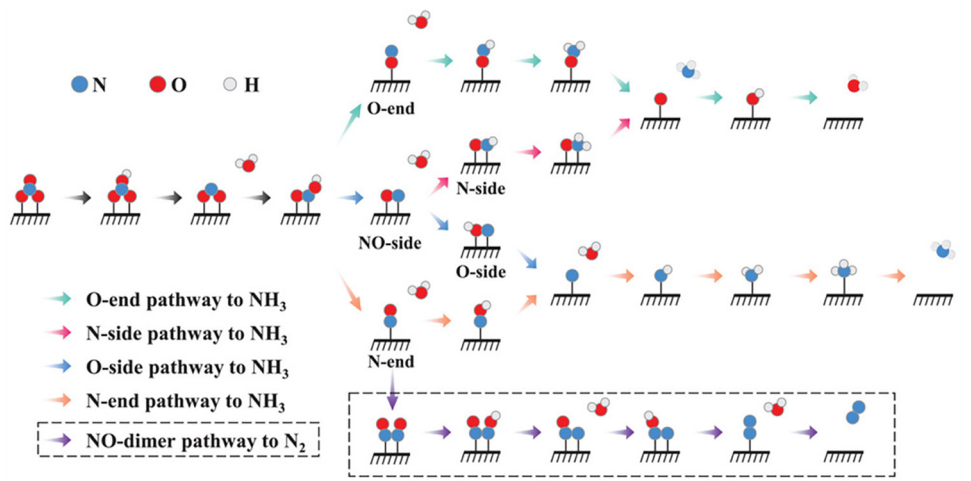

Fig. 5 Atomic-scale adsorption pathways and free energy landscape for nitrate reduction, detailing how distinct *NO chemisorption modes (O-end, N-end, NO-side) dictate the reaction trajectory and ultimate selectivity towards NH_3 *versus* N_2.[59] Reproduced from ref. 59, with permission from John Wiley & Sons, Copyright [2020].

further reduce to *N or *HNOH, with *N following a pathway to ammonia, while *HNOH converts to $*H_2NOH$ and then to ammonia.[4] Ultimately, selectivity is directed by the catalyst's capacity to stabilize specific intermediates thereby steering the pathway toward N–O cleavage and N–H formation over the HER.[62]

A singular focus on the cathodic mechanism of the nitrate reduction reaction obscures a fundamental limitation in the overall electrochemical process which is an anodic half-reaction. Conventionally, nitrate reduction reaction is paired with the OER ($2H_2O \rightarrow O_2 + 4H^+ + 4e^-$) which is notoriously sluggish and requires high overpotentials contributing significantly to the total energy consumption of the system without producing a valuable co-product.[63] The mechanistic understanding of nitrate reduction illuminates a more transformative pathway to the strategic design of paired electrocatalysis. As shown in Fig. 6, replacing the OER (1.23 V *vs.* SHE) with a thermodynamically favorable AOR such as the oxidation of waste contaminants or the valorization of renewable organics radically reduces the operational cell voltage.[64] This paradigm shift transcends mere electrochemical remediation enabling integrated systems that simultaneously purify wastewater and synthesize valuable chemicals.

Consequently, the mechanistic pursuit of high-performance nitrate reduction reaction catalysts must be conducted with an awareness of the anodic partner. These necessities a rigorous evaluation of performance that extends beyond intrinsic catalytic activity to encompass the full-cell energy landscape. Catalysts should be designed not only for high ammonia selectivity and yield but also for compatibility within a paired system that operates at low cell voltage, maximizing both energy efficiency and economic return. This holistic approach of integrating cathodic mechanism with anodic innovation is essential for translating electrocatalytic nitrate to ammonia conversion from a laboratory concept into a scalable and sustainable technology.

2.2. Performance metrics for electrochemical ammonia production systems

Evaluating the performance of electrocatalytic nitrate-to-ammonia conversion requires a holistic set of metrics that extend beyond traditional half-cell activity descriptors. While intrinsic catalyst properties such as overpotential, Tafel slope and current density provide insights into reaction kinetics and efficiency, a comprehensive assessment must incorporate system-level parameters including full-cell voltage, faradaic efficiency, selectivity, stability and economic viability. These indicators collectively determine the feasibility of scaling up this process for sustainable and energy-efficient ammonia synthesis.[65] Crucially, the advent of paired electrolysis configurations necessitates an integrated perspective, where the performance of both cathodic and anodic reactions dictates the overall energy footprint, environmental impact and economic potential of the technology.

2.2.1. Activity and kinetics: overpotential, Tafel slope and current density. The intrinsic activity of an electrocatalyst is primarily gauged by its overpotential (η), Tafel slope and operational current density. The overpotential, defined as the deviation from the thermodynamic potential for nitrate-to-ammonia conversion (0.69 V *vs.* RHE), arises from kinetic barriers associated with multi-electron/proton transfers and the cleavage of robust N–O bonds. A lower η signifies superior catalytic efficiency and reduced energy consumption.[66] Complementarily, the Tafel slope quantifies the potential increase required to augment the current density (j) by an order of magnitude.[67] The Tafel equation is:

$$\eta = a + b \times \log(j) \quad (1)$$

where j is the current density in mA cm^{-2}, b is the Tafel slope in mV dec^{-1}, a is the exchange current density and η is the overpotential in mV.[67] A lower Tafel slope indicates favorable reaction kinetics and an efficient electron transfer pathway often linked to the initial nitrate-to-nitrite step as the potential-determining stage. Meanwhile, the applied current density directly governs the reaction rate and product distribution.[12] While elevated current densities can enhance nitrate removal rates, they often promote competing side reactions notably the HER thereby compromising ammonia selectivity.[68] Therefore, optimizing this triad of parameters is essential for achieving high reaction rates at minimal energy penalties.

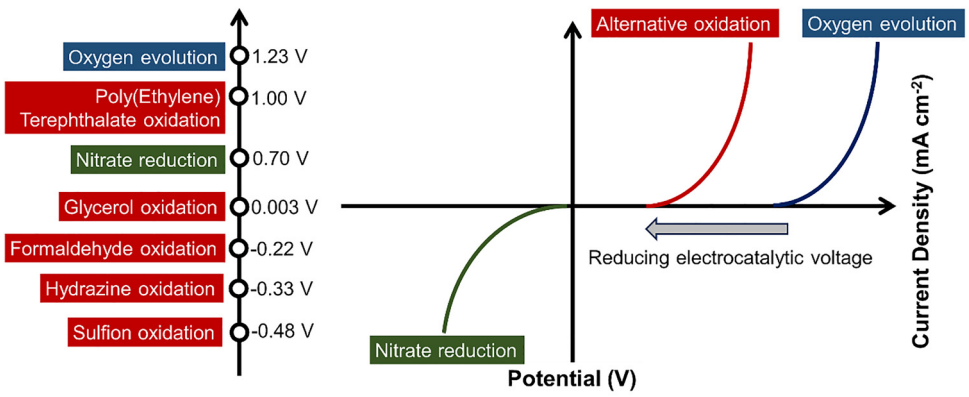

Fig. 6 Polarization curves for nitrate reduction paired with the AOR, low-potential anodic reactions (V *vs.* SHE).

2.2.2. Efficiency and selectivity: faradaic efficiency and product distribution. FE and selectivity are paramount for assessing the practical utility of the nitrate reduction reaction. FE quantifies the fraction of electrons channeled toward the desired ammonia product relative to the total charge passed, calculated as:

$$\text{FE}\ (\%) = \frac{Q_{\text{NH}_3}}{Q_{\text{total}}} \times 100\% = \frac{n \times F \times c \times V}{M \times Q_{\text{total}}} \times 100\% \qquad (2)$$

where M is the molecular mass of ammonia, V is the volume of electrolyte, c is the concentration of ammonia produced, F is the Faraday constant, n is the number of electrons transferred and Q_{total} is the total charge passed through the system during the reaction.[43] High FEs (>70%) are often attainable due to the more facile activation of N–O bonds compared to N≡N bonds which are critical for process efficiency.[65] However, FE alone is insufficient thus product selectivity must be concurrently high to minimize the generation of undesirable by-products (NO_2^-, N_2O) and simplify downstream separation. The equation to calculate the selectivity is:

$$\text{Selectivity} = \frac{C_{\text{NH}_3}}{\Delta C_{\text{NO}_3^-}} \times 100\% \qquad (3)$$

where $\Delta C_{\text{NO}_3^-}$ is the change of nitrate ion concentration over time and C_{NH_3} is the concentration of ammonia produced.[43] A system exhibiting high nitrate conversion is only technologically viable if coupled with near-perfect ammonia selectivity as this drastically reduces purification costs and energy burdens.[69]

From an environmental perspective, the direct electrochemical reduction of nitrate to nitrogen is even more desirable, as it offers complete detoxification of nitrate without forming secondary products. Yet this pathway remains instrinsically challenging. The fundamental difficulty lies in the multistep, eight-electron, nine-proton transfer process that requires the precise coupling of intermediate species such as $*NO_2^-$, *NO, *NHO, and $*N_2O$. The kinetic barrier for N–N bond formation (2.7 eV) is substantially higher than that for the successive hydrogenation steps leading to ammonia (on the order of 0.1–0.4 eV), rendering the NH_3 pathway thermodynamically and kinetically favoured under most electrochemical conditions.[70] Moreover, controlling the adsorption and desorption energetics of these intermediates is complex as achieving selective N_2 evolution demands a delicate balance between *NO stabilization for dimerization and suppression of overhydrogenation towards $*NH_x$ species. Current Cu- and Co-based catalysts predominantly facilitate proton-coupled electron transfer mechanisms that accelerate hydrogenation to NH_3 rather than N–N coupling to N_2.

While FE and selectivity quantify the electron utilization and pathway specificity, the ammonia yield rate provides an indispensable measure of the catalyst's practical productivity, typically expressed in mass or molar units per time per geometric or mass-normalized area (mg h^{-1} cm^{-2} or mmol h^{-1} $gcat^{-1}$).[71] This parameter directly reflects the system's capability to convert nitrate into ammonia at a commercially relevant throughput bridging the gap between fundamental catalytic properties and industrial applicability. A high yield rate sustained under industrially significant current densities is a non-negotiable prerequisite for the economic viability of decentralized ammonia synthesis.[72] Therefore, a comprehensive performance evaluation must synergistically consider FE, selectivity and the ammonia yield rate to holistically assess the technological potential of any electrocatalytic system. In paired electrolysis, this paradigm extends to the anode where the FE for the valorized oxidation product must also be high to validate the economic premise of co-production.

2.2.3. System-level viability: full-cell voltage, stability and economic potential. The transition from laboratory curiosity to industrial application hinges on system-level performance metrics.[39] Replacing the anodic OER with a thermodynamically favorable AOR can slash the full-cell voltage (E_{cell}) by up to 50%, as the thermodynamic and kinetic overpotentials at the anode are dramatically reduced.[64] This directly translates to profound energy savings per mole of ammonia produced. Long-term operational stability (>1000 hours) under industrially relevant current densities (>200 mA cm^{-2}) is a non-negotiable prerequisite.[73] Degradation mechanisms including catalyst fouling by nitrogenous intermediates, anodic dissolution and membrane degradation must be mitigated through intelligent catalyst and system design.[74,75] Finally, economic viability is fundamentally redefined in paired electrolysis. The evaluation framework must expand to encompass the formation rate and market value of the co-produced anodic chemical such as formate, sulfur, terephthalic acid.[76] The objective is to transform the electrochemical reactor from a net energy consumer into a distributed, modular and profitable chemical manufacturing unit thereby challenging the economic dominion of the Haber–Bosch process.[22,77]

2.3. State-of-the-art electrocatalyst modifications for nitrate reduction to ammonia

The rational design and sophisticated engineering of electrocatalysts constitute the cornerstone of advancing nitrate reduction to ammonia, a process plagued by inherent challenges such as multi-electron/proton transfer complexities, competitive sides reactions and intermediate-induced deactivation.[45] This subsection provides a critical and comprehensive analysis of the forefront strategies in electrocatalyst modifications, meticulously examining how structural, defect, doping, single-atom and bimetallic engineering paradigms synergistically enhance catalytic performance. Herein, by elucidating the interplay between atomic-scale active sites, electronic structure modulation and reaction pathway optimization, this work unravels how state-of-the-art Cu- and Co-based electrocatalysts achieve unprecedented activity, selectivity and stability in paving the way for scalable and sustainable electrochemical ammonia synthesis.

2.3.1. Structure engineering. Various structural engineering strategies such as facet, morphology, modifications with metals and others have been employed to improve the electrocatalytic nitrate to ammonia reduction.[78,79] The structural engineering of electrocatalysts has great promise for modulating catalytic activity for specific applications.[80,81] Facet engineering is

regarded as a prospective strategy to control the desired crystalline ratio of a surface.[82] Due to anisotropy, differently oriented crystalline surfaces usually have chemical and physical properties associated with the facets, resulting in variations in hydrogen intermediates or oxygen adsorption energies.[83] The facets can expose more electrocatalytically active sites, which greatly improves the mass activity of active sites. This allows for better control over reaction pathways and increases the overall efficiency of the nitrate reduction process.

In this domain, the use of Cu-based catalysts, particularly in conjunction with structural engineering strategies such as facets has been highlighted for enhancing nitrate to ammonia conversion. Research by Fu *et al.*[84] presented a detailed investigation into Cu nanosheet catalysts derived from CuO, showcasing their high ammonia yield rate of 1.41 mmol h^{-1} cm^{-2} and partial current density of 665 mA cm^{-2} due to the tandem interaction of Cu (111) and Cu (100) facets (Fig. 7(a)). According to Fig. 7(b), a high-resolution transmission electron microscopy (HRTEM) picture revealed that the CuO nanosheets had been transformed into metallic Cu, with lattice spacing of 0.18 nm for Cu (100) and 0.21 nm for Cu (111). Besides, ammonia FE remained above >80% across a broad potential range of −0.19 to −0.59 V *vs.* RHE (Fig. 7(c)). The catalyst has high stability up to 700 hours at 365 mA cm^{-2} with an ammonia FE of about 88% (Fig. 7(d)). The Cu (100) facets predominantly adsorbed nitrate and turned the nitrate to nitrite, while the Cu (111) facets were more beneficial for the consequential hydrogenation of *NO to *NOH for ammonia production. In another study, Hu *et al.*[16] emphasizes the synthesis of Cu nanobelts (Cu-NBs) with preferential exposure of Cu (100) facets and abundant surface defects, achieved through *in situ* electrochemical reduction. The synergistic interaction between Cu (100) facets and surface defects has been shown to significantly enhance the reduction of nitrate to ammonia while inhibiting the competitive HER and upshifting the d band center of Cu. The Cu (100) facet and surface defects achieve a FE of 95.3% for ammonia. Additionally, Shih *et al.*[15] examined the effect of crystal facet and morphology on Cu nanoparticles supported on nickel foam (Cu/Ni), emphasizing the important role of Cu facet in fostering nitrate reduction. The preferential facet orientation of Cu surfaces enhanced the electron transfer process. According to batch kinetics tests conducted at constant voltage and current, effective electrochemical nitrate reduction required the selective adsorption of nitrate and nitrite on the Cu {111} facet. Thus, the facet engineering and surface modifications through nanosheet formation, nanobelts synthesis or supported nanoparticles are essential for improving the electrocatalytic performance of Cu-based catalysts for nitrate to ammonia reduction.[85]

Interestingly, Co_3O_4-based catalysts exhibited tremendous potential for electrocatalytic nitrate reduction due to their facet-dependent properties. For Co_3O_4, facet engineering has a significant impact on the geometric coordination and valence of Co on the Co_3O_4 surface, leading to large differences in catalytic activity.[86] For instance, a study by Lu *et al.*[48] showcased the development of Co_3O_4 hexagonal nanosheets with selectively exposed {111} and {112} facets, demonstrating that the {111} facet notably outperformed the {112} facet in nitrate to ammonia conversion. As can be seen from Fig. 7(f) and (g), the adsorption energy of *H on the {111} facet (−3.10 eV) is significantly lower when compared to that of the {112} facet (1.39 eV). The {111} facet's Co site and *H have a stronger interaction, which prevents hydrogen from forming and increases the conversion of nitrate and NH_x intermediates to ammonia. Out of these, Co_3O_4-{111} has a superior FE of >99% at −0.7 V *vs.* RHE and obtained the highest ammonia yield rate of 5.73 mg mg_{cat}^{-1} h^{-1} at −0.9 V *vs.* RHE. Moreover, the rate-determining step (*NO_3H to *NO_2) energy barrier is lower for Co_3O_4-{111} compared to Co_3O_4-{112} (*NO_2 to *NO_2H). Complementing these finding, Zhu *et al.*[87] highlighted the facet related behaviour spinel Co_3O_4 nanostructures catalysts with various exposed facets, including {100}, {111}, {110} and {112} which were prepared using a hydrothermal-calcination method for electrochemical nitrate reduction reactions (Fig. 7(h)). It is found that the {111} facet has superior catalytic activity compared to other facets and plays a key role in facilitating the formation of oxygen vacancies as well as promoting the phase transition to $Co(OH)_2$ under electrochemical conditions. This transition provides abundant active sites for the stabilization of *NH_2 intermediates, thereby improving the efficiency and selectivity of ammonia synthesis. These findings suggest that Co_3O_4 with {111} facets could be the catalyst of choice for improved performance in further studies of Co_3O_4-based catalysts.

In addition to facet engineering, morphology is another aspect of structural engineering. By designing catalysts with customized shapes, such as nanosheets, nanospheres, nanorods or others, researchers can maximize the surface area and ensure that active sites are more accessible. As a 21st-century strategic resource, Co-based catalysts with nanosheet or nanosheet arrays have an inherent catalytic capability for nitrate reduction. In particular, Wang *et al.*[88] reported ultrathin cobalt oxide (CoO_x) nanosheets with abundant surface oxygen introduced through a simple one-pot method (Fig. 8(a) and (b)). In detail, this contributed to an exceptionally high FE and ammonia production with 93.4% and 82.4 mg h^{-1} mg_{cat}^{-1}, respectively at −0.3 *vs.* RHE. This morphology is enriched with surface oxygen, which reduces the HER, stabilizes adsorbed hydrogen and promotes more efficient nitrate to ammonia reduction through the NHO pathway with a lower energy barrier. On another note, Du *et al.*[75] carried out the cobalt iron layered double hydroxide (CoFe LDH) nanosheet arrays on Ni foam (NF) with 97.68% FE and 97.68% selectivity. As displayed in Fig. 8(c) and (d), CoFe LDH is a three-dimensional (3D) porous structure with vertical and conterminous nanosheets evenly spread on the NF substrate surface. Impressively, the nitrate to ammonia reduction performance of the CoFe LDH is maintained at a high level after 12 cycles totalling 36 hours (Fig. 8(e)). DFT calculations signify that CoFe LDH can adjust the d band centre to balance nitrate and nitrite adsorption as well as ammonia desorption, providing an optimal active site and excellent performance. Building this paradigm, constructing

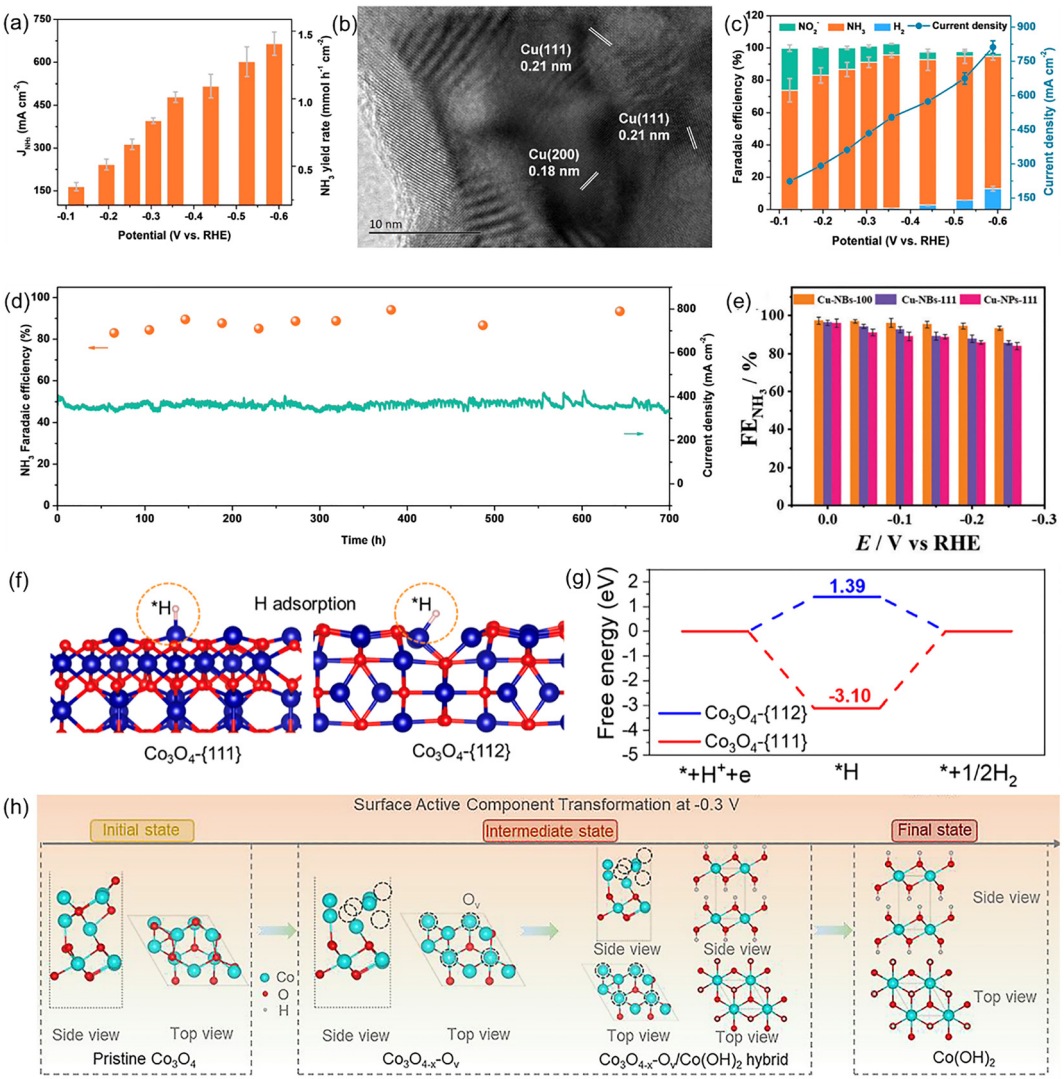

Fig. 7 Electrocatalytic nitrate to ammonia performance in flow cells. (a) Ammonia partial current density and yield rate over Cu nanosheets. (b) HRTEM images of Cu nanosheets after reduction. (c) FE and total current density of various products over Cu nanosheets. (d) Time-dependent NH_3 faradaic efficiency and current density over Cu nanosheets during long-term stability testing over the course of 700 h. (e) FE of Cu (100) nanobelts, Cu (111) nanobelts and Cu nanoparticles with Cu (111).[84] Reproduced from ref. 84, with permission from John Wiley & Sons, Copyright [2023]. (f) Adsorption configuration of *H on the Co sites of Co_3O_4-{111} and Co_3O_4-{112}. (g) Free energy profiles for the HER on Co_3O_4-{111} and Co_3O_4-{112}.[48] Reproduced from ref. 48, with permission from American Chemical Society, Copyright [2024]. (h) Illustration on the structure evolution of the Co_3O_4 {111} upon electrocatalytic nitrate reduction operation.[87] Reproduced from ref. 87, with permission from American Chemical Society, Copyright [2024].

hierarchical nanoarrays with multiple active components represents a powerful morphology engineering strategy. Liu *et al.*[89] demonstrated this approach by electrodepositing Cu nanoparticles onto $NiCo_2O_4$ nanowire arrays creating hierarchical Cu–$NiCo_2O_4$ heterostructures. SEM images (Fig. 8(f) and (g)) confirm the preserved nanowire scaffold with rough surface after Cu decoration while TEM (Fig. 8(h)) verifies the intimate integration of crystalline $NiCo_2O_4$ and metallic Cu phases. This architecture creates a synergistic tandem system where Cu reduces nitrate to nitrite while $NiCo_2O_4$ provides crucial *H species for hydrogenation, achieving an exceptional NH_3 yield of 3.56 mmol h^{-1} cm^{-2} with 95.2% FE at −0.2 V *vs.* RHE. This case illustrates that hierarchical morphologies integrating complementary functionalities are transformative for developing superior electrocatalysts.

Remarkably, cobalt phosphide (CoP)-based catalysts show enormous promise in electrocatalytic nitrate reduction due to their unique structure. For example, Ye and coworkers narrated CoP nanosheet arrays grown on carbon fiber cloth (CoP NAs/CFC) exhibit nearly perfect FE (∼100%) and excellent stability.[90] This work proved that phosphorus is pivotal for optimizing the energetic barrier and stabilizing the active phase of the nitrate reduction reaction. Furthermore, *in situ* X-ray absorption fine structure (XAFS) analysis firstly indicates that the 3d–4p electronic transition in Co, induced by an electric field, is intimately linked to the nitrate reduction reaction. This structural and electronic synergy between Co and P not only enhances the selective conversion of nitrate to ammonia but also mitigates the HER (Fig. 9(a)–(c)). In another

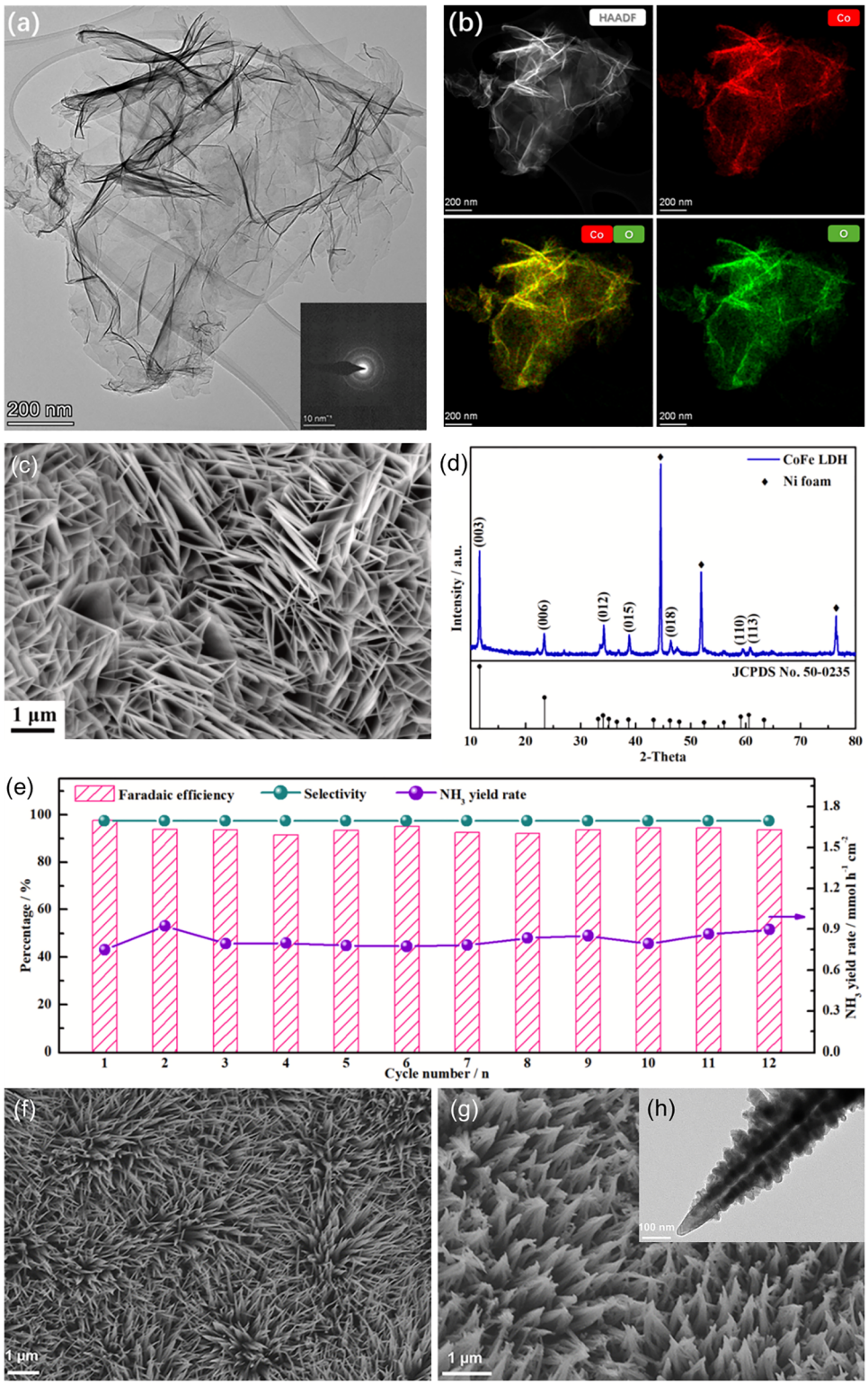

Fig. 8 (a) TEM image and the corresponding SAED pattern. (b) HAADF-STEM image and the corresponding elemental EDX maps of the CoO_x nanosheets.[88] Reproduced from ref. 88, with permission from American Chemical Society, Copyright [2021]. (c) SEM image of CoFe LDH. (d) XRD pattern of CoFe LDH. (e) The consecutive recycling test of CoFe LDH at −0.45 V *vs.* RHE in 1 M KOH electrolyte with 1400 ppm NO_3^-–N.[75] Reproduced from ref. 75, with permission from Elsevier, Copyright [2022]. SEM images of the (f) $NiCo_2O_4$ and (g) hierarchical Cu–$NiCo_2O_4$ nanoarrays on Ni foam. (h) TEM image showing Cu nanoparticles deposited on a $NiCo_2O_4$ nanowire.[89] Reproduced from ref. 89, with permission from The Royal Society of Chemistry, Copyright [2025].

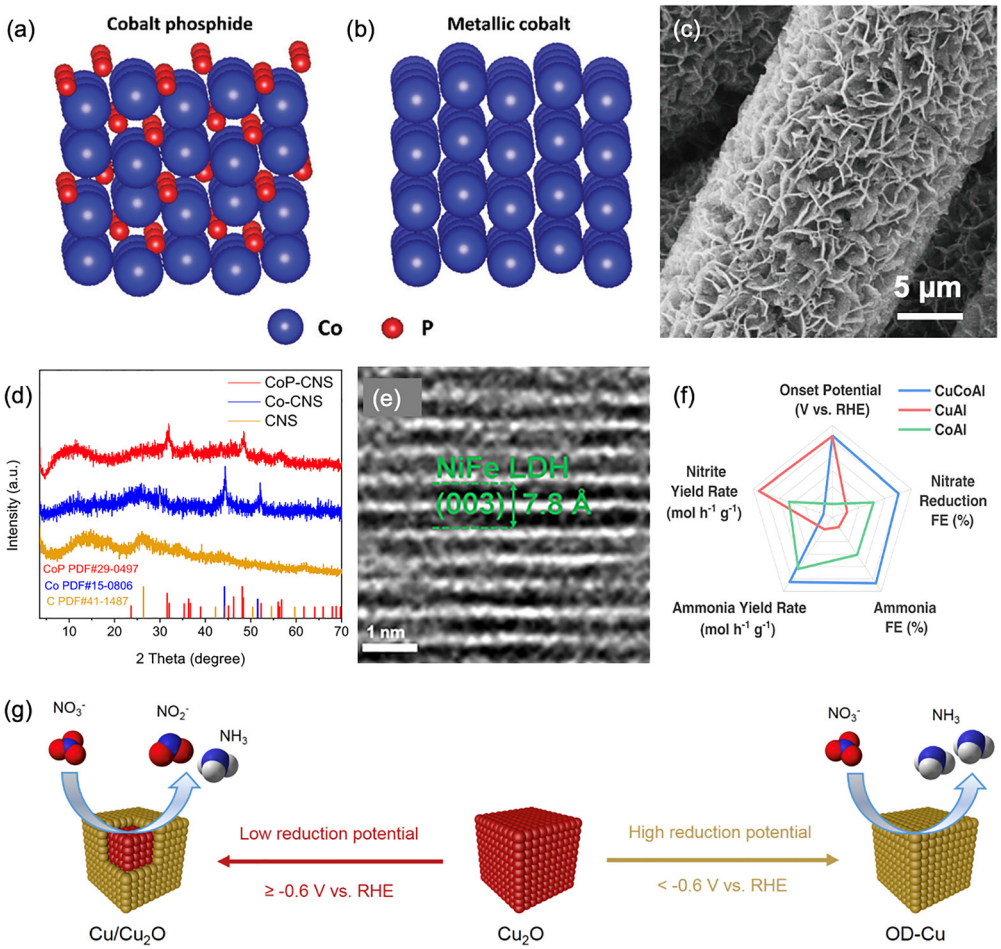

Fig. 9 Crystallographic structures of (a) CoP and (b) metallic Co.[90] Reproduced from ref. 90, with permission from The Royal Society of Chemistry, Copyright [2022]. (c) SEM images of CoP-CNS. (d) XRD pattern.[91] Reproduced from ref. 91, Springer Nature, Open Access [2022]. (e) HR-TEM image of Ni_3Fe–CO3 LDH.[92] Reproduced from ref. 92, with permission from The Royal Society of Chemistry, Copyright [2023]. (f) Radar plot of the nitrate reduction performance of multimetallic LDH catalysts.[93] Reproduced from ref. 93, with permission from American Chemical Society, Copyright [2023]. (g) Schematic illustration of potential-induced electrochemical reconstruction of Cu_2O cubes with different chemical states of Cu toward NO_3^- reduction to different products (NH_3 and NO_2^-).[98] Reproduced from ref. 98, with permission from American Chemical Society, Copyright [2023].

study, Fan *et al.*[91] synthesized a hollow CoP nanosphere electrocatalyst on a self-supported carbon nanosheet array (CoP-CNS) with a high ammonia yield rate of 8.47 mmol h^{-1} cm^{-2}. Both theoretical and experimental research have demonstrated that better ammonia is produced when active hydrogen is generated in dynamic equilibrium on CoP and promptly consumed by nitrogen intermediates. Besides, the CoP-CNS performs with outstanding stability for more than 123 hours, with FE $>80\%$ and the yield rate of ammonia remaining virtually unchanged. The crystal structure of CoP-CNS was validated by the X-ray diffraction (XRD) pattern analysis (Fig. 9(d)), which revealed distinct peaks corresponding to CoP and demonstrated the effective integration of phosphorus. These studies highlight the immense possibilities of CoP-based catalysts for efficient and stable electrocatalytic nitrate reduction, highlighting the structural and electronic synergies of phosphorus in enhancing ammonia production, reducing the HER and maintaining long-term catalytic stability.

In addition to the morphology of catalysts discussed above, significant results have been achieved with strategies involving the design of complex structures. In the work of Kim *et al.*,[92] a Ni_3Fe–CO_3 LDH/Cu foam hybrid structure was developed to enhance the electrocatalysis of nitrate reduction by exploiting the collaborative effect between LDH and conductive Cu foam substrate. Fig. 9(e) shows a high-resolution transmission electron microscopy (HRTEM) image in which the nanoplatelet morphology of Ni_3Fe–CO_3 LDH shows a lattice edge of 0.78 nm. Ni_3Fe–CO_3 LDH manifests an appropriate kinetic potential for the generation of hydrogen radicals at the Volmer step and inhibits the formation of H–H bonds by dampening the Heyrovsky step. The structure has been designed to greatly improve catalytic performance, with an 8.5-fold increase in ammonia production and an impressive 98.5% nitrate conversion compared to pure copper. These outcomes demonstrate that this hybrid structure has a Ni_3Fe–CO_3 LDH coating that facilitates the transfer or generation of hydrogen radicals, as well as a

highly porous copper foam that selectively binds nitrate. Moreover, Wang *et al.*[93] proposed an LDH electrocatalyst with trimetallic CuCoAl composition. This catalyst has a lamellar structure containing active Cu, Co and Al sites and lattice spacing of 0.66 nm and attains a high FE of 99.5%. The nitrate reduction onset potential was positively shifted by 0.3 V when Cu was present, confirming that Cu plays a key role in reducing the electrochemical activation barrier and igniting the nitrate upcycling process. The radar plot in Fig. 9(f) illustrates the superior performance of the CuCoAl LDH compared to CuAl and CoAl. These studies underscore the effectiveness of hybrid structures and multimetallic LDH compositions in significantly enhancing nitrate reduction performance by improving catalytic kinetics, optimizing hydrogen radical generation and improving nitrate adsorption properties.[94–96] In another study, Yoon *et al.*[97] well-defined Cu_2O cubes, demonstrating that these structures undergo significant restructuring under electrochemical conditions, forming distinct active sites that influence selectivity towards ammonia production.

Aside from facet and morphology, modification with metals is also a crucial aspect of structure engineering to enhance the catalytic properties of nitrate reduction reactions. For example, Zhou *et al.*[98] explored the potential-induced synthesis of oxide-derived Cu^0 (OD-Cu) cube electrocatalysts fabricated through *in situ* electrochemical reconstruction from Cu_2O (Fig. 9(g)). According to theoretical computations, well-designed pulsed electrolysis tests and *in situ* Raman analysis, the presence of the Cu/Cu_2O interface promoted nitrite synthesis at low reduction potentials.[99] At the same time, ammonia was predominantly formed on OD-Cu at high reduction potentials. DFT calculations implied that the high selectivity on OD-Cu was attributed to the enhanced adsorption of nitrate which promotes the formation of key intermediate *NOH and inhibits competitive HERs. Noteworthily, Liu *et al.*[69] devised an advanced electrocatalyst for highly efficient nitrate to ammonia reduction by loading atomically precise silver nanoclusters (Ag_9 NCs) on Ti_3C_2 MXene (Ag_9/MXene) for ambient ammonia synthesis with enhanced robustness in neutral media. In comparison to Ag_9 NCs, Ag_9/MXene has superior stability with no decay in current density after 108 hours of reactions. The double layer capacitance (C_{dl}) value of 12.2 mF cm^{-2} for Ag_9/MXene is greater than 0.13 mF cm^{-2} for Ag_9 NCs, which indicates that Ag_9/MXene has more active reaction sites. Thus, the existence of Ag clusters facilitated the conversion of nitrate to nitrite, which acted as an intermediate in the tandem catalytic reaction process on MXene, dramatically improving the FE and selectivity of ammonia.

To conclude, structure engineering is indispensable in enhancing the catalytic performance of materials for nitrate to ammonia conversion. The profound impact of structural engineering on catalytic performance is systematically benchmarked in Table 1 which reveals that tailored facet exposure and morphology in Cu- and Co-based systems consistently result in FE exceeding 95% with exceptional long-term stability. Advanced electrocatalysts were developed with improved efficiency, selectivity and stability through various strategies such

Table 1 Performance comparison of structurally engineered electrocatalysts for nitrate reduction

Catalyst	FE (%)	Electrolyte	Stability (h)	Current density (mA cm^{-2})	Ammonia yield rate	Ref.
Cu-NBs-100	95.3% at −0.15 V *vs.* RHE	1 M KOH + 0.5 M NO_3^-	20	398 at −0.25 V *vs.* RHE	650 mmol g^{-1} h^{-1} at −0.15 V *vs.* RHE	16
Co_3O_4-{111}	>99% at −0.7 V *vs.* RHE	0.1 M K_2SO_4 + 500 ppm KNO_3	—	—	5.73 mg mg^{-1} h^{-1} at −0.9 V *vs.* RHE	48
Ag_9/MXene	80.2% at −0.95 V *vs.* RHE	0.5 M K_2SO_4 + 200 ppm NO_3^-	108	—	—	69
CoFe LDH/NF	97.68% at −0.95 V *vs.* RHE	1 M KOH + 1400 ppm NO_3^-–N	36	—	0.93 mmol h^{-1} cm^{-2} at −0.45 V *vs.* RHE	75
Cu nanosheets with Cu(100) and Cu (111)	95% at −0.36 V *vs.* RHE	1 M KOH + 0.2 M KNO_3	700	665 at −0.59 V *vs.* RHE	1.41 mmol h^{-1} at −0.59 V *vs.* RHE	84
Co_3O_4 with {111}	99.1 ± 1.8% at−0.6 V *vs.* RHE	1 M KOH + 100 mM NO_3^-	—	—	35.2 ± 0.6 mg h^{-1} cm^{-2} at −0.6 V *vs.* RHE	87
Ultrathin CoO_x nanosheets with abundant surface oxygen	93.4 ± 3.8% at −0.3 V *vs.* RHE	0.1 M KOH + 100 mM NO_3^-	—	—	82.4 ± 4.8 mg h^{-1} mg^{-1} at −0.3 V *vs.* RHE	88
CoP NAs/CFC	~100	1 M NaOH + 1 M $NaNO_3$	12	—	0.569 mol g^{-1} h^{-1} at −0.3 V *vs.* RHE	90
Hollow CoP-CNS	88.6	1.0 M OH^- + 1.0 M NO_3^-	123	1000	8.47 mmol h^{-1} cm^{-2} at −1.03 V *vs.* RHE	91
Ni_3Fe–CO_3 LDH/Cu foam	96.8	1.0 M KOH + 5 mM NO_3^-	—	−79.4	1.261 mg cm^{-2} h^{-1} at −0.2 V *vs.* RHE	92
CuCoAl LDH	99.5% at −0.8 V *vs.* RHE	0.5 M phosphate buffer + 50 mM KNO_3	32	—	0.22 mol h^{-1} g^{-1} at −0.8 V *vs.* RHE	93
OD-Cu cube	93.9% at −0.9 V *vs.* RHE	0.1 M PB + 0.1 M KNO_3	—	52.8 at −1.0 V *vs.* RHE	219.8 μmol h^{-1} cm^{-2} at −0.9 V *vs.* RHE	98

as facet engineering, morphology customization and metal modification. Facet engineering optimizes active site activity and modulates reaction pathways, while morphology control increases surface area and accessibility though nanosheets and nanobelts. The addition of metals to catalyst structures has been validated to be an efficient intermediate stabilization and others. These approaches highlight the structure engineering as a transformative tool for maximizing the reduction of nitrate to ammonia.

2.3.2. Vacancy engineering. Among other methods to modify the electronic structure of catalysts, defect engineering has been a popular topic in electrocatalysis in recent years.[100] Defect engineering enables the chemical properties of the catalyst, electronic energy band structure and fine-tuning of local microstructure.[101] Defects are categorized into point defects, line defects and others. Point defects are the simplest form of crystal defects, representing a deviation from the typical crystal structure within a node or adjacent microscopic region.[102] There are two classical types of point defects, namely vacancies and doping. In particular, vacancies are empty spaces in the lattice of a material due to missing atoms. Noticeably, recent literature has shown that vacancy engineering provides a facile and effective strategy for accelerating their catalytic performance.

Oxygen vacancies are identified as localized cave structures in the oxide matrix, which arise from the absence of an O atom in the atomic scale structure. It plays a critical role in enhancing the performance of electrocatalytic nitrate reduction by improving catalytic efficiency and product selectivity. For instance, Jia *et al.*[103] and Zhang *et al.*[17] illustrate the potential of oxygen vacancies for advancing this process with both investigations focusing on modification to TiO_2 structures that increase the density of oxygen vacancies and maximizing their catalytic potential. Jia *et al.* reported the synthesis of oxygen vacancies TiO_{2-x} as electrocatalytic nitrate reduction catalysts on titanium foil using electrochemical anodic oxidation and subsequent high temperature reduction with hydrogen.[103] Fig. 10(a) shows the electron paramagnetic resonance (EPR) after hydrogen treatment, TiO_{2-x} has a stronger signal near g = 2.002 which exemplifies the introduction of rich oxygen vacancies in TiO_{2-x}. TiO_{2-x} with more oxygen vacancies demonstrated higher selectivity, FE and conversion in ammonium synthesis than TiO_2, recording 87.1%, 85.0% and 95.2% correspondingly (Fig. 10(b)). Compared to TiO_2 (101) with a single vacancy (Fig. 10(c)), TiO_2 (101) with two vacancies (Fig. 10(d)) requires a higher reaction barrier for HNO_2, thereby reducing by-product formation. Consequently, oxygen vacancies not only accommodate oxygen from nitrate to weaken the N–O bond but also adjust the interaction between catalysts and intermediates to enhance the reaction pathway and minimize by-product generation. Next, the work by Zhang *et al.* investigated the combination of TiO_{2-x} with 10% of the loading amount of copper clusters ($10Cu/TiO_{2-x}$), which leverages the catalytic activity of copper as well as the enhanced nitrate adsorption and optimized hydrogenation pathways provided by oxygen vacancies.[17] Fig. 10(e) displays an excellent performance of $10Cu/TiO_{2-x}$ catalyst with a yield rate of 0.1143 mmol h^{-1} mg^{-1} and FE of 81.34%. Differential electrochemical mass spectrometry (DEMS) results in Fig. 10(f) show that NH_2OH is the main intermediate, providing insight into the reaction mechanism facilitated by oxygen vacancies and copper. Hence, TiO_{2-x} whether used alone or in combination with other catalytic elements can significantly elevate the performance of ammonia synthesis, providing a promising approach for sustainable nitrate reduction technologies.

Moving on, recent studies on Cu_2O-based catalysts designed for nitrate reduction in a lively manner have demonstrated the presence of oxygen vacancies. For example, the study by Xu *et al.* explores hierarchical defect incorporation in Pd–Cu_2O corner-etched octahedra (CEO), which uses ultralow Pd content to facilitate oxygen vacancies and cavity formation on Cu_2O (Fig. 11(a)–(c)).[49] The synergistic effect of cavity and oxygen vacancy defects plays a conspicuous role in weakening the N–O bond, suppressing the formation of by-products and facilitating the adsorption of nitrate. Moreover, the Pd site as an active centre for the accumulation of hydrogenated substances facilitates the ammonia generation reaction pathway. This dual-defect structure significantly enhances the efficiency of nitrate to ammonia reduction, achieving a high FE of 96.56% and selectivity of 95.31% at optimum potential (−1.3 V *vs.* SCE). Meanwhile, Gong *et al.* and Zhong *et al.* both delve into the strategic role of oxygen vacancies and hydroxyl group densities in enhancing nitrate reduction efficiency on Cu_2O surfaces. In 2022, Gong *et al.* utilized plasma treatment to increase oxygen vacancies and hydroxyl group densities on Cu_2O surfaces (Fig. 11(d)).[104] The oxygen vacancies can enhance nitrate reduction through selective adsorption and proton transfer while hydroxyl groups on the surface inhibit competing HERs.[105] Likewise, Zhong *et al.* extended this defect focused methodology through facet engineering on Cu_2O crystals, showing that (111) facets contain higher oxygen vacancies and hydroxyl densities than other facets.[106] The above studies exemplify that vacancy engineering through hierarchical structuring, plasma treatment or facet engineering can drastically improve the performance of Cu_2O-based catalysts in nitrate reduction.

Aside from the previously discussed oxygen vacancies, the addition of other anionic vacancies such as sulfur vacancies has potential in enhancing electrocatalytic performance for nitrate to ammonia reduction.[107] Sulfur vacancies can create localized electron-rich sites, leading to unique electronic properties, which are particularly effective in modifying catalysts to achieve high efficiency and selectivity. This was demonstrated by the work of Tao *et al.*[108] in which they introduced sulfur-rich vacancies with $Ni_3Co_6S_8$ nanospheres (NCS-2) growing on a nickel foam substrate by developing a facile Joule heating method (Fig. 11(e)). NCS-2 with reasonable concentration of sulfur vacancies exhibited excellent performance in electrocatalytic reduction of nitrate to ammonia while preserving their structural integrity, with FE of 85.3%, selectivity of 98.2% and yield rate of 2388.4 μg h^{-1} cm^{-2} (Fig. 11(f)). The DFT calculation and structural characterizations indicated that the addition of sulfur vacancy allows more 3d electrons to be localized at Co sites, which reduces the energy barrier for the rate

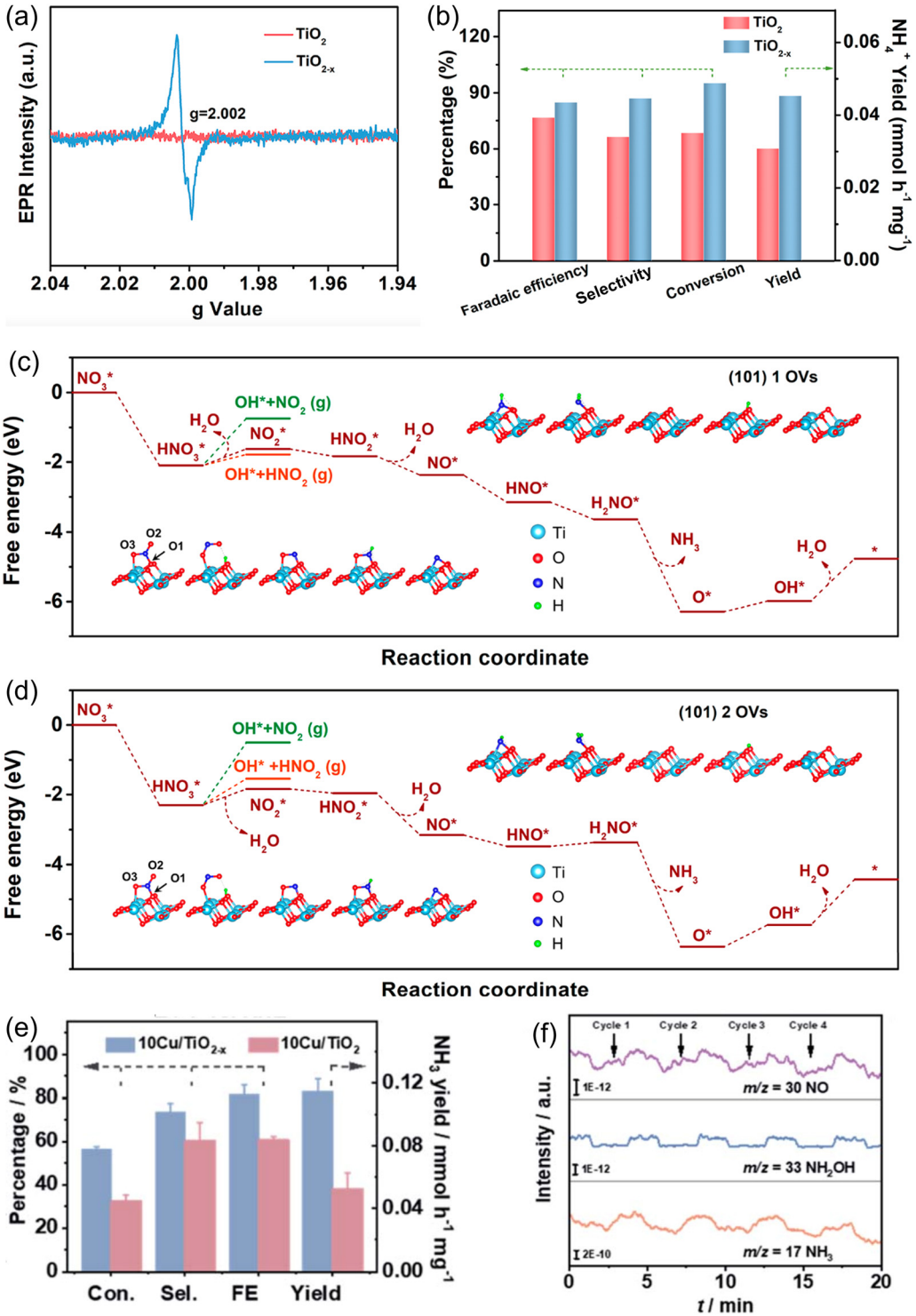

Fig. 10 (a) EPR spectra. (b) Faraday efficiency, selectivity, yield and nitrate conversion among TiO_{2-x} and TiO_2. (c and d) Free energy plot of nitrate reduction on TiO_2 (101) surface with (c) one and (d) two oxygen vacancies.[103] Reproduced from ref. 103, with permission from American Chemical Society, Copyright [2020]. (e) Conversion rate, selectivity, FE and yield of ammonia between $10Cu/TiO_{2-x}$ and $10Cu/TiO_2$. (f) DEMS measurement of nitrate electroreduction on $10Cu/TiO_{2-x}$.[17] Reproduced from ref. 17, with permission from The Royal Society of Chemistry, Copyright [2022].

determining step in the conversion of HNO_3* to NO_2*. Similarly, Li *et al.*[109] explored sulfur vacancies within Cu-doped SnS_2 nanoflowers, which trigger a cooperative interaction between sulfur vacancies and Cu and increase the exposure of active metal centers. DFT calculations revealed that sulfur vacancies enable free electron transfer to Sn for improved adsorption ability. The presence of copper further modulates the electron distribution and stabilizes the intermediates, resulting in a

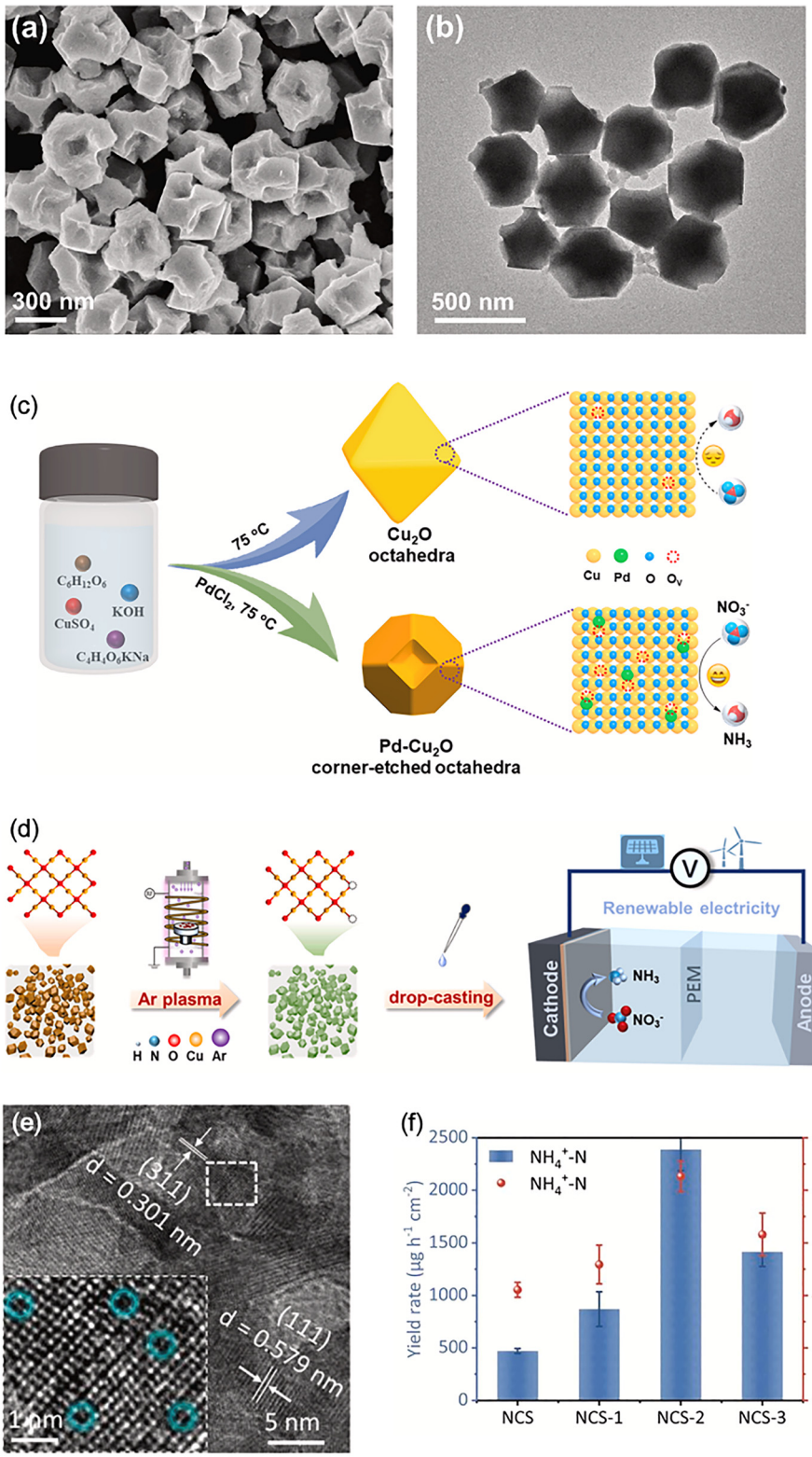

Fig. 11 (a) SEM image of Pd–Cu_2O CEO. (b) TEM image of Pd–Cu_2O CEO. (c) Schematic illustration of the synthesis process of the Pd–Cu_2O CEO and Cu_2O octahedra.[49] Reproduced from ref. 49, with permission from Elsevier, Copyright [2022]. (d) Schematic illustration of the synthesis process of the Cu_2O with plasma strategy and its application in electrochemical nitrate reduction.[104] Reproduced from ref. 104, with permission from Elsevier, Copyright [2022]. (e) HRTEM images of NCS-2. (f) Yield rate and FE of catalyst.[108] Reproduced from ref. 108, with permission from Elsevier, Copyright [2023].

rapid reduction of nitrate to ammonia. These characteristics enabled Cu–SnS_{2-x} to achieve a high FE of 93.8% and a high ammonia production of 0.63 mmol h^{-1} mg_{cat}^{-1} at −0.7 *vs.* RHE. According to this research, the sulfur vacancy is a flexible engineering technique that, like the oxygen vacancy, may be employed to optimize nitrate reduction performance by adjusting the catalytic characteristics through intermediate stabilization and electronic structure manipulation.

In short, vacancies have unique functions in the process of nitrate reduction. A primary benefit of vacancies is their capacity to modify the catalyst's electronic structure. In order to enhance electron transport during catalytic processes, vacancies create new energy levels by introducing localized states inside the band structure. This alteration in electronic structure enhances the activation and adsorption of reactant molecules, leading to impact reaction selectivity and kinetics. As summarized in Table 2, the strategic introduction of anionic vacancies serves as a powerful lever to modulate electronic structures with oxygen- and sulfur-deficient catalysts demonstrating a dramatic reduction in the energy barriers for key hydrogenation steps. Furthermore, vacancies can optimize catalyst active sites by enabling precise control over their density and arrangement. This strategic targeting creates active sites with desirable properties such as improved coordination, enhanced accessibility and tuned binding strength that are expected to enhance catalytic activity, promote specific reaction pathways and increase selectivity for target products.

2.3.3. Doping engineering. The inclusion of foreign atoms in the lattice of pristine materials is considered a viable method to improve the performance of nitrate to ammonia reduction.[110] Heteroatom doping can be employed to modify the adsorption or desorption of intermediates and to adapt the electronic structure and the electrochemical properties.[111,112] Besides, heteroatoms can act as extra centers of activity for nitrate to ammonia reduction, creating a strong synergy effect and contributing to better performance. Doping has the possibility of causing electron density redistribution and lattice distortion, enlarging the catalyst's surface area and improving electrical conductivity.[4,113]

Heteroatom doped transition metals would be effective catalyst electrodes for electrocatalytic conversion of nitrate to ammonia. For instance, Zhang *et al.* developed an iron doped nickel phosphide (Fe/Ni_2P) catalyst which was prepared from the phosphorization of NiFe LDH (Fig. 12(a)).[114] Based on Fig. 12(b), ultraviolet photoelectron spectroscopy (UPS) spectra showed that the d band center was shifted downward by 0.36 eV after doping with Fe atoms. The change in charge density provides additional proof that the addition of Fe atoms improves NO_3^- adsorption on the Ni site (Fig. 12(c) and (d)). The Fe/Ni_2P reaches a conversion rate of nearly 100% and high FE of 94.3% which is better compared to that of Ni_2P. Following this, Niu *et al.*[115] reported that Cu doping resulted in a shift of the d band centroid position of Co_3O_4 towards the center, which optimized the free energy changes of the reaction intermediates, particularly for $*NO_x$ (x = 1, 2 and 3). The findings showed that at −0.6 V *versus* RHE, Cu–Co_3O_4 had the maximum ammonia production of FE, at 86.5%. In another study, cobalt doped Fe@Fe_2O_3 (Co–Fe@Fe_2O_3) catalyst derived from a metal–organic framework (MOF) showed high performance in tuning the Fe d band center, inhibiting hydrogen generation and modulating the adsorption energies for intermediates (Fig. 12(e)).[116] The Tafel slope showed that 70.73 mV dec^{-1} for Co–Fe@Fe_2O_3 is smaller than Fe@Fe_2O_3 and Co. This indicated the kinetics of nitrate to ammonia reduction is faster for Co–Fe@Fe_2O_3. In short, doping fine-tunes the d band centers of the metal-based catalysts and enhanced the adsorption of intermediates to produce higher FE, selectivity and nitrate removal during nitrate-to-ammonia reduction.

Doping strategies in electrocatalysis have become a potent way to improve the efficiency and selectivity of nitrate reduction for ammonia production. In a recent study, Wan *et al.*[117] developed a Ru–$Ni(OH)_2$ catalyst that exhibits interfacial H_2O behaviour and accelerates nitrate hydrogenation to ammonia at ultralow overpotentials. The hydroxide regulation technique greatly enhances the hydrogen spillover process, achieving a nearly 100% FE with an energy efficiency of 44.6% at 0.1 V. *In situ* characterization showed that the $Ni(OH)_2$ disrupts the rigid hydrogen bonding network, promotes the availability of *H and enhances the nitrate conversion at the Ru site. Subsequently, Wang *et al.*[30] showed that doping of BaO in a Cu catalyst resulted in a yield of 356.9 mmol h^{-1} g^{-1} and an FE of 97.3% for ammonia production. DFT calculations reveal that elemental Ba enhances the localized electronic states of Cu and promotes protonation, adsorption and desorption of key N-intermediates. The Cu–BaO catalyst also exhibits excellent nitrate reduction performance over a wide concentration range

Table 2 Catalytic performance of vacancy engineered electrocatalysts for nitrate reduction

Catalyst	FE (%)	Electrolyte	Stability (h)	Current density (mA cm^{-2})	Ammonia yield rate	Ref.
10Cu/TiO_{2-x}	81.34	0.1 M Na_2SO_4+ 200 ppm NO_3^-	—	—	0.1143 mmol h^{-1} mg^{-1} at −0.75 V *vs.* RHE	17
Pd–Cu_2O CEO	96.56	0.5 M K_2SO_4 + 50 ppm KNO_3	—	—	925.11 μg h^{-1} mg^{-1} at −1.3 V *vs.* SCE	49
TiO_{2-x} (oxygen-vacancy-enriched)	85.0	0.5 M Na_2SO_4+ 50 ppm NO_3^-	—	—	0.045 mmol h^{-1} mg^{-1} at −1.6 V *vs.* SCE	103
Ar-40 plasma-treated Cu_2O	89.54	0.5 M Na_2SO_4 + 200 ppm NO_3^-	—	30	0.0825 mmol h^{-1} mg^{-1} at −1.2 V *vs.* Ag/AgCl	104
Cu_2O (111)	94.27	0.5 M Na_2SO_4 + 200 ppm NO_3^-	48	—	∼0.45 mmol h^{-1} g^{-1} at −1.4 V *vs.* Ag/AgCl	106
$Ni_3Co_6S_8$ nanospheres (NCS-2)	85.3	1 M KOH + 50 mg L^{-1} NO_3^-–N	12	—	2388.4 μg h^{-1} cm^{-2} at −0.4 V *vs.* RHE	108
Cu–SnS_{2-x}	93.8	0.1 M KOH + 0.1 M KNO_3	24	−36	0.63 mmol h^{-1} mg^{-1} at −0.7 V *vs.* RHE	109

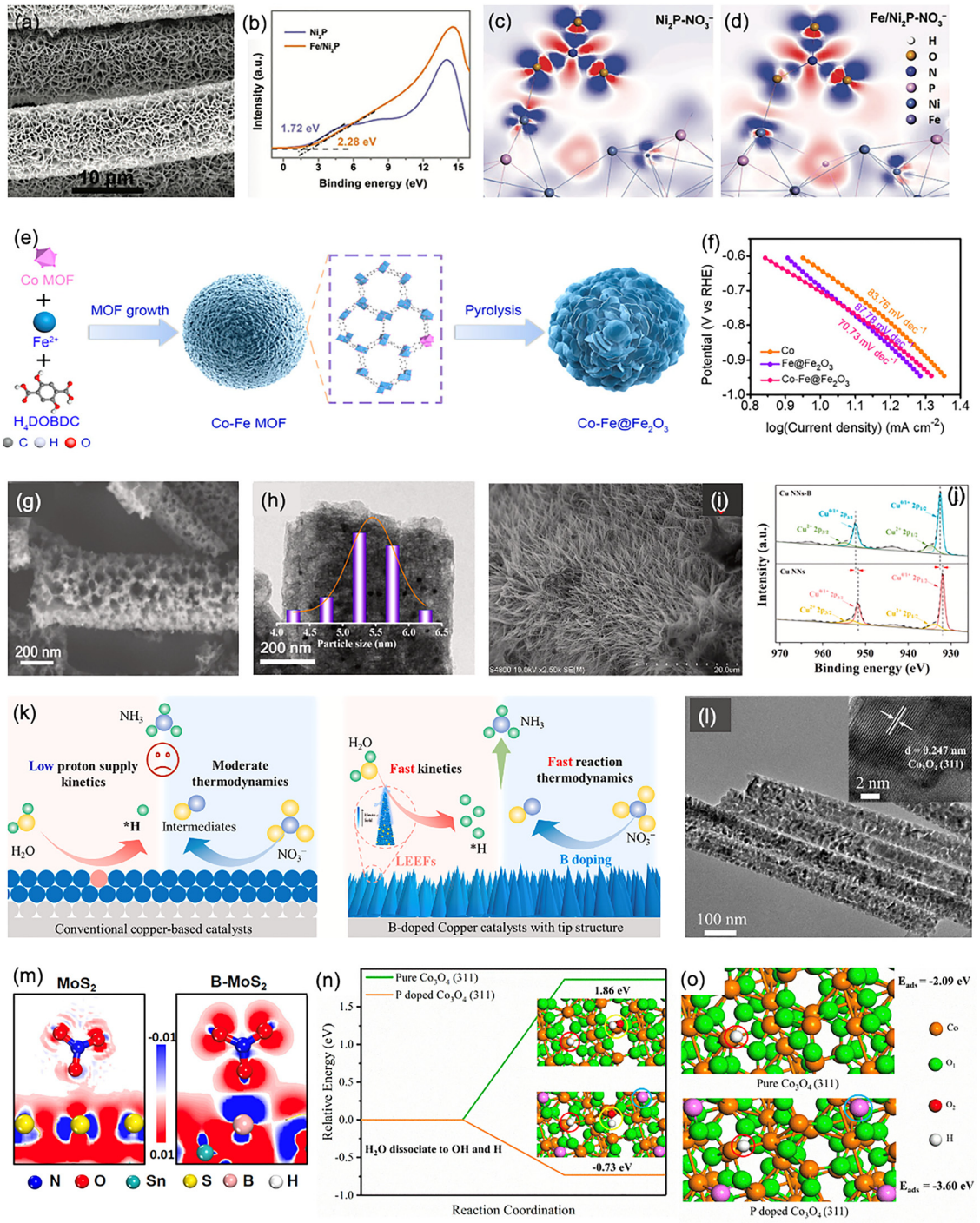

Fig. 12 (a) SEM image of Fe/Ni_2P. (b) UPS spectra of Ni_2P and Fe/Ni_2P. (c and d) The charge density difference of Ni_2P and Fe/Ni_2P after adsorbing NO_3^-. Blue and red regions indicate the increase and depletion of the electron density, respectively.[114] Reproduced from ref. 114, with permission from John Wiley & Sons, Copyright [2022]. (e) Synthesis of Co–Fe@Fe_2O_3. (f) Morphology of Ni_3N/N–C by SEM. (g) SEM of Ni_3N/N–C nanohybrids. (h) TEM image of Ni_3N/N–C nanohybrids.[50] Reproduced from ref. 50, with permission from Elsevier, Copyright [2022]. (i) SEM of Cu-NNs-B. (j) Cu 2p XPS spectra of Cu NNs-B and Cu NN. (k) Schematic diagram of conventional copper-based catalyst and B-doped copper catalyst with tip structure.[120] Reproduced from ref. 120, with permission from Elsevier, Copyright [2025]. (l) TEM and HRTEM images of $P_{2.1}$–Co_3O_4.[122] Reproduced from ref. 122, with permission from Elsevier, Copyright [2020]. (m) The charge density differences of NO_3^- on MoS_2 and B–MoS_2. red: electron accumulation, blue: electron depletion.[121] Reproduced from ref. 121, with permission from Elsevier, Copyright [2023]. (n) The relative energy for H formation from H_2O dissociation. (o) Adsorption energy for H atom on pure Co_3O_4 (311) and P doped Co_3O_4 (311).[122] Reproduced from ref. 122, with permission from Elsevier, Copyright [2020].

of 5–100 mM with stable cycling. In a complementary study, Li *et al.*[118] demonstrated that Cu doping in FeP creates a highly efficient catalyst for nitrate-to-ammonia conversion in neutral media achieving a notable NH_3 faradaic efficiency of 92.5% and

a yield of 0.787 mmol h^{-1} cm^{-2}. The incorporation of Cu increases the electrochemically active surface area and modulates the electronic structure, which facilitates nitrate adsorption and enhances the binding of key intermediates without altering the host crystal lattice. The Cu–FeP catalyst also exhibits exceptional stability across multiple cycles. This study solidifies cation doping as a versatile strategy for activating transition metal phosphides positioning them as durable and selective catalysts for sustainable ammonia synthesis. As a whole, these findings highlight the critical role of doping in electronic state modulation and interfacial engineering to promote effective and selective nitrate electroreduction to ammonia.

Aside from metal atoms, non-metal dopants including nitrogen, phosphorus, boron, and oxygen have drawn a lot of interest because of their capacity to control the chemical characteristics of materials and electron structures, provide abundant active sites, and enhance catalytic activity. In recent years, nitrogen doped carbon-based materials have been extensively studied in terms of the relationship between doped structures and active nanoparticles. For example, Yang and coworkers designed electron-deficient Co nanocrystals by incorporating them with pyridine nitrogen doped carbon (Co/PN-C), which enhances nitrate adsorption and lowers the energy barrier of *NH to $*NH_2$ and nitrate adsorption energy.[119] According to DFT calculations, PN-C is able to extract more electrons from interacting Co than both graphitic nitrogen doped carbon (GN–C) and carbon. This electron-deficient environment around Co enhances its electrophilic nature, significantly improving nitrate adsorption as it attracts the electron-rich nitrate ions. In a study by Zhang *et al.*,[50] nitrogen doped carbon nanorods were employed to support Ni_3N nanoparticles resulting in highly effective catalysts for electrocatalytic nitrate reduction. The Ni_3N/N–C nanohybrids were synthesized *via* simple calcination and acid etching processes (Fig. 12(f)–(h)). The embedding with carbon material enhances its stability and protects the aggregation of particles. At the same time, the porous structure enables the Ni_3N/N–C nanohybrids not only to have a large specific surface area of 665.7 m^2 g^{-1}, but also to provide a convenient channel for the transfer of the reactants and a fast conduction of electrons. In addition, the ultrafine size (5.3 nm) of Ni_3N provides an abundance of active sites due to the size effect. This work exemplifies the effectiveness of nitrogen doping in stabilizing metal nanoparticles, improving nitrate conversion and providing stable structures for long-term catalytic use.

Moving forward, boron with empty orbitals has a propensity to manipulate the local electronic state of the metal and accept electrons, which can effectively tune the electrochemical behaviour. Inspired by these, Wu *et al.*[120] well demonstrated in boron doped copper nanoneedles (Cu NNs-B) that high-curvature nanoneedles create a localized enhanced electric field (LEEFs), which expedite hydrolysis for the production of active hydrogen (*H) (Fig. 12(i)). Based on the Cu 2p XPS spectra in Fig. 12(j), the binding energy of $Cu^{0/1+}$ in Cu NNs-B has changed to a larger energy value in the comparison to Cu NNs. This indicates that electrons are transformed from Cu atoms to B atoms and some of the Cu^0 is changed to Cu^+. As a result, boron doping introduces Cu/Cu^+ active sites that can improve the activation and adsorption of reactants or intermediates, thereby promoting ammonia electrosynthesis by enhancing thermodynamics and kinetics aspects of the reaction (Fig. 12(k)). In another study, a B-doped MoS_2 nanosheet array grown on carbon cloth (B–MoS_2/CC) was developed by Luo *et al.*[121] Fig. 12(m) shows that there is a larger electron cloud between B–MoS_2 and nitrate compared to MoS_2, which means that their interaction is enhanced and nitrate can be intensely absorbed on the B–MoS_2 surface. DFT calculations identify B dopants as the active sites to enhance intermediate stabilization and encourage nitrate adsorption, leading to a high ammonia FE of 92.3%. These studies pose a new pathway for exploring nitrate to ammonia reduction catalysts.

Notably, 3D interconnected NF and 3D pinewood-derived carbon have proven to be highly effective supports for doped catalysts in electrocatalytic applications. For instance, a study by Gao *et al.*[122] showcased the fabrication of P-doped 3D Co_3O_4 cathode supported on NF (P–Co_3O_4/NF) by employing a combination of hydrothermal and low temperature annealing with NaH_2PO_2 serving as the P source (Fig. 12(l)). The 3D interconnected NF known for its low cost and high electrical conductivity, offers efficient diffusion and a multidimensional electron transport avenue.[123] Fig. 12(n) and (o) show that the relative energy for dissociating H_2O into OH^- and H* (Volmer step) on the P-doped Co_3O_4 surface is −0.73 eV, indicating a thermodynamically favourable reaction. In contrast, the same reaction on pure Co_3O_4 requires a high relative energy of 1.86 eV, highlighting that P doping significantly promotes H* formation. This structural sympathy between P-doped Co_3O_4 and NF improves active site exposure, electronic conductivity and durability under reaction conditions. Likewise, Fe-doped Co_3O_4 supported on a pinewood-derived 3D carbon scaffold (Fe–Co_3O_4/PC) improves electrical conductivity and structural robustness, while iron doping generates electron-rich active sites that promote nitrate adsorption and ammonia formation.[124] This structural and electronic synergy provided by the 3D frameworks in both systems optimizes the exposure of active sites and provides high durability under reaction conditions, making them highly effective in electrocatalytic nitrate reduction.

Therein, heteroatom doping efficiently adjusts the electronic structure, creating active sites that facilitate adsorption and stabilization of intermediates, which are critically important for high efficiency nitrate reduction. The efficacy of heteroatom doping in reconfiguring the local coordination and d band center of active sites is quantitatively compared in Table 3, highlighting how both metallic and non-metallic dopants synergistically enhance intermediate adsorption to achieve near-unity FE. This approach strengthens the catalytic activity, selectivity and durability and solves the key challenge of ammonia reduction by nitrate. In addition, when combined with 3D support frameworks such as nickel foam and pine-derived carbon, these doped catalysts provide enhanced active site exposure, improved electrical conductivity and structural

Table 3 The influence of heteroatom doping on the electrocatalytic nitrate reduction performance

Catalyst	FE (%)	Electrolyte	Stability (h)	Current density (mA cm^{-2})	Ammonia yield rate	Ref.
Ni_3N/N–C	89.5	0.5 M Na_2SO_4 + 0.05 M NO_3^-	12	—	9.185 mmol h^{-1} mg^{-1} at −1.45 V *vs.* SCE	50
Fe/Ni_2P	94.3	0.2 M K_2SO_4 + 50 mM KNO_3	11	75	4.17 mg h^{-1} cm^{-2} at −0.4 V *vs.* RHE	114
Cu–Co_3O_4	86.5	0.1 M Na_2SO_4 + 500 ppm NO_3^-	—	—	36.71 mmol h^{-1} g^{-1} at −0.6 V *vs.* RHE	115
Co/PN-C	97.8	1 M NaOH + 0.1 M $NaNO_3$	10	1390	109 mg h^{-1} cm^{-2} at −1.55 V *vs.* RHE	119
Cu NNs-B	98.6	0.5 M Na_2SO_4 + 50–1500 ppm NO_3^-N	—	—	1.33 mmol h^{-1} cm^{-2} at –0.6 V *vs.* RHE	120
B–MoS_2/CC	92.3	0.5 M Na_2SO_4 + 0.1 M $NaNO_3$	—	—	10.8 mg h^{-1} cm^{-2} at −0.7 V *vs.* RHE	121
Fe–Co_3O_4/PC	96.5	0.1 M NaOH	—	—	0.55 mmol h^{-1} cm^{-2} at −0.5 V *vs.* RHE	124

integrity, which contribute to their excellent electrochemical performance. The combination of optimized electronic properties through doping and the multidimensional benefit of 3D supports underscores the potential of these systems in overcoming existing limitations in nitrate reduction.

2.3.4. Single atom engineering. Single atom catalysts (SACs) have attracted growing interest in the field of electrocatalytic nitrate to ammonia reduction due to their excellent catalytic performance in terms of their unique electronic structure, unsaturated coordination environment and outstanding atom utilization efficiency.[5,125] These catalysts give a chance to fine-tune the durability, selectivity, and activity of this type of electrocatalysts by modifying precisely defined metal active sites, which are made up of individual metal species atomically distributed on the support structure.[4,126] The wide distribution of active sites boosts the interaction between the catalyst and nitrate intermediates, lowering the energy barrier and improving the reaction pathway, which makes SACs highly efficient for ammonia synthesis.[127]

To date, there are several research papers about electrocatalytic nitrate to ammonia reduction on single atom Cu catalysts. For example, a single atom Cu catalyst was developed by Cheng *et al.*[128] with coordination symmetry breaking by introducing a *cis*-configuration of two oxygen and nitrogen atoms (Cu-*cis*-N_2O_2). It was produced by equilibrium annealing of salen–Cu coordination (Fig. 13(a)). The *cis* coordination enhances the polarity of the active sites, subsequently increasing the accumulation of nitrate on the catalyst surface and facilitating the efficient formation of intermediate *ONH *via* π-complex, which reduces the energy barrier compared to traditional σ-complexes. Surprisingly, the Cu-*cis*-N_2O_2 catalyst attained an industrial-level current density of 366 mA cm^{-2} and preserved high stability over 2000 hours, balancing catalytic performance and durability through the structural benefits of symmetry breaking. Enthrallingly, Li *et al.*[129] presented a pulsed electrosynthesis of ammonia from nitrate with a Cu single atom gel (Cu SAG) catalyst. Fig. 13(b) and (c) show the porous structure and abundant 3D channels of the cross-linking by nanoparticles. This approach facilitates the accumulation and reduction processes of nitrite intermediates in tandem within a 3D framework, which effectively reduces competitive HER and improves the FE and yield.[130] The Cu SAG provides unique spatial confinement and kinetic enhancement for selective conversion of nitrate to nitrite and nitrite to ammonia, which demonstrates the potential of SAC paired with tailored electrolysis methods to optimize the efficiency of the nitrate reduction reaction.

Moving forward, a recent study by Zhao *et al.*[131] anchored a single atom Cu catalyst on nitrogen doped porous carbon (Cu_{SA}NPC) which was prepared by carbonization of Cu-containing a Zeolitic Imidazolate Framework (ZIF-8) precursor. DFT calculations showed that the CuN_4 sites effectively boost the formation of *NO and the consequent generation of ammonia in a continuous downslope free-energy pathway, thus providing excellent catalytic performance compared to conventional Cu nanoparticle catalysts (Fig. 13(d)). The structural stability of Cu_{SA}NPC also contributed to its stable performance, as it maintains high FE and ammonia yield over ten times of cycling. In another case, Zhu *et al.*[132] synthesized a single Cu atom stabilized by nitrogenated carbon nanosheets (Cu–N–C-800) using MOF pyrolysis at 800 °C. The single Cu atoms on carbon nanosheets may be seen in the high-angle annular dark field-scanning transmission electron microscopy (HAADF-STEM) picture, as shown in Fig. 13(e). Time-course NO_3–N proportion indicates that Cu–N–C-800 interacts more strongly with nitrate and nitrite than bulk metal and Cu nanoparticles, with a 97.3% reduction in nitrate (Fig. 13(f) and (g)). At the same time, Cu–N–C-800 significantly inhibits the production of nitrite. After twenty consecutive cycles, the NO_3–N conversion may still be maintained, indicating its strong endurance. These findings underline the vast possibilities of single-atom copper catalysts for selective and efficient nitrate reduction by minimizing the formation of unwanted by-products and increasing the accessibility of the active site.

Following the advancements in Cu-based SAC, Co SAC have concurrently emerged as a highly attractive class of materials for electrocatalytic nitrate to ammonia conversion, capitalizing on their distinct d band electronic structure and versatile coordination chemistry to achieve exceptional performance. As exemplified by the Co–NC catalyst, isolated Co atoms are anchored within a nitrogen-doped carbon framework (Fig. 14(h)), the atomic dispersion is unequivocally confirmed by HAADF-STEM which reveals a uniform distribution of bright spots corresponding to single metal atoms.[51] Electrochemical evaluation demonstrates that the Co–NC catalyst achieves a notable ammonia FE of approximately 78% at −0.3 V *vs.* RHE, underscoring its intrinsic activity for the nitrate reduction reaction. However, a comparative analysis with the bimetallic CoCu–NC system reveals a key limitation of the monoatomic Co site. DFT calculations illustrate that while Co–NC facilitates the initial

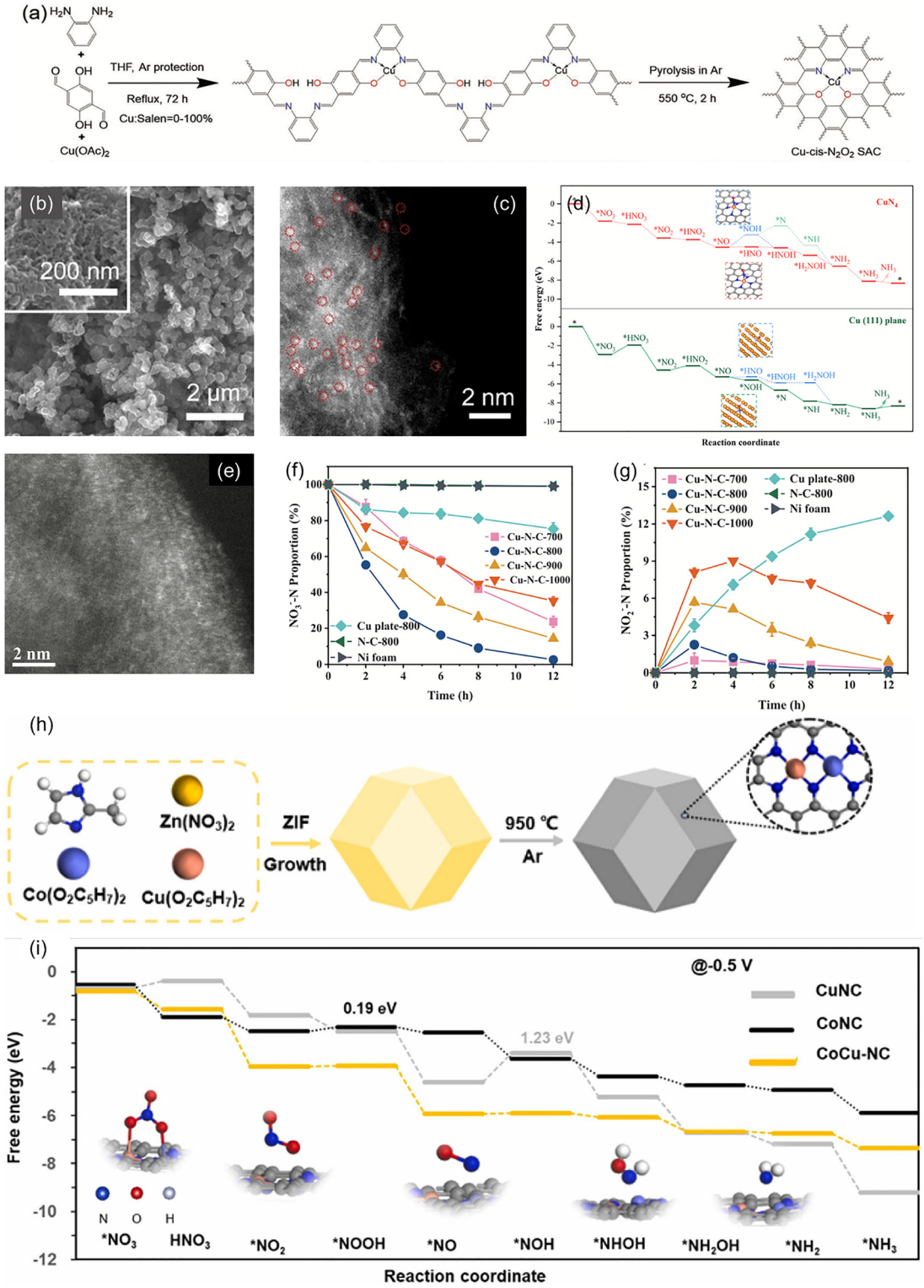

Fig. 13 (a) Synthetic process of Cu-*cis*-N_2O_2 single atom catalyst.[128] Reproduced from ref. 128, with permission from John Wiley & Sons, Copyright [2022]. (b) SEM of CuSAGs. (c) TEM images of CuSAGs.[129] Reproduced from ref. 129, with permission from American Chemical Society, Copyright [2023]. (d) Free energy diagrams of ammonia generation *via* nitrate reduction on the CuN_4 site and Cu (111) plane.[131] Reproduced from ref. 131, with permission from Elsevier, Copyright [2023]. (e) HAADF-STEM images Cu–N–C-800. (f) Comparisons of time-course NO_3^-–N proportion. (g) Time-course NO_2^-–N proportion.[132] Reproduced from ref. 132, with permission from John Wiley & Sons, Copyright [2020]. (h) Schematic illustration of the synthesis of CoCu–NC. (i) Free-energy DFT calculations diagram for the NO_3RR over CoCu–NC, Co–NC and Cu–NC.[51] Reproduced from ref. 51, with permission from Elsevier, Copyright [2025].

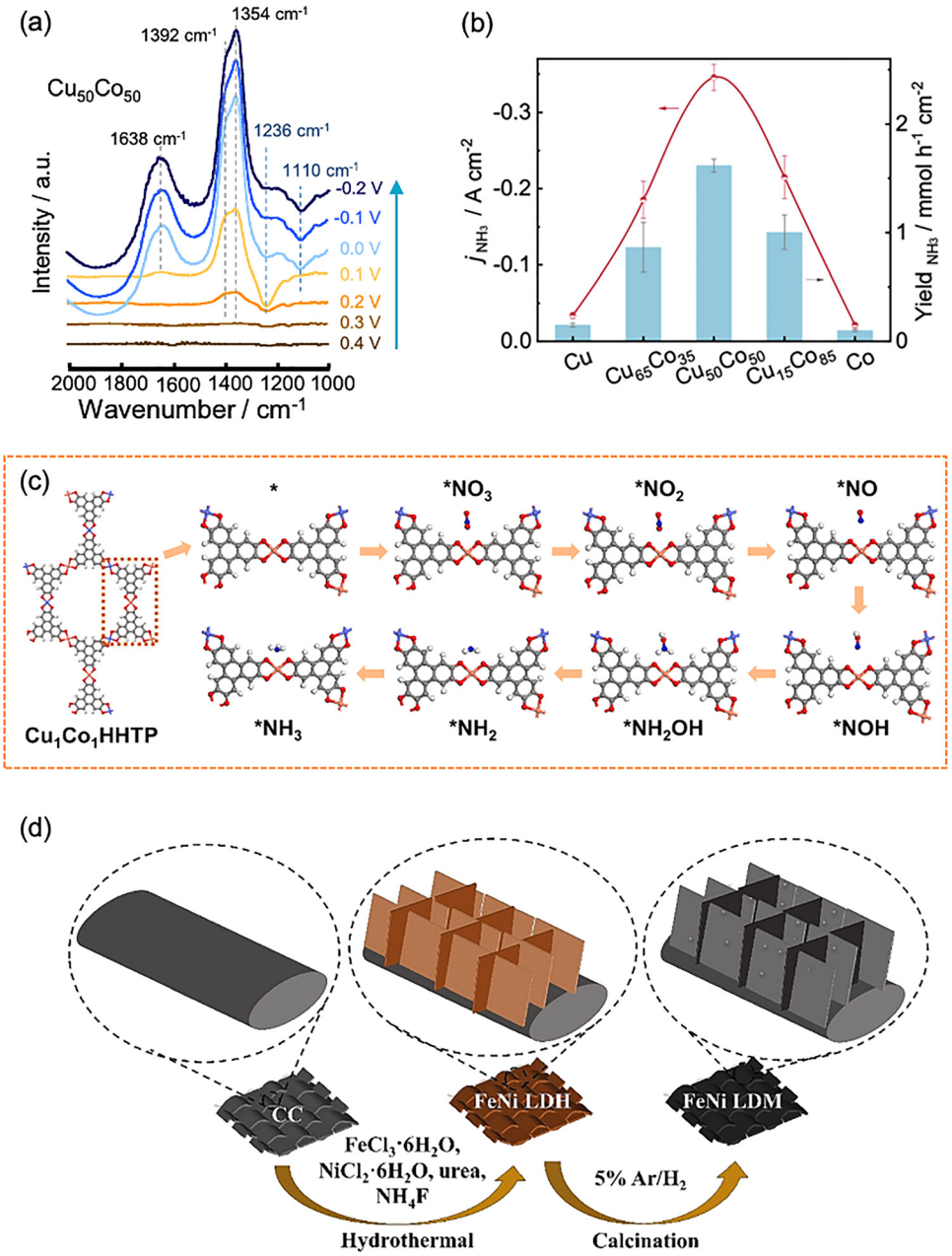

Fig. 14 (a) Electrochemical thin-layer *in situ* FTIR spectra of NO_3^-RR on $Cu_{50}Co_{50}$. (b) The ratio of NO_2^- to NH_3 generated.[137] Reproduced from ref. 137, Springer Nature, Open Access [2022]. (c) Cu_1Co_1HHTP slab with optimized intermediate adsorption.[138] Reproduced from ref. 138, with permission from Elsevier, Copyright [2023]. (d) Schematic illustration of the preparation of Fe_4Ni_1 LDM arrays.[140] Reproduced from ref. 140, with permission from Elsevier, Copyright [2023].

adsorption of $*NO_3$, the subsequent hydrogenation step, particularly the critical *NO to *NOH conversion presents a substantial energy barrier of 1.23 eV, acting as a kinetic bottleneck (Fig. 14(i)). This insight underscores that while monoatomic Co sites provide a foundational platform with high atom utilization efficiency, their performance is intrinsically governed by the adsorption energetics of key intermediates. The subsequent integration of Co into a dual-atom configuration, as realized in the CoCu–NC and the Co–Cu mixed single-atom/cluster catalyst (SCC), strategically addresses this limitation.[46,51,133] This tandem mechanism effectively bypasses the rate-limiting steps associated with isolated Co sites, thereby optimizing the entire reaction pathway and pushing the catalytic performance encompassing FE, yield rate, and operational stability to the forefront of the field.

Overall, SACs have a huge potential for electrocatalytic nitrate to ammonia reduction due to unsaturated environments to lower energy barriers, precisely coordinate active sites, prevent undesired by-products and optimize reaction pathways. Table 4 encapsulates the supreme atom-utilization efficiency of

Cu- and Co-based SACs where the maximized density of unsaturated sites enables high catalytic activity and stability, pushing the boundaries of ammonia yield rates under industrially relevant current densities. Through innovations in single-atom design, support structures and coordination environments, SACs open promising avenues for sustainable, high-performance electrocatalysts to advance green chemistry and energy applications.

2.3.5. Bimetallic engineering and alloying. Bimetallic engineering and alloying have emerged as vital strategies in the pursuit of efficient and selective electrocatalytic nitrate reduction to ammonia. These approaches allow the combination of two metals in the catalyst structure, which usually enhances the catalytic performance due to synergistic effects.[134,135] By combining different metal atoms, bimetallic catalysts can strike an optimal balance between the adsorption of intermediate species and the activation energy, resulting in improved catalytic activity and selectivity. In alloying, atomic interactions between two metals result in an optimized electronic structure, commonly by adjusting the d band center, thus optimizing the adsorption strength of reaction intermediates and regulating the reaction pathways more eloquently.

The Cu–Co bimetallic catalyst is one of the most economical systems for simulating the natural nitrate reduction process since Co has been shown to be an effective element in pushing electrocatalytic conversion of nitrate to ammonia.[136] As a typical study, Fang and coworkers[137] created a CuCo bimetallic nanosheet catalyst on nickel foam inspired by copper type nitrite reductase, which enables efficient and selective nitrate to ammonia reduction under mild conditions. This CuCo catalyst has a unique bifunctional design in which Cu effectively adsorbs NO_x^- and Co acts as an electron or proton donor. With this collaborative interaction between the Cu and Co, the $Cu_{50}Co_{50}$ nanosheet catalyst exhibits nearly 100% FE at an ampere-level current density of 1035 mA cm^{-2}. According to Raman spectroscopy and electrochemical *in situ* Fourier transform infrared (FTIR) spectroscopy (Fig. 14(a)), there is a synergistic interaction between Cu and Co, with Co sites favouring the adsorption of *H and promoting the hydrogenation of nitrate to ammonia. Their results suggest that a moderate Cu/Co ratio is essential to maintain high catalytic performance (Fig. 14(b)). Besides that, He *et al.*[33] presented a Cu–Co tandem catalyst by transforming Cu–Co binary sulfides into core–shell Cu/CuO_x and Co/CoO phases. From *in situ* scanning electrochemical microscopy (SECM), the inner Cu/CuO_x core effectively catalyzed the nitrate to nitrite reduction, while the Co/CoO shell completed the reduction to ammonia. The formation of multiple active phases allows a rapid, cooperative reduction of nitrate to ammonia at low overpotentials with high selectivity, overcoming typical scaling limitations. Similarly, Liu *et al.*[138] developed a Cu–Co bimetallic conductive MOF (cMOF) labelled Cu_1Co_1HHTP, which exhibited enhanced catalytic properties through electronic modulation (Fig. 14(c)). According to DFT simulations, the Co sites alter the Cu sites' electron structure, reducing the potential determining step's ΔG and enhancing nitrate adsorption. In summary, these studies demonstrate the potent synergy in Cu–Co bimetallic catalysts, whose interaction dramatically improves the nitrate to ammonia reduction by optimizing electron transfer, adsorption and reaction kinetics.

Subsequently, other bimetallic catalysts such as Cu–Pt and Fe–Ni have shown impressive capabilities in enhancing nitrate to ammonia reduction. In the research of Cerron-Calle *et al.*,[139] a Cu–Pt bimetallic 3D electrocatalyst was introduced to enhance the performance. They created bimetallic nanodomains that took advantage of both metals' electrical characteristics by electrodepositing Pt on a Cu foam substrate. This synergy enabled the catalyst to achieve 94% nitrate conversion in 120 minutes. A remarkable feature of this Cu–Pt electrode is that even with minimal Pt content (<0.50 wt%), the hybridisation mechanism of the hydrogenation reduction process and catalytic electrochemistry is possible, emphasizing the synergistic effect between the Cu and Pt nanointerfaces. These interactions effectively reduce the energy required for nitrate reduction, resulting in significantly lower energy consumption compared to single metal catalysts. Following this, Ma and coworkers[140] developed a bimetallic FeNi LDM catalyst which could adjust the d band centers of FeNi facilitating an optimal balance in intermediate adsorption and desorption. This leads to fast conversion of nitrate. The FeNi LDM is produced through a hydrothermal process where FeNi LDH nanosheets were uniformly rooted on the carbon cloth and calcination in 5% H_2/Ar (Fig. 14(d)). In five consecutive cycle tests, the FeNi LDM showed excellent operational durability. Therein, the remarkable synergies achieved by Cu–Pt and FeNi bimetallic catalysts, where structural tuning and strategic material combinations lead to lower energy consumption, higher stability and higher nitrate conversion efficiencies making them ideal solutions for sustainable electrocatalysis.

Impressively, in addition to bimetallic catalysts, alloying is also an efficient way to improve catalyst activity and stability as well as reduce costs.[140] In a recent study, Wang *et al.*[141] fabricated RuMo alloy nanoflowers (NFs) with a unique face-centered cubic (fcc) phase and hexagonal close-packed/fcc (hcp/fcc) heterophase using a one-pot solvothermal method

Table 4 Performance of SACs for selective nitrate to ammonia conversion

Catalyst	FE (%)	Electrolyte	Stability (h)	Current density (mA cm^{-2})	Ammonia yield rate	Ref.
Co–NC	78	0.1 M Na_2SO_4 + 0.2 M KNO_3	12 cycles	~100	~2.41 mg h^{-1} cm^{-2} at −0.6 V *vs.* RHE	51
CoCU–NC	95.3	0.1 M Na_2SO_4 + 0.2 M KNO_3	12 cycles	100	2.41 mg h^{-1} cm^{-2} at −0.6 V *vs.* RHE	51
Cu-*cis*-N_2O_2	80	0.5 M Na_2SO_4 + KNO_3	>2000	366	27.84 mg h^{-1} cm^{-2} at −1.2 V *vs.* RHE	128
Cu SAG	78	0.1 MPBS + 20 mM NO_3^-	—	—	440 μg h^{-1} cm^{-2} at −0.8 V *vs.* RHE	129
Cu_{SA}NPC	87.2	0.01 M PBS	—	—	2602 μg h^{-1} cm^{-2} at −1.1 V *vs.* RHE	131

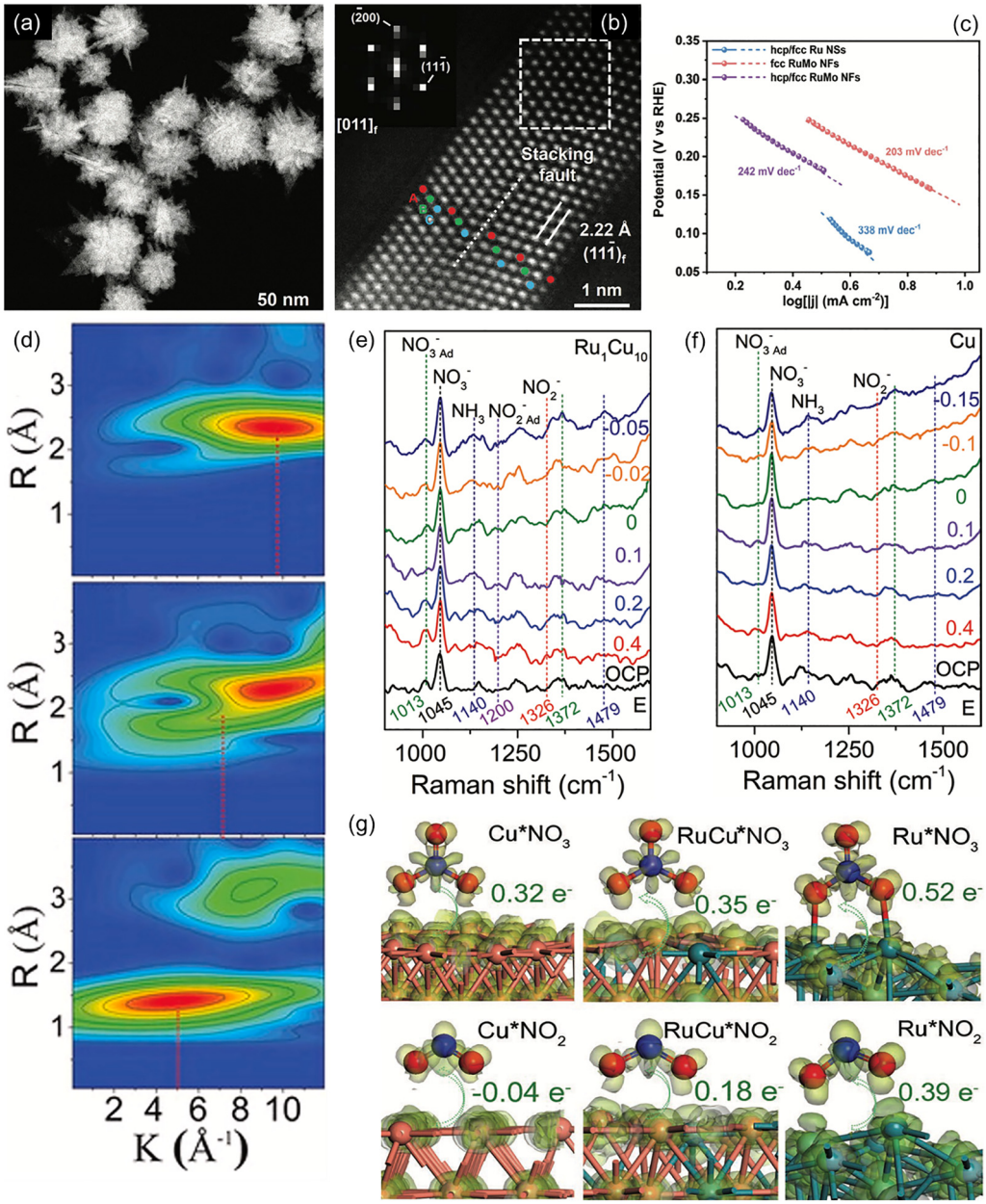

Fig. 15 (a) Atomic resolution HAADF-STEM. (b) Images of fcc RuMo NFs. (c) Tafel plots of hcp/fcc Ru NSs, fcc RuMo NFs, and hcp/fcc RuMo NFs.[141] Reproduced from ref. 141, with permission from John Wiley & Sons, Copyright [2024]. (d) k^2-weighted wavelet transforms for the Ru K-edge XAFS of Ru_1Cu_{10}/rGO, RuO_2 and Ru foil based on Morlet wavelets. (e) *In situ* Raman spectra of Ru_1Cu_{10}. (f) *In situ* Raman spectra of Cu. (g) Charge density differences and charge transfer of Cu, Ru, and RuCu solid solution after adsorption of nitrate and nitrite, respectively.[52] Reproduced from ref. 52, with permission from John Wiley & Sons, Copyright [2023].

(Fig. 15(a) and (b)). Due to the strong Ru–Mo interaction and high intrinsic activity of the unusual fcc phase, this structure has the highest d band center and superior electroactivity. The enhancement of the electronic properties of the fcc phase of RuMo alloys also suppressed the HER substantially, thus maintaining a high selectivity for ammonia. Based on the Tafel slope in Fig. 15(c), it shows that the fcc RuMo NFs exhibit a lower Tafel slope of 203 mV dec^{-1} than the hcp/fcc Ru nanosheets (338 mV dec^{-1}) and hcp/fcc RuMo NFs (242 mV dec^{-1}). This indicated that the fcc RuMo NFs have rapid reaction kinetics and fast electron transfer efficiencies. Gao *et al.*[52] designed a RuCu alloy supported on a reduced-graphene-oxide catalyst (Ru_xCu_x/rGO). The k^2-weighted wavelet transforms analysis of the Ru K-edge XAFS (Fig. 15(d)) reveals a distinct lobe at 1.9 Å and 7.3 Å^{-1} for Ru_1-Cu_{10}/rGO, which ascribed to the Ru–Cu contribution, validating formation of the RuCu solid solution alloy. *In situ* Raman spectra (Fig. 15(e) and (f)) show a gradually decrease and ultimate disappearance of the aqueous nitrite peak as the potential decreases to 0.1 V. Concurrently, a peak corresponding to adsorbed nitrite appears at 0.1 V and persists as the potential changes. Additionally,

the bands representing ammonia and ammonium intensify with increasing applied potential. The results indicate that the Ru_1Cu_{10} alloy catalyst facilitates the processes of nitrite generation, adsorption, desorption and its subsequent conversion to ammonia through a relay catalysis mechanism. Moreover, the charge density difference plots (Fig. 15(g)) show that RuCu alloys adsorb nitrate and nitrite more favorably than individual Ru or Cu, highlighting their excellent catalytic properties. Moreover, Jia *et al.*[142] developed a Cu/A–Ru tandem catalyst by facile chemical reduction coupled with an electrostatic adsorption strategy. The Cu/Ag heterostructure facilitates nitrate adsorption and electron transfer due to the synergistic effect, while Ru enhance hydrogenation activity. This $((Cu_7/Ag_3)_7$–Ru/C demonstrated long-term stability over 60 hours in a membrane electrode assembly, highlighting its industrial scale applicability. The catalyst achieved 93.48% of FE and ammonia yield of 3.45 mmol h^{-1} cm^{-2}. Online DEMS and ATR-FTIR spectroscopy confirmed that the catalyst encouraged the creation of adsorbed nitric oxide, which experienced a quick conversion to ammonia through a sequential deoxygenation and progressive hydrogenation process. The above studies exemplify the effectiveness of alloying strategies in achieving advanced catalytic performance.

Likewise, the catalytic efficiency of the nitrate–ammonia reduction reaction was significantly improved by alloying Cu with Ni. In a study by Yu and coworkers,[143] CuNi alloy nanoparticles on Cu foil (CuNi NPs/CF) by laser irradiation were manufactured. The added Ni sites have a significant capacity for H* supply and a great ability to activate O–H, which is advantageous for the ammonia synthesis's subsequent hydrogenation steps. The result indicated the strong Cu–Ni coupling of CuNi NPs and the electron transfer from Ni to Cu as compared with the single metal component. Excitedly, the alloy achieved a FE of 97.03% and maintained excellent stability over prolonged cycles. Next, Cai *et al.*[144] introduced an innovative single atom Ni-alloyed Cu catalyst (Ni_1Cu-SAA). This Ni_1Cu alloy structure enhances the energies of the unoccupied antibonded N 2p states above the Fermi level and modulates the gap between the d band center of N 2p and Ni 3d orbitals. XAFS and DFT simulations displayed that the interaction between nickel atoms and the key NOOH* intermediate greatly inhibited the formation of the product and lowered the limiting potential. Ni_1Cu-SAA has a maximum FE close to 100% and an ammonia yield of 326.7 μmol h^{-1} cm^{-2}, which is 10.7 times higher than that of the unalloyed counterpart. In another breakthrough, Bu *et al.*[145] explored a Cu–Ni tandem catalyst that utilizes a programmable electrical pulse to achieve self-repairing Cu/Cu_2O heterojunctions for efficient electrocatalytic nitrate to ammonia reduction. Incorporating Ni into the alloy effectively resolves the rate imbalance between the nitrate-to-nitrite and nitrite-to-ammonia reactions. This enhancement is achieved by facilitating hydrogenation through improved water dissociation at the $Ni/Ni(OH)_2$ interface under pulsed conditions, driving the conversion process forward even at low overpotentials.

Herein, bimetallic engineering and alloying have emerged as transformative strategies for enhancing the nitrate to ammonia reduction reaction. The synergistic electronic interplay inherent to bimetallic and alloyed architecture is demonstrated in Table 5 where Cu- and Co-based tandem catalysts achieve ampere-level current densities by optimizing discrete reaction steps across adjacent metal sites. These systems produce high FE and ammonia yields by efficiently balancing adsorption energies and suppressing competing processes. The alloying introduces tailored electronic structures and innovative reaction mechanisms including relay catalysis and self-repairing heterojunctions. These alloy systems improve catalytic activity, selectivity, and durability by utilizing atomic-scale modifications and strong metal–metal interactions.

3. Paired electrolysis for nitrate reduction with alternative oxidation reaction

Paired electrolysis is an innovative electrocatalytic method that combines cathodic nitrate reduction with alternative anodic oxidation reactions. This provides a sustainable and energy-efficient pathway for ammonia synthesis. Typically, a nitrate reduction reaction is coupled with an OER at the anode. This process is energy intensive and produces limited value-added products. Pairing nitrate reduction with alternative oxidation processes, including sulfion oxidation, organic oxidation or plastic oxidation, not merely lowers energy consumption overall but also produces useful byproducts that increase the process's overall economic feasibility.[20] Utilizing this bifunctional design, the paired electrolysis system addresses the challenges of low selectivity, high operating costs, competitive hydrogen evolution and optimizes resource utilization, which could create a path to a scalable and environmentally friendly ammonia production solution.[63]

Table 5 Synergistic performance of bimetallic and alloyed catalysts for nitrate reduction

Catalyst	FE (%)	Electrolyte	Stability (h)	Current density (mA cm^{-2})	Ammonia yield rate	Ref.
Cu/Co tandem catalyst	93.3	0.1 M KOH + 0.1 M KNO_3	—	—	1.17 mmol h^{-1} cm^{-2} at −0.175 V *vs.* RHE	33
Ru_xCu_x/rGO	98	1 M KOH + 0.1 M KNO_3	—	120	0.38 mmol h^{-1} cm^{-2} at −0.05 V *vs.* RHE	52
CuCo nanosheets	∼100	1 M KOH + 0.1 M KNO_3	—	1035	4.8 mmol h^{-1} cm^{-2} at −0.2 V *vs.* RHE	137
Cu/Co bimetallic cMOF	96.4	0.5 M Na_2SO_4 + 0.1 M $NaNO_3$	—	—	299.9 μmol h^{-1} cm^{-2} at −0.6 V *vs.* RHE	138
RuMo alloy NFs (fcc)	95.2	0.1 M KOH + 0.1 M KNO_3	—	68.3	32.7 mg h^{-1} mg^{-1} at −0.1 V *vs.* RHE	141
CuNi NPs/CF	97.03	1 M NaOH + 44.2 g L^{-1} NO_3^-	—	1200	94.57 mg h^{-1} cm^{-2} at −0.48 V *vs.* RHE	143
Ni_1Cu-SAA	∼100	0.5 M K_2SO_4 + 200 ppm NO_3^-	—	165.8	326.7 μmol h^{-1} cm^{-2} at −0.55 V *vs.* RHE	144

The integration of electrocatalytic nitrate reduction to ammonia with the sulfion oxidation reaction represents a paradigm shift in electrochemical nitrogen management, simultaneously tackling the environmental burdens of nitrate and sulfide pollution while enabling energy-efficient and value-added chemical synthesis. This innovative paired electrolysis system circumvents the thermodynamically demanding and kinetically sluggish OER which is a primary source of energy inefficiency in conventional electrolyzers. A seminal study by Ren *et al.* demonstrated this transformative concept through the design of a bifunctional dimethylamine-borane (DMAB)-modified Co-based metal–organic framework (DMAB-Co-MOF/NF) precatalyst.[146] This precatalyst undergoes *in situ* electrochemical reconstruction under operational conditions to yield two distinct highly active phases; a heterogeneous $CoOOH/Co(OH)_2$ structure on the cathode for nitrate reduction and an amorphous boron-doped cobalt sulfide (B–Co–S) on the anode for sulfion oxidation (Fig. 16(a)). The reconstructed cathode, $CoOOH/Co(OH)_2$ exhibits exceptional nitrate reduction performance achieving an ammonia yield rate of 0.238 mmol h^{-1} cm^{-2} and a near unity FE of 94.16% at a low potential of −0.2 V *vs.* RHE. This high activity attributed to the synergistic redox interplay between Co^{2+} and Co^{3+} species within the heterogeneous structure which facilitates efficient electron transfer for the nitrate reduction pathway. Concurrently, the *in situ* formed amorphous B–Co–S anode demonstrates superior sulfion oxidation activity requiring a low potential of 0.268 V *vs.* RHE to achieve a current density of 100 mA cm^{-2}. The amorphous nature of B–Co–S characterized by abundant defects and unsaturated coordination sites alongside the electronic modulation induced by boron doping, optimizes the adsorption of reactants and enhances charge transfer kinetics. The two-electrode nitrate reduction to an ammonia and sulfion oxidation reaction system (NRA||SOR) operates a dramatically low cell voltage of 1.062 V to deliver a current density of 50 mA cm^{-2} (Fig. 16(b)), starkly contrasting the much higher voltage required for a traditional NRA||OER configuration. This substantial reduction in energy consumption coupled with the simultaneous production of valuable ammonia at the cathode and elemental sulfur at the anode (Fig. 16(c)) establishes an economically viable platform for the collective value-added recycling of wastewater pollutants.

Further cementing the transformative potential of paired electrolysis, Wang *et al.* demonstrated a remarkably efficient system coupling nitrate reduction on a metallic copper catalyst with sulfion oxidation.[38] This study is underpinned by DFT calculations which revealed that the metallic Cu(111) surface provides a more favorable pathway for the critical conversion of NO_2^- intermediates to ammonia compared to Cu_2O facilitating efficient ammonia generation as shown in Fig. 16(d). The synthesized chemically reduced Cu (CR-Cu) catalyst was further treated by an electrochemical reduction method (ER-Cu) and delivered exceptional performance achieving a near-unity FE of 96.0% and a high ammonia yield rate of 0.391 mmol h^{-1} cm^{-2} at a low cathodic potential of −0.2 V *vs.* RHE. By replacing the anodic OER with sulfion oxidation on a sulfur-doped Ni/Fe hydroxide anode ($S–(Ni,Fe)O_xH_y$) on Ni foam which operates at a significantly lower onset potential, 0.288 V *vs.* RHE for sulfion oxidation and 1.366 V *vs.* RHE for OER, the overall cell voltage was drastically reduced. The integrated nitrate reduction reaction and sulfion oxidation reaction (NO_3RR-SOR) system required an ultralow cell voltage of just 1.2 V to achieve a current density of 85 mA cm^{-2}, a 50% reduction from the 2.387 V needed for a conventional NO_3RR-OER configuration illustrated in Fig. 16(e). This monumental decrease in energy demand was further showcased by powering the entire process with a single 1.2 V commercial battery which sustained an ammonia yield rate of 0.316 mmol h^{-1} cm^{-2} (Fig. 16(f)). Beyond its exceptional energy efficiency, this system establishes a circular economy paradigm simultaneously valorizing two pollutants into valuable products, ammonia and elemental sulfur thus offering a sustainable pathway for wastewater remediation and resource recovery.

Another approach of this coupling of nitrate reduction with the glycerol oxidation simultaneously valorizes a biodiesel byproduct into formate, a high-value chemical. In a landmark study, Li *et al.*[147] engineered a highly efficient nitrate reduction with glycerol oxidation system centered on a bifunctional carbon nanosheet array-supported cobalt phosphide electrocatalyst (CNs@CoP). The cathodic nitrate reduction to ammonia performance of CNs@CoP is exceptional, achieving a FE of 95.1% at a low potential of −0.30 V *vs.* RHE and record ammonia yield rate of 43.9 mg h^{-1} cm^{-2} under high current densities of 440 mA cm^{-2} at 1.0 V *vs.* RHE. This superior activity stems from a synergistic core@shell architecture where the CN promotes water dissociation to generate active hydrogen species (*H) which then spill over to adjacent CoP sites. Combined experimental and DFT analyses revealed that this H enrichment on CoP (forming CoP-H) state) significantly lowers the energy barrier for the rate-determining step (NO to *NOH) from 1.57 eV to 1.33 eV thus accelerating the protonation of key intermediates and enhancing the overall nitrate reduction kinetics as illustrated in Fig. 17(a). Crucially, the full nitrate reduction reaction and glycerol oxidation reaction (NITRR||GOR) system delivered dramatically enhanced performance compared to a conventional NITRR||OER setup in a two electrode membrane-electrode assemble flow reactor. At a cell voltage of just 1.8 V, the system achieved a high current density of 600 mA cm^{-2} simultaneously producing ammonia at a rate of 15.2 mg h^{-1} cm^{-2} (FE of 96.4%) (Fig. 17(b)) and formate at 111 mg h^{-1} cm^{-2} (FE of 93.5%) (Fig. 17(c)). This coupling strategy reduced the operational cell voltage by approximately 0.2 V at 300 mA cm^{-2} translating to substantial energy savings of 1.4×10^3 kW h per ton of ammonia. A preliminary techno-economic analysis confirmed the profound economic advantage by shifting the process from a net cost of $$ −2629 per ton NH_3 for NITRR||OER to a significant profit of $1217 per ton NH_3 for NITRR||GOR with potential for further valorizaation by converting formate to potassium diformate (KDF) (Fig. 17(d)).

In another breakthrough study that exemplifies the power of integrated system design, Li *et al.*[39] introduced a bifunctional Cu-doped NiCo alloy catalyst supported on nickel foam (Cu–NiCo/NF) for the concurrent electrocatalytic valorization of nitrate and glycerol. This innovative paired electrolysis system

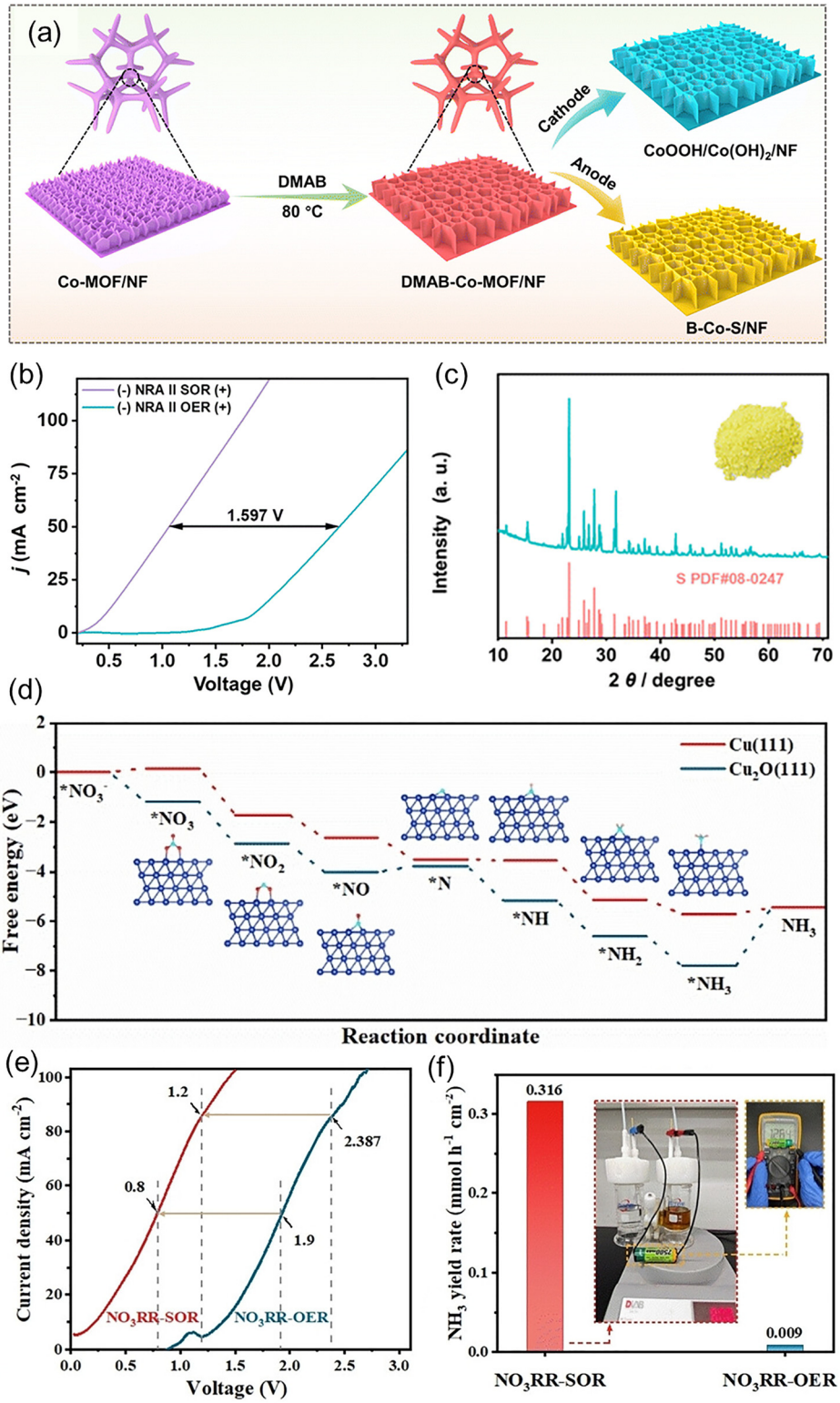

Fig. 16 (a) Schematic of the synthesis process for $CoOOH/Co(OH)_2$/NF and B–Co–S/NF electrodes. (b) LSV curves of the DMAB-Co-MOF/NF precatalyst as the cathode and anode in NRA||SOR and NRA||OER. (c) XRD pattern and photographic image (inset) of the collected sulfur (S) powder product.[146] Reproduced from ref. 146, with permission from The Royal Society of Chemistry, Copyright [2023]. (d) Calculated Gibbs free energy diagrams for NO_3^--to-NH_3 conversion on Cu and Cu_2O catalysts. The blue, red, cyan and pink balls represent copper, oxygen, nitrogen and hydrogen atoms, respectively. (e) Polarization curves of the two-electrode NO_3RR-SOR and NO_3RR-OER. (f) NH_3 yield rate for the NO_3RR-SOR system powered by a 1.2 V commercial battery.[38] Reproduced from ref. 38, with permission from John Wiley & Sons, Copyright [2023].

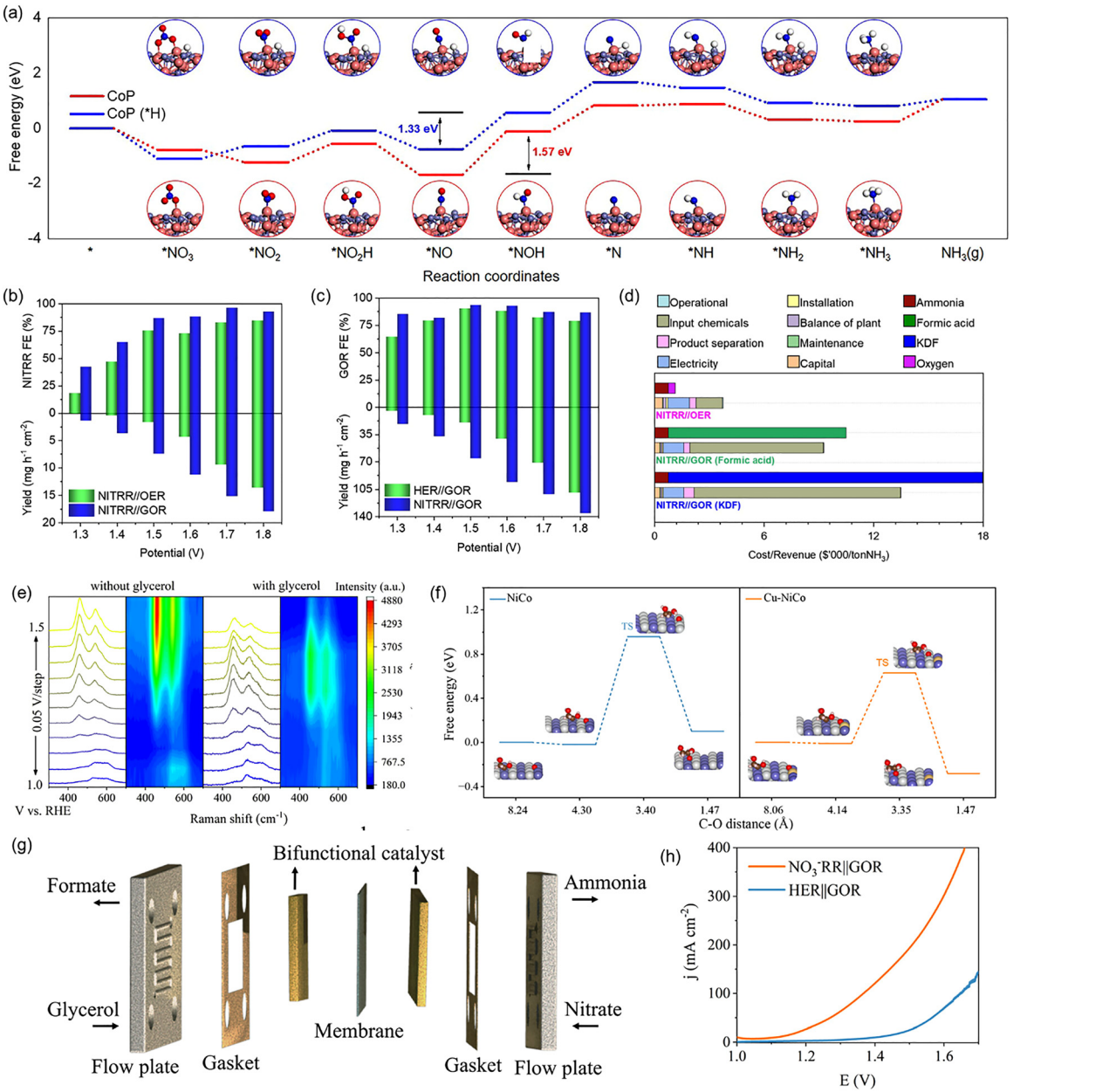

Fig. 17 (a) Free energy diagram of NITRR intermediates on CoP and CoP–H catalysts. Atom colors: Co (orange), P (purple), N (blue), O (red), and H (white). Performance metrics: (b) FE of NITRR and yield rate of NH_3 as a function of potential for NITRR||GOR and NITRR||OER. (c) FE of GOR and yield rate of formic acid as a function of the potential for NITRR||GOR and HER||GOR. (d) Technoeconomic analysis of NITRR||GOR and NITRR||OER.[147] Reproduced from ref. 147, with permission from Elsevier, Copyright [2023]. (e) *In situ* Raman spectra at applied potentials ranging from 1.0 to 1.5 V *vs.* RHE. (f) Energy barrier investigation of *O and *$C_2H_5O_2$ coupling for Cu–NiCo and NiCo, showing C–O distance at the transition state (TS). (g) Schematic of the MEA flow reactor for the NO_3^-RR||GOR system. (h) LSV curves comparing the NO_3^-RR||GOR and HER||GOR.[39] Reproduced from ref. 39, with permission from John Wiley & Sons, Copyright [2024].

couples the nitrate reduction reaction to ammonia with the glycerol oxidation reaction to formate demonstrates exceptional performance metrics. The Cu–NiCo/NF cathode achieves a near-unity FE of 100% for ammonia production while the anode simultaneously generates formate with a remarkable FE of 93.8%. The system's robustness is underscored by its ability to maintain continuous electrolysis for 144 hours at a steady current density of 10 mA cm^{-2}, showcasing outstanding operational stability. Mechanistic investigations including *in situ* Raman spectroscopy reveal that the superior activity originates from the rapid electrogeneration of high-valence Ni^{3+}–OOH and Co^{3+}–OOH species (460 and 541 cm^{-1}) on the alloy surface which serve as the true active sites shown in Fig. 17(e). DFT calculations provide atomic-level insight of Cu doping significantly facilitating the critical coupling between surface-adsorbed oxygen species (*O) and reactive intermediates, *$C_2H_5O_2$, lowering the energy barrier

of this step from 0.96 eV for pristine NiCo to 0.63 eV for Cu–NiCo (Fig. 17(f)). This synergistic effect optimizes the reaction pathway, dramatically enhancing the kinetics of both the C–O bond formation during glycerol oxidation and the hydrogenation steps during nitrate reduction. When configured as a full nitrate reduction reaction and glycerol oxidation reaction (NO_3^-RR||GOR) membrane electrode assembly (MEA) flow reactor (Fig. 17(g)), the system requires only 1.11 V and 1.37 V to deliver current densities of 10 and 100 mA cm^{-2}, respectively which is approximately 290 mV lower than a conventional HER||GOR counterpart (Fig. 17(h)). This study not only presents a high-performance bifunctional catalyst but also establishes a transformative paradigm for energy-saving electrochemical refineries that co-produce high-value chemicals from waste streams.

Following the promising results with sulfion and glycerol oxidation, Xiao *et al.*[18] demonstrated a ground-breaking paired electrolysis system coupling cathodic nitrate reduction with anodic formaldehyde oxidation over Cu_2O catalysts achieving unprecedented energy efficiency. This innovative approach capitalizes on the unique redox chemistry of Cu_2O which facilitates an ultra-low onset potential of −0.03 V *vs.* RHE for the formaldehyde oxidation *via* an electrocatalytic oxidative dehydrogenation pathway. At potentials exceeding 0.42 V *vs.* RHE, a tandem reaction mechanism is activated, where Cu_2O is electrochemically oxidized to $Cu(OH)_2$ then spontaneously reduced back to Cu_2O by formaldehyde. *In situ* Raman spectroscopy provides direct evidence of the self-repairing tandem cycle (Fig. 18(a)). Under anodic potential, the characteristic Cu_2O signal (220 cm^{-1}) diminishes as $Cu(OH)_2$ signals (299 and 490 cm^{-1}) emerge confirming oxidation reaction. Upon formaldehyde (HCHO) introduction, the $Cu(OH)_2$ signals vanish while the Cu_2O signal instantly recovers demonstrating the spontaneous aldehyde-driven reduction that prevents catalyst deactivation. Hence it enables exceptional stability sustaining a high current density of 300 mA cm^{-2} at 0.81 V *vs.* RHE, 1.56 V lower than the potential required for the OER at the same current density (Fig. 18(b)). Crucially, an integration of two-electrode nitrate reduction with a formaldehyde oxidation (NO_3^-RR||FOR) cell system with Cu_2O at both electrodes requires an ultralow cell voltage of −0.19 V to achieve 10 mA cm^{-2} reducing the energy input compared to conventional NO_3^-RR||OER systems. This configuration simultaneously delivers a near-unity FE of 99.77% for ammonia production and generates formic acid as a valuable anodic co-product at a remarkable rate of 9.64 mmol cm^{-2} h^{-1}. This work establishes a transformative paradigm for simultaneous environmental remediation of hazardous pollutants (NO_3^- and HCHO) and the co-production of high-value chemicals (NH_3 and HCOOH) highlighting the profound potential of paired electrolysis to enhance both the economic viability and sustainability of electrochemical ammonia synthesis.

A subsequent revolutionary study by Zhang *et al.*[76] has dramatically established the viability of coupling nitrate reduction with formaldehyde oxidation. Their work introduces high-performance bifunctional Ag single-atom-decorated Cu_2O nanowire catalysts (Ag_1@Cu_2O) grown on Cu foam which achieve unprecedented current densities and enable an innovative tandem electrochemical–chemical route for scalable ammonia production and fixation into high-value ammonium formate ($HCOONH_4$). The Ag_1@Cu_2O catalyst exhibits exceptional bifunctionality achieving a two-ampere level current density of 2.3 A cm^{-2} for the bitrate reduction at −1 V *vs.* RHE in a 0.5 M NO_3^- electrolyte alongside a near-unity NH_3 FE of >90% across a wide concentration range (0.01–0.5 M). Concurrently at the anodic side formaldehyde oxidation attains a large current density of 300 mA cm^{-2} at a mere 0.31 V *vs.* RHE with near 100% FE for formate production. This remarkable performance stems from an elucidated Ag–Cu inter-site synergistic mechanism, where single-atom Ag acts as an accelerator for active hydrogen (*H) generation and stabilization on neighboring Cu sites, thereby boosting the hydrogenation kinetics of N-containing intermediates *via* the favorable *NHO pathway, as confirmed by *in situ* studies and DFT calculations (Fig. 18(c)). Leveraging this bifunctionality, MEA-based pair nitrate reduction and formaldehyde oxidation reaction (NO_3^-RR/FOR) electrolysis (Fig. 18(d)) was implemented at an ultralow cell voltage of 1.6 V for 100 hours. This configuration successfully co-produced NH_3 and formate with high FEs (96% for NH_3 and 97% for formate), enabling the subsequent chemical combination, isolation and recovery of 10.7 g of high-purity solid $HCOONH_4$ with a collection efficiency of 84.8% (Fig. 18(e)). A preliminary techno-economic analysis estimated a production cost as low as $237.4 per ton, underscoring the profound economic viability of this integrated route for simultaneous wastewater purification and value-added chemical synthesis. The adaptability of this tandem electrochemical–chemical strategy was further validated by extending it to other nitrate/aldehyde pairs, specifically coupling NO_3^-RR with the oxidation of 4-pyridinecarboxaldehyde (4-PCA) and 5-hydroxymethylfurfural (HMF) (Fig. 18(f)). This expansion highlights the broad applicability and modularity of the approach for upgrading ammonia into diverse, high-value ammonium salts from various industrial aldehyde pollutants.

A pioneering paired electrolysis system has recently been demonstrated for the coupled upgrading of nitrate pollution and waste polyethylene terephthalate (PET) plastics leveraging electro-reconstructed transition metal electrodes to achieve exceptional energy efficiency and economic viability.[148,149] Wang *et al.*[54] developed a dual-electrode system employing a reconstructed Co on copper foam (R-Co/CF) cathode for the nitrate reduction reaction and a reconstructed NiCo on nickel foam (R-NiCo/NF) anode for the oxidation of PET hydrolysate, specifically targeting ethylene glycol (EG) oxidation to formic acid (FA). The R-Co/CF cathode exhibited outstanding performance achieving FE of 96.2% for NH_3 production at −0.2 V *vs.* RHE with a production rate of 0.87 mmol h^{-1} cm^{-2}. This high activity stems from a tandem mechanism between Co and Cu sites (Fig. 19(a)), where Cu facilitates the initial reduction of NO_3^- to NO_2^-, and Co promotes the subsequent hydrogenation to NH_3 (Fig. 19(b)) as confirmed by both experimental analysis and DFT calculations. Concurrently, the R-NiCo/NF anode demonstrated exceptional catalytic activity for the EG oxidation

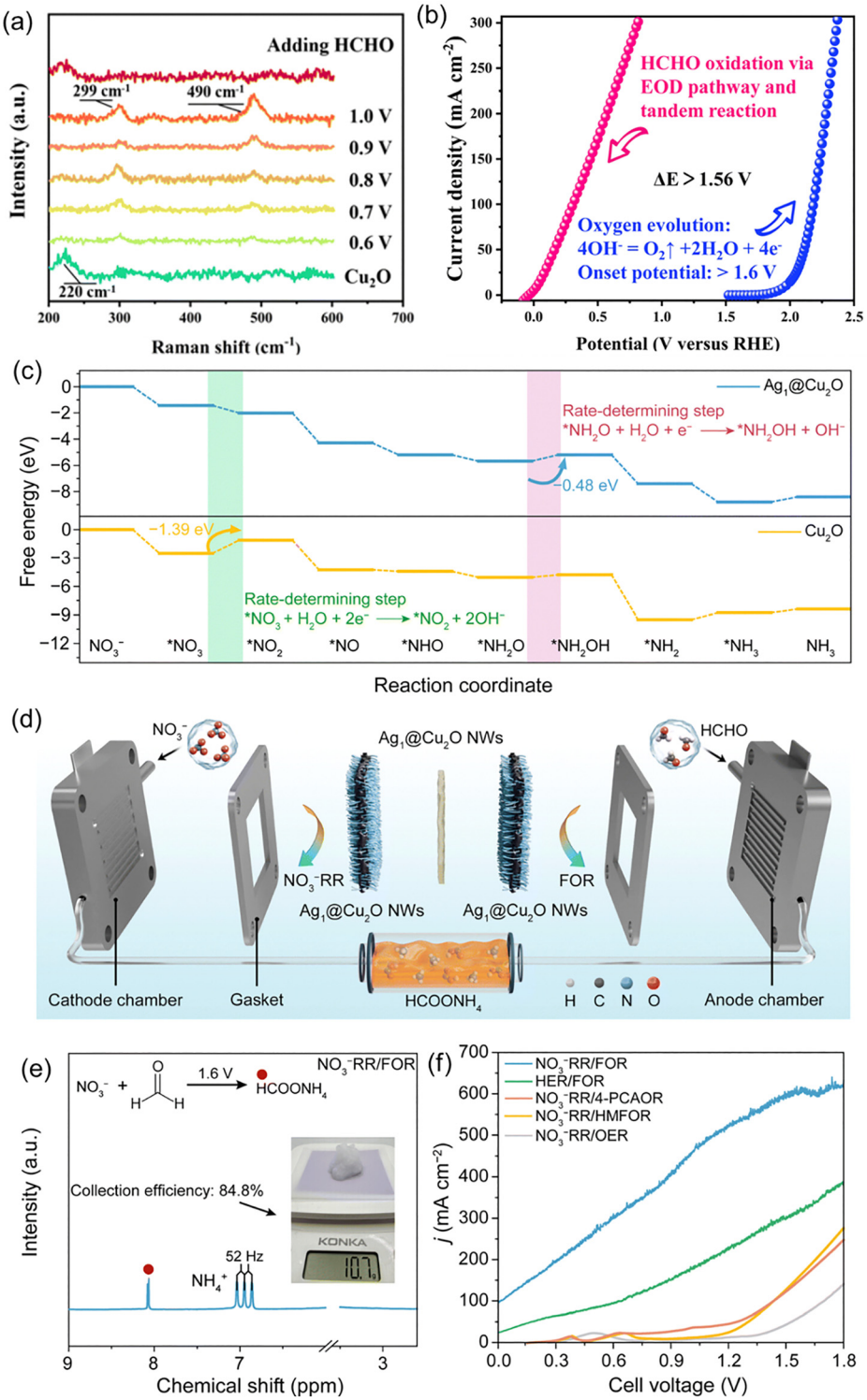

Fig. 18 (a) *In situ* Raman spectroscopy of Cu_2O after holding various potentials from 0.6 V to 1.0 V for 100 s without HCHO and finally adding HCHO. (b) HCHO oxidation over Cu_2O and OER over Pt.[18] Reproduced from ref. 18, with permission from The Royal Society of Chemistry, Copyright [2023]. (c) Gibbs free energy diagrams of NO_3^-RR on Ag_1@Cu_2O and Cu_2O. (d) Schematic illustration of the configuration of the MEA electrolyzer. (e) ^{1}H NMR spectrum of the $HCOONH_4$ product; inset is a photograph of the 10.7 g of $HCOONH_4$ solid isolated. (f) Performance of MEA-based electrolysis for the NO_3^-RR/OER, NO_3^-RR/FOR, NO_3^-RR/4-PCAOR and NO_3^-RR/HMFOR pairs.[76] Reproduced from ref. 76, with permission from The Royal Society of Chemistry, Copyright [2025].

reaction attaining FE of 98.2% for FA at 1.45 V *vs.* RHE with a production rate of 0.63 mmol h^{-1} cm^{-2}. The incorporation of Co was found to accelerate the formation of Ni^{3+} active species, thereby enhancing both the adsorption of EG and the cleavage

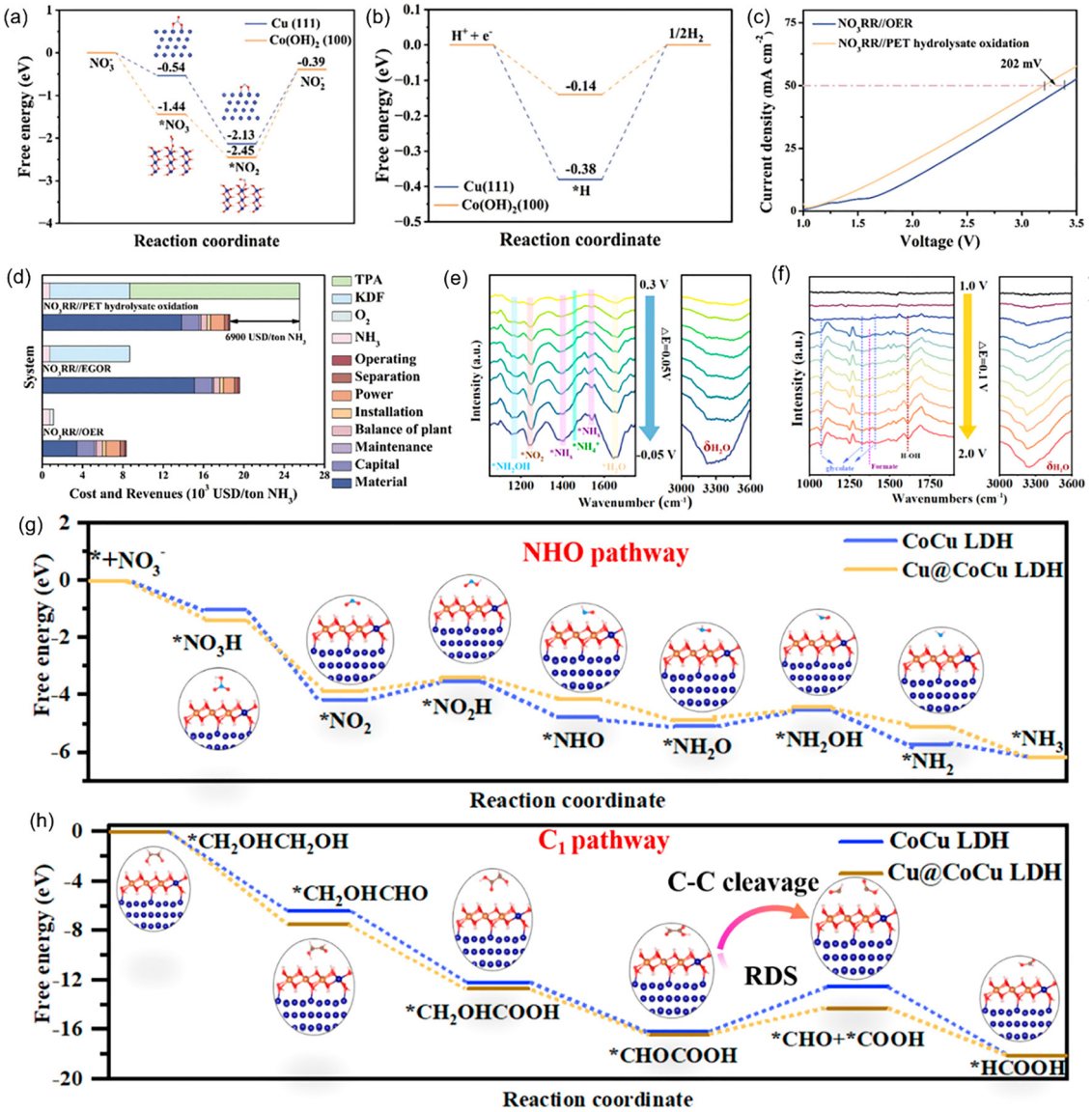

Fig. 19 Free energy profiles (a) for NO_3^- to NO_2^- and (b) for the HER on Cu and $Co(OH)_2$. (c) LSV curves of NO_3RR||PET hydrolysate oxidation and NO_3RR||OER. (d) Technoeconomic analysis of NO_3RR||OER, NO_3RR||EGOR and NO_3RR||PET hydrolysate oxidation (USD/tonne NH_3).[54] Reproduced from ref. 54, with permission from John Wiley & Sons, Copyright [2025]. The operando FTIR spectra of the (e) NO_3 reduction reaction and (f) of the EG oxidation reaction for the Cu@CoCu LDH. The Gibbs free energy diagrams of the (g) NO_3RR and (h) EGOR on both the CoCu LDH and Cu@CoCu LDH. The insets are the corresponding adsorbed structures of different intermediates.[19] Reproduced from ref. 19, with permission from American Chemical Society, Copyright [2024].

of C–C bonds critical for selective FA production. When integrated into a full nitrate reduction and PET hydrolysate oxidation (NO_3RR||PET) coupled system, the electrolyzer required a cell voltage of only 1.526 V to achieve a current density of 50 mA cm^{-2} which is 202 mV lower than that of a conventional NO_3RR||OER system (Fig. 19(c)). This substantial reduction in operational voltage translates directly into significant energy savings. Post-electrolysis, the system enabled the recovery of high-purity terephthalic acid (TPA) and KDF, a valuable derivative of FA through straightforward acidification and crystallization processes. A comprehensive techno-economic analysis revealed that, compared to the NO_3RR||OER benchmark, the NO_3RR||PET hydrolysate oxidation system could save approximately 2.8 × 10^3 kW h per tonne of NH_3 in electricity consumption while generating an estimated $6900 in revenue per tonne of NH_3 (Fig. 19(d)). This transformative approach not only simultaneously remediates two pervasive waste streams, nitrate-contaminated water and plastic waste but also upgrades them into valuable commodities, establishing a circular and economically competitive pathway for distributed chemical synthesis and environmental management.

Further extending the paradigm of paired electrolysis to the valorization of plastic waste, a groundbreaking study by Wu *et al.* demonstrated an exceptionally efficient coelectrolysis

system coupling nitrate reduction with the oxidation of PET-derived EG.[19] The authors engineered a bifunctional electrode comprising Cu nanoparticle-anchored CoCu layered double hydroxide heterostructural nanosheets on carbon cloth (Cu@CoCu LDH/CC) *via* a one-step electrochemical deposition strategy. In a MEA electrolyzer for the concurrent nitrate reduction and EG oxidation reaction, the Cu@CoCu LDH/CC achieved near-unity FE for both ammonia, 98.6% and formate, 98.1% at a low cell voltage of 1.3 V. The system delivered a high ammonia yield rate of 0.793 mmol h^{-1} cm^{-2} at 1.6 V and exhibited outstanding operational stability, maintaining high FE for both products over 120 hours of continuous operation at 1.3 V, a durability that significantly surpasses most reported coelectrolysis systems. Further exploration through a mechanistic study which supported *in situ* FTIR spectroscopy, revealed that the Cu@CoCu LDH heterostructure fosters the favorable formation of key reaction intermediates of $*NH_2OH$, $*NH_x$ for nitrate reduction reaction (Fig. 19(e)) and glycolate for EG oxidation reaction (Fig. 19(f)). DFT calculations further confirmed that the interfacial electronic interaction between Cu nanoparticles and the CoCu LDH substrate optimizes the electronic structure, leading to a substantial reduction in the energy barrier for the rate-determining steps of both the nitrate reduction, NO_2 to $*NO_2H$ (Fig. 19(g)) and the EG oxidation, and C–C bond cleavage in glyoxylate (Fig. 19(h)). This work establishes a transformative and highly efficient circular economy model, simultaneously remediating nitrate wastewater and upcycling waste plastics into valuable ammonia and formate.

Building upon the innovative paradigm of replacing the OER with thermodynamically more favourable oxidation processes, the integration of electrocatalytic nitrate reduction with the oxidation of hydrazine hydrate ($N_2H_4{\cdot}H_2O$) has recently emerged as a particularly compelling strategy. This approach capitalizes on the exceptionally low oxidation potential of hydrazine enabling a dramatic reduction in the overall cell voltage required for ammonia synthesis. Yuan *et al.*[55] exemplifies the transformative potential of this approach, reporting the synthesis of hierarchical $CuCo_2O_4$ nanodendrites (NDs) composed of ultrathin nanosheet subunits *via* a simple coprecipitation-annealing method (Fig. 20(a)). This unique architecture characterized by a spinel structure with well-defined Cu–Co pairs, provides a large specific surface area (167.15 m^2 g^{-1}) and abundant exposed active sites. The catalyst's electronic structure, probed by XPS and XAFS confirms strong electronic interactions between Cu and Co leading to electron redistribution that optimizes intermediate adsorption and hydrogenation kinetics. In the cathodic nitrate reduction of 1 M KOH with 0.05 M KNO_3, the $CuCo_2O_4$ NDs achieve FE of 97.86% with an ammonia yield rate of 34.23 mg h^{-1} mg_{cat}^{-1} at a low potential of −0.3 V *vs.* RHE (Fig. 20(b)), significantly outperforming monometallic CuO nanorods (NRs) and Co_3O_4 (nanosheets) NSs. The true innovation of this work lies in the construction of a symmetric $CuCo_2O_4$ NDs electrolyzer where the anodic OER is replaced by hydrazine oxidation. As illustrated in Fig. 20(c), the nitrate reduction and hydrazine oxidation reaction ($NO_3RR||HzOR$) system requires a remarkably low cell voltage of only 0.997 V to achieve 10 mA cm^{-2} which is 573 mV lower than that of the conventional $NO_3RR||OER$ configuration. Furthermore, the system demonstrates excellent stability during prolonged operation (Fig. 20(d)), maintaining consistent performance and highlighting the practical viability of this paired approach. The integration of HzOR drastically cuts energy consumption and enables the simultaneous remediation of two nitrogenous pollutants, nitrate and hydrazine valorizing them into valuable ammonia and environmentally benign nitrogen gas, respectively.

Concurrently, the strategic pairing of nitrate reduction with the hydrazine oxidation reaction has been advanced as a quintessential model for achieving ''bidirectional nitrogen neutralization'', simultaneously remediating nitrogen pollutants in high NO_3^- and low oxidation N_2H_4 while co-producing valuable NH_3 and benign N_2. Chen *et al.*[150] engineered a sponge-like porous nitrogen-doped carbon encapsulated Cu nanoparticle electrocatalyst (Cu NPs@NDC) specifically for the $NO_3RR||$HzOR (Fig. 20(e)). The spatial confinement of Cu NPs within the NDC matrix effectively mitigates nanoparticle aggregation and detachment while the electronic interaction between the N-doped carbon and Cu optimizes the d band structure enhancing nitrate adsorption and activation (Fig. 20(f)). In a conventional $NO_3RR||OER$ configuration the optimized 1-Cu NPs@NDC catalyst exhibits a NH_3 yield of 502.30 μmol h^{-1} mg^{-1} and FE of 71.69% at −1.1 V *vs.* RHE. The transformative performance leap was achieved by replacing the anodic OER with the thermodynamically favored HzOR (−0.33 V *vs.* RHE). This substitution dramatically accelerated the reaction kinetics, reducing the charge transfer resistance (R_{ct}) from 19.69 Ω in the $NO_3RR||OER$ system to 13.28 Ω in the $NO_3RR||HzOR$ system as confirmed by electrochemical impedance spectroscopy. Consequently, the $NO_3RR||HzOR$ system achieved a spectacular NH_3 yield of 484.83 μmol h^{-1} mg^{-1} and FE of 99.85% at a significantly lower cathodic potential of −0.9 V *vs.* RHE (Fig. 20(g)). This represents a 1.5-fold enhancement in both yield and FE compared to the OER-coupled system under equivalent conditions. Furthermore, the system demonstrated robust stability over multiple cycles with the FE NH_3 consistently exceeding 96% and effectively degraded ∼74.48% of the anodic hydrazine pollutant within 4 hours validating its dual-functionality for environmental remediation and sustainable synthesis.

The transformative potential of paired electrolysis is conclusively quantified in Table 6 which showcases how replacing the OER with thermodynamically favorable alternatives slashes cell voltages by up to 50% while co-producing valuable chemicals, fundamentally rewriting the process economics.[155] It is critically underpinned by the sophisticated design of Cu- and Co-based electrocatalysts, which have emerged as the cornerstone for enabling these energy-efficient coupled reactions. The remarkable versatility of Cu whether in its metallic, oxide or alloyed forms, consistently facilitates the critical hydrogenation steps in nitrate reduction, while its ability to form synergistic interfaces with promoters like Ag single atoms dramatically enhances *H supply and intermediate stabilization.[156–158] Concurrently, Co-based systems, particularly in reconstructed

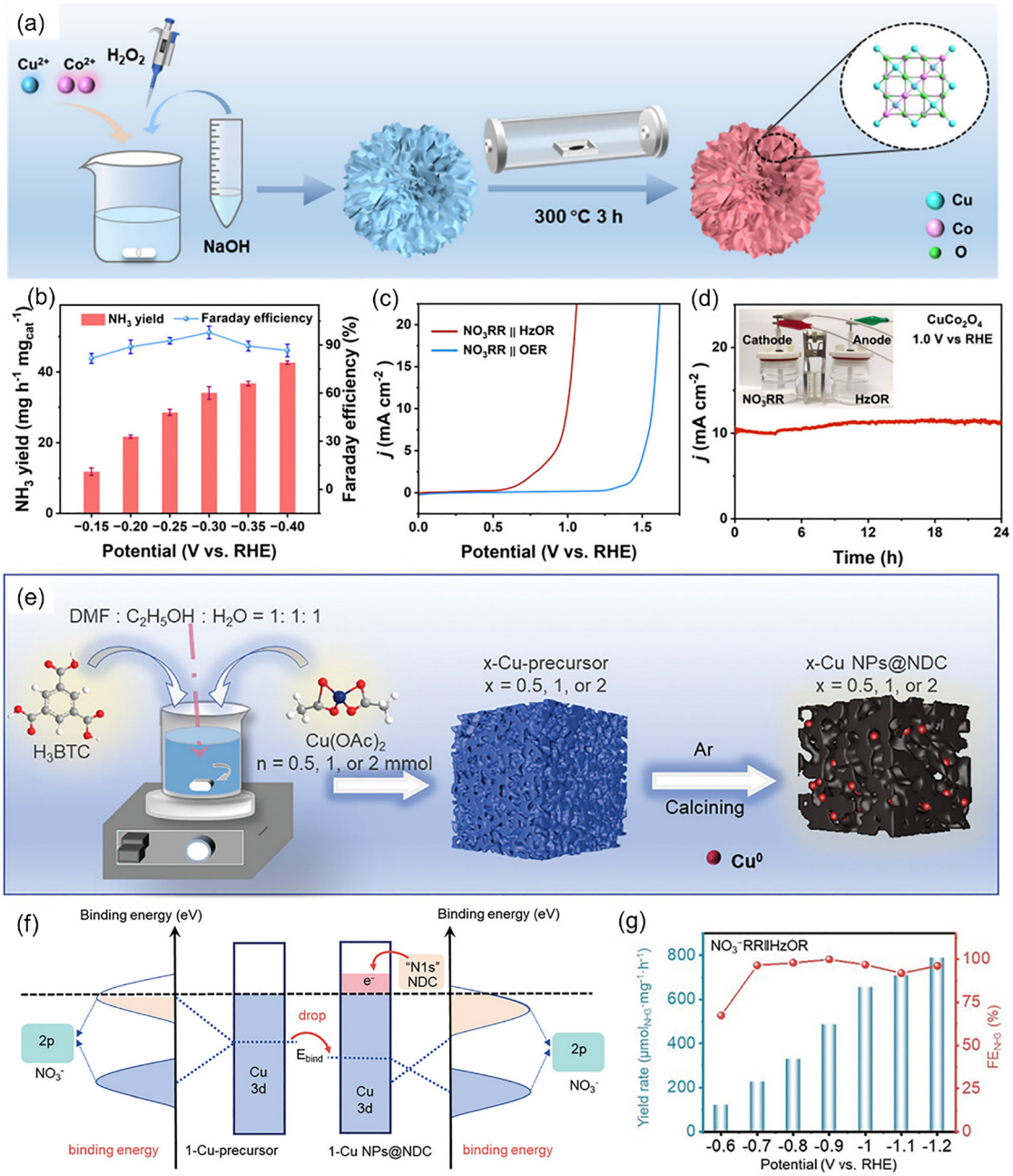

Fig. 20 (a) Schematic diagram of the synthesis of $CuCo_2O_4$ NDs. (b) NH_3 yield and FE of $CuCo_2O_4$ NDs at different potentials (1 M KOH with 0.05 M KNO_3). (c) LSV curves for the electrochemical NH_3 production in 1 M KOH electrolyte with and without 0.3 M N_2H_4. (d) The chronoamperometry curve of bifunctional $CuCo_2O_4$ NDs.[55] Reproduced from ref. 55, with permission from American Chemical Society, Copyright [2025]. (e) Schematic illustration of the synthesis routes for *x*-Cu NPs@NDC. (f) Schematic diagram illustrating the electron interaction between N 1s and Cu 3d orbitals. (g) NH_3 yield and FE_{NH_3} of the 1-Cu NPs@NDC catalyst at different applied potentials for electrocatalytic NO_3^-RR in the NO_3^-RR||HzOR system.[150] Reproduced from ref. 150, with permission from John Wiley & Sons, Copyright [2025].

heterostructures or as components in spinel oxides like $CuCo_2O_4$, exhibit exceptional bifunctionality, leveraging their dynamic redox interplay between Co^{2+}/Co^{3+} states to drive both cathodic nitrate-to-ammonia conversion and anodic oxidations of diverse substrates.[159–161] The strategic integration of Cu and Co into bimetallic or heterostructured architectures creates a powerful synergy, optimizing electronic structures and fostering tandem reaction pathways that collectively lower the energy barriers for both half-reactions. The development of sophisticated bifunctional catalysts and the engineering of tandem reaction mechanisms are pivotal in overcoming the fundamental limitations of conventional processes, ensuring not only remarkable energy efficiency but also unprecedented catalyst stability. Beyond the extensively discussed coupling with the SOR,[162,163] GOR,[164,165] and FOR,[44,166] the scope of viable anodic partners is broad and highly promising. In addition, coupling

Table 6 Performance summary of paired electrolysis systems for nitrate reduction coupled with alternative oxidation reactions

Anodic reaction	Catalyst system (cathode||anode)	Cell voltage (V)@current density (mA cm^{-2})	NH_3 FE (%)/yield rate	Anodic product/FE (%)	Ref.
SOR	$CoOOH/Co(OH)_2$/NF||B–Co–S/NF	1.062@50	94.2%/0.238 mmol h^{-1} cm^{-2}	Elemental S/—	146
SOR	ER-Cu||S–$(Ni,Fe)O_xH_y$	1.2@85	96.0%/0.391 mmol h^{-1} cm^{-2}	Elemental S/—	38
SOR	$CuCo_2O_4$@CC||$CuCo_2O_4$@CC	0.45@100	98.5%/445.6 μmol h^{-1} cm^{-2} (at −0.4 V *vs.* RHE in half-cell)	Polysulfide (S_x^{2-})/—	53
GOR	CNs@CoP||CNs@CoP	1.8@600	96.4%/15.2 mg h^{-1} cm^{-2}	Formate/93.5%	147
GOR	Cu–NiCo/NF||Cu–NiCo/NF	1.11@10	∼100%/—	Formate/93.8%	39
FOR	Cu_2O||Cu_2O	−0.19@10	99.8%/—	Formate/—	18
FOR	Ag_1@Cu_2O||Ag_1@Cu_2O	1.6@—	96%/—	Formate/97%	76
EGOR	R-Co/CF||R-NiCo/NF	1.526@50	96.2%/0.87 mmol h^{-1} cm^{-2}	Formate/98.2%	54
EGOR	Cu@CoCu LDH/CC||Cu@CoCu LDH/CC	1.3@—	98.6%/0.793 mmol h^{-1} cm^{-2}	Formate/98.1%	19
HzOR	$CuCo_2O_4$ NDs||$CuCo_2O_4$ NDs	0.997@10	97.9%/34.23 mg h^{-1} mg_{cat}^{-1}	N_2/—	55
HzOR	Cu NPs@NDC||Cu NPs@NDC	−0.9@—	99.9%/ 484.83 μmol h^{-1} mg^{-1}	N_2/—	150
HzOR	$Co_{0.5}$NiS-NSs/NF||$Co_{0.5}$NiS-NSs/NF	0.36@10	92.2%/ 0.250 mmol h^{-1} cm^{-2} (at −0.15 V *vs.* RHE in half-cell)	N_2/—	151
MOR	Cu–CoO/NF||Cu–CoO/NF	2 V@60 mA cm^{-2}	70.1%/0.46 mmol h^{-1} cm^{-2}	Formate/72%	152
HMFOR	Ag–$Ni(OH)_2$/Cu NW||Ag–$Ni(OH)_2$/Cu NW	1.57 V@50 mA cm^{-2}	98.1%/ 3.17 mg h^{-1} cm^{-2}	FDCA/99.7% Selectivity	153
HMFOR	CuO/Co_3O_4||CuO/Co_3O_4	1.80@20 mA cm^{-2}	77%/ 1.01 mmol h^{-1} cm^{-2} (at −0.60 V half-cell)	FDCA/79.9%	154

nitrate reduction with the HzOR can drive the overall cell at dramatically low voltages while simultaneously remediating two nitrogenous pollutants.[167,168] Similarly, reactions such as the alcohol oxidation reaction,[169,170] methanol (MOR)[27,171] and 5-hydroxymethylfurfural oxidation (HMFOR)[172,173] co-produce valuable organic chemicals like formic acid or furandicarboxylic acid significantly enhancing the process's economic viability by creating dual revenue streams. The valorization of wastewater contaminants and renewable organic feedstocks at the anode elevates these systems beyond simple ammonia production transforming them into versatile and decentralized electrochemical refineries. This integrated approach which couples cathodic and anodic valorization charts a direct course toward a circular nitrogen economy. Thereby it offers a unified solution to the pressing issues of environmental pollution and the high carbon footprint of conventional fertilizer synthesis establishing a new standard for distributed energy-smart manufacturing.

4. Conclusions and future perspectives

Electrocatalytic nitrate reduction to ammonia has emerged as a transformative strategy for sustainable nitrogen management simultaneously addressing the dual challenges of environmental nitrate pollution and the carbon intensive Haber–Bosch process. This review explores the fundamental mechanisms underlying the nitrate reduction reaction, emphasizing critical parameters including overpotential, Tafel slope, FE, selectivity and current density. This review has comprehensively detailed the fundamental mechanisms, performance metrics and the state-of-the-art in catalyst engineering with a dedicated focus on Cu- and Co-based systems. Through sophisticated design strategies including structural, vacancy, doping, single-atom and bimetallic engineering, significant strides have been made in enhancing the activity, selectivity (FE often exceeding 95%) and stability of these catalysts. The inherent advantages of Cu and Co such as their optimal electronic structures for nitrate adsorption and activation, cost-effectiveness and natural abundance firmly establish them as among the most promising candidate materials for this reaction. Beyond these catalyst level advancements, a broader system level reflection is essential to assess the realistic role of electrocatalytic nitrate reduction within the future nitrogen economy. Despite the remarkable progress achieved, it is imperative to acknowledge that electrocatalytic nitrate reduction is unlikely to completely supplant the Haber–Bosch process in the near term, primarily due to the limited availability of nitrate feedstock at a global scale, approximately 21 million tonnes in 2022 and is expected to grow slowly at a CAGR of about 3.63%.[174] However, this technology holds immense potential as a complementary or distributed route within a hybrid nitrogen economy. The natural and anthropogenic nitrate reservoirs such as industrial and agricultural wastewater and municipal effluents represent abundant localized sources (over 60–70% of nitrate) that can be directly valorized.[175,176] Harnessing these waste-derived nitrates not only offsets the environmental burden of nitrate pollution but also enables the co-production of green ammonia under mild conditions thereby decoupling fertilizer synthesis from fossil-based hydrogen and high-pressure operations. Thus, while large scale replacement of the Haber–Bosch process remains aspirational, integrating electrocatalytic nitrate-to-ammonia modules into existing water treatment infrastructures offers a realistic and sustainable pathway towards a decentralized nitrogen cycle. Looking ahead, this vision can be further strengthened by coupling these catalytic systems within paired electrolysis configurations, enabling synergistic gains in both energy efficiency and economic viability.

Furthermore, the integration of these advanced cathodes into paired electrolysis systems represents a paradigm shift, dramatically improving the energy and economic viability of electrochemical ammonia synthesis. Cell voltages can be reduced by up to 50% enabling simultaneous wastewater remediation and the co-production of valuable chemicals by replacing the kinetically sluggish OER with thermodynamically favorable alternative oxidation reactions (SOR, GOR, FOR, EGOR, and HzOR). This innovative approach transcends mere electrocatalysis, paving the way for distributed, energy-smart electrochemical refineries. The synergistic potential of integrating sophisticated catalyst design with paired electrolysis configurations to simultaneously address environmental remediation and sustainable chemical synthesis is powerfully illustrated in Fig. 21, which encapsulates the transformative roadmap for next-generation nitrogen management technologies. Despite remarkable progress, several challenges must be overcome to transition this technology from laboratory breakthroughs to industrial-scale implementation. Future research should focus on the following key directions.

4.1. Advanced catalyst design for enhanced stability and selectivity

The pursuit of next-generation electrocatalysts must continue, prioritizing designs that mitigate deactivation from intermediate poisoning (*NO) and suppress the hydrogen HER under industrial-relevant current densities. Future catalysts must aim to consistently achieve ammonia yield rates exceeding 1 mmol h^{-1} cm^{-2} and faradaic efficiencies above 95% at current densities >200 mA cm^{-2} to meet the economic thresholds for decentralized ammonia synthesis.[137,177] High-entropy alloys, multi-metallic hybrids and catalysts with dynamically self-repairing active sites have immense promise for concurrently unlocking this triumvirate of high activity, unprecedented durability (>1000 hours) and near-perfect selectivity in complex real-world wastewater matrices.[178] The integration of such high-performance materials is paramount for transforming laboratory breakthroughs into viable and scalable electrochemical ammonia technologies.

4.2. Expanding the horizon: paired electrolysis and C–N coupling for urea synthesis

A particularly compelling and nascent frontier is the co-reduction and C–N coupling of NO_3^- and carbon dioxide (CO_2) for the direct synthesis of urea. Urea, a vital fertilizer and chemical feedstock, is currently produced *via* the energy-intensive Bosch–Meiser process. Electrocatalytic urea synthesis offers a sustainable alternative by using waste pollutants (NO_3^- and CO_2) as feedstocks. In this context, Cu-based catalysts are exceptionally promising due to their unique capability to activate and catalyze the reduction of both NO_3^- and CO_2. Their ability to facilitate C–N bond formation, a critical step in urea generation, makes them ideal candidates for exploring this complex reaction pathway. Similarly, Co-based catalysts, known for their hydrogenation prowess, could be engineered in tandem or alloyed with Cu to optimize the supply of key intermediates like $*NH_2$ and *CO, thereby enhancing urea selectivity and yield. Research should focus on elucidating the complex mechanism of C–N coupling and designing bifunctional sites that can simultaneously manage the reaction landscapes of both nitrogen and carbon species.

4.3. System engineering and scalability

The development of robust and self-supported electrodes on 3D conductive substrates (Ni foam, carbon nanotubes) is crucial for enhancing mass transport and mechanical integrity in flow reactors and MEAs. Scaling up requires optimized reactor designs that minimize energy losses, facilitate product

Fig. 21 The integrated design of performance metrics, electrocatalyst modification and paired electrolysis – AOR enables circular and distributed ammonia synthesis from nitrate wastewater.

separation and enable efficient ammonia recovery. Long-term stability tests (>1000 hours) under continuous flow conditions with real wastewater feeds are non-negotiable for de-risking technological translation.

4.4. Integration of advanced characterization and computational intelligence

The combination of operando spectroscopic and microscopic techniques with computational methods, particularly DFT and machine learning (ML) will be indispensable. This synergy allows for the real-time observation of active sites and reaction intermediates, guiding the rational design of catalysts. ML-driven high-throughput screening can rapidly identify novel material compositions, accelerating the discovery cycle beyond traditional trial-and-error approaches.

4.5. Synergy with renewable energy and circular systems

To truly realize its sustainable potential, electrocatalytic nitrate reduction reaction must be integrated with renewable energy sources such as solar and wind. This integration can enable decentralized, off-grid ammonia production. Furthermore, coupling nitrate reduction with the oxidation of biomass-derived compounds or plastic waste hydrolysates can establish a circular economy model, transforming waste streams into value-added products and drastically improving the overall process economics.

In conclusion, electrocatalytic nitrate-to-ammonia conversion, particularly when leveraging the unique strengths of Cu- and Co-based catalysts and innovative paired electrolysis systems, stands at the forefront of sustainable chemistry. Addressing these existing challenges *via* interdisciplinary research focused on advanced materials, system engineering and renewable integration, this technology has the definitive potential to revolutionize ammonia production, contribute to a circular nitrogen economy and establish a new standard for distributed, clean chemical manufacturing.

Conflicts of interest

There are no conflicts of interest to declare.

Data availability

This review is based on the analysis and synthesis of existing literature; as such, all data are contained within the manuscript.

Acknowledgements

The authors would like to acknowledge the financial support provided by the Ministry of Higher Education Malaysia under the Fundamental Research Grant Scheme (FRGS) (ref no. FRGS/1/2024/TK08/XMU/02/1). This work was supported by the PETRONAS-Academia Collaboration Dialogue (PACD 2023) grant, provided by PETRONAS Research Sdn. Bhd. (PRSB). The authors would like to thank the Ministry of Science, Technology and Innovation (MOSTI) Malaysia under the Strategic Research Fund (SRF) (S.22015). The authors gratefully acknowledge Agilent Technologies Malaysia Sdn. Bhd. for their contribution through chromatography. This research was supported by the National Natural Science Foundation of China (ref no: 22202168) and the Guangdong Basic and Applied Basic Research Foundation (ref no: 2021A1515111019). The authors would also like to acknowledge the financial support from the State Key Laboratory of Physical Chemistry of Solid Surfaces, Xiamen University (ref no: 2023X11). This work was supported by the Embassy of the People's Republic of China in Malaysia (EENG/0045). This work was also funded by a Xiamen University Malaysia Investigatorship Grant (grant no: IENG/0038) and Xiamen University Malaysia Research Fund (ICOE/0001, XMUMRF/2021-C8/IENG/0041 and XMUMRF/2025-C15/IENG/0080).

References

1 A. E. Giblin, C. R. Tobias, B. Song, N. Wetson, G. T. Banta and V. H. Rivera-Monroy, *Oceanography*, 2015, **26**, 124–131.
2 B. Z. Houlton, M. Almaraz, V. Aneja, A. T. Austin, E. Bai, K. G. Cassman, J. E. Compton, E. A. Davidson, J. W. Erisman, J. N. Galloway, B. Gu, G. Yao, L. A. Martinelli, K. Scow, W. H. Schlesinger, T. P. Tomich, C. Wang and X. Zhang, *Earth's Future*, 2019, **7**, 865–872.
3 X. Zou, C. Chen, C. Wang, Q. Zhang, Z. Yu, H. Wu, C. Zhuo and T. C. Zhang, *Sci. Total Environ.*, 2021, **800**, 149645.
4 C. Liang, X.-Y. Wei, W. Liu, Y.-Z. Zhang, Z.-J. Ma, H.-Y. Liu, C.-G. Niu and L.-S. Jiang, *Coord. Chem. Rev.*, 2025, **522**, 216174.
5 L. Shan, Y. Ma, S. Xu, M. Zhou, M. He, A. M. Sheveleva, R. Cai, D. Lee, Y. Cheng, B. Tang, B. Han, Y. Chen, L. An, T. Zhou, M. Wilding, A. S. Eggeman, F. Tuna, E. J. L. McInnes, S. J. Day, S. P. Thompson, S. J. Haigh, X. Kang, B. Han, M. Schröder and S. Yang, *Commun. Mater.*, 2024, **5**, 104.
6 X. Sheng, Y. Wang and J. Xu, *Mater. Horiz.*, 2025, **12**, 9087–9093.
7 Q. Wu, S. Ji, J. Chen, X.-Q. Tan, W.-J. Ong, R. Du, P. Wang, H. Wang, Y. Qiu, K. Yan, Y. Zhao, W.-W. Zhao, K.-S. Peng, Y.-Y. Chen, S.-F. Hung, L. Zhou, X. Wang, G. Qiu and G. Chen, *Nat. Water*, 2025, **3**, 1291–1302.
8 W. Qiu, Y. Liu, M. Xie, Z. Jin, P. Li and G. Yu, *EES Catal.*, 2024, **2**, 202–219.
9 C. Smith, A. K. Hill and L. Torrente-Murciano, *Energy Environ. Sci.*, 2020, **13**, 331–344.
10 H. Lee, K.-H. Kim, R. R. Rao, D. G. Park, W. H. Choi, J. H. Choi, D. W. Kim, D. H. Jung, I. E. L. Stephens, J. R. Durrant and J. K. Kang, *Mater. Horiz.*, 2024, **11**, 4115–4122.
11 N. F. Agesta, Y.-L. Woo, J. Y. Loh, F. M. Yap, X. Zeng and W.-J. Ong, *J. Mater. Chem. A*, 2025, **13**, 40213–40228.
12 L. Su, K. Li, H. Zhang, M. Fan, D. Ying, T. Sun, Y. Wang and J. Jia, *Water Res.*, 2017, **120**, 1–11.

13 D. Zhang, B. Wang, X. Gong, Z. Yang and Y. Liu, *Chem. Eng. J.*, 2019, **359**, 1195–1204.
14 J. Gao, B. Jiang, C. Ni, Y. Qi, Y. Zhang, N. Oturan and M. A. Oturan, *Appl. Catal., B*, 2019, **254**, 391–402.
15 Y.-J. Shih, Z.-L. Wu, Y.-H. Huang and C.-P. Huang, *Chem. Eng. J.*, 2020, **383**, 123157.
16 Q. Hu, Y. Qin, X. Wang, Z. Wang, X. Huang, H. Zheng, K. Gao, H. Yang, P. Zhang, M. Shao and C. He, *Energy Environ. Sci.*, 2021, **14**, 4989–4997.
17 X. Zhang, C. Wang, Y. Guo, B. Zhang, Y. Wang and Y. Yu, *J. Mater. Chem. A*, 2022, **10**, 6448–6453.
18 L. Xiao, W. Dai, S. Mou, X. Wang, Q. Cheng and F. Dong, *Energy Environ. Sci.*, 2023, **16**, 2696–2704.
19 J. Wu, X. Cheng, Y. Tong, Z. Yu, C. Lin, N. Zhang, L. Chen and P. Chen, *ACS Catal.*, 2024, **14**, 18095–18106.
20 M. Du, T. Sun, X. Guo, M. Han, Y. Zhang, W. Chen, M. Han, J. Ma, W. Yuan, C. Zhou, V. Nicolosi, J. Shang, N. Zhang and B. Qiu, *Mater. Horiz.*, 2025, **12**, 3743–3751.
21 H. Zhang, J. Ran, Y. Ding, L. Zhou, H. Wang, Y. Wang, Y. Cao and Y. Wang, *Appl. Catal., B*, 2026, **381**, 125830.
22 H. M. A. Sharif, H. M. F. Khan, S. Ullah, Y. Wang, M. Ahmad, B. Yang, C. Li and M. B. Asif, *J. Energy Chem.*, 2024, **95**, 380–406.
23 K. Lu and Y. Shen, *Adv. Funct. Mater.*, 2025, **35**, 2424311.
24 J. Wei, Y. Li, H. Lin, X. Lu, C. Zhou and Y.-Y. Li, *Environ. Sci. Ecotechnology*, 2024, **20**, 100383.
25 Z. Li, C. Yang, B. Xu, L. Yao, W. Zhu and Y. Cui, *Energy Mater.*, 2024, **4**, 400046.
26 C. Yang, Y. Chen, Z. He, R. Li and X. Gou, *Front. Chem.*, 2025, **13**, DOI: 10.3389/fchem.2025.1629904.
27 X. Cheng, Z. Xie, S. Zha, Q. Xu, S. Ci and Z. Wen, *J. Mater. Chem. A*, 2025, **13**, 13286–13294.
28 X. Peng, H.-X. Liu, Y. Zhang, Z.-Q. Huang, L. Yang, Y. Jiang, X. Wang, L. Zheng, C. Chang, C.-T. Au, L. Jiang and J. Li, *Chem. Sci.*, 2021, **12**, 7125–7137.
29 S. Jiang, X. Tang, H. Liu, J. Fang, Z. Jin, M. Liu and Y. Liu, *J. Hazard. Mater.*, 2025, **492**, 138266.
30 R. Wang, S. Jia, L. Wu, L. Zhang, X. Song, X. Tan, C. Zheng, W. Li, X. Ma, Q. Qian, X. Kang, Q. Zhu, X. Sun and B. Han, *Angew. Chem., Int. Ed.*, 2025, **64**, e202425262.
31 C. Wang, Y. Zhang, H. Luo, H. Zhang, W. Li, W.-X. Zhang and J. Yang, *Small Methods*, 2022, **6**, 2200790.
32 Z. Wang, E. M. Ortiz, B. R. Goldsmith and N. Singh, *Catal. Sci. Technol.*, 2021, **11**, 7098–7109.
33 W. He, J. Zhang, S. Dieckhöfer, S. Varhade, A. C. Brix, A. Lielpetere, S. Seisel, J. R. C. Junqueira and W. Schuhmann, *Nat. Commun.*, 2022, **13**, 1129.
34 K. Zhang, Y. Liu, Z. Pan, Q. Xia, X. Huo, O. C. Esan, X. Zhang and L. An, *EES Catal.*, 2024, **2**, 727–752.
35 C. Cang, R. Hua, G. Shen, M. Ma, Y. Chen and H. Zheng, *Adv. Sustainable Syst.*, 2024, **9**, 2400523.
36 D. T. González, J. A. Baeza, L. Calvo and M. Á. Gilarranz, *ACS ES&T Water*, 2025, **5**, 1595–1604.
37 I. A. Cechanaviciute and W. Schuhmann, *ChemSusChem*, 2025, **18**, e202402516.
38 Z. Wang, N. Zhou, J. Wang, D. Wang, J. Zeng, H. Zhong and X. Zhang, *ChemSusChem*, 2024, **17**, e202301050.
39 C. Li, H. Li, B. Zhang, H. Li, Y. Wang, X. Wang, P. Das, Y. Li, X. Wu, Y. Li, Y. Cui, J. Xiao and Z.-S. Wu, *Angew. Chem., Int. Ed.*, 2024, **63**, e202411542.
40 S. Sun, C. Dai, P. Zhao, S. Xi, Y. Ren, H. R. Tan, P. C. Lim, M. Lin, C. Diao, D. Zhang, C. Wu, A. Yu, J. C. J. Koh, W. Y. Lieu, D. H. L. Seng, L. Sun, Y. Li, T. L. Tan, J. Zhang, Z. J. Xu and Z. W. Seh, *Nat. Commun.*, 2024, **15**, 260.
41 W. Qiao, I. Waseem, G. Shang, D. Wang, Y. Li, F. Besenbacher, H. Niemantsverdriet, C. Yan and R. Su, *ACS Catal.*, 2021, **11**, 13510–13518.
42 Z. Zhang, N. Zhang, J. Zhang, B. Deng, Z. Cao, Z. Wang, G. Wei, Q. Zhang, R. Jia, P. Xiang and S. Xia, *Chem. Eng. J.*, 2024, **483**, 148952.
43 H. Zhang, K. Fang, J. Yang, H. Chen, J. Ning, H. Wang and Y. Hu, *Coord. Chem. Rev.*, 2024, **506**, 215723.
44 L. Thapa, S. Mallobarman and C. R. Raj, *ACS Appl. Mater. Interfaces*, 2025, **17**, 57803–57838.
45 Y. Feng, J.-T. Ren, M.-L. Sun and Z.-Y. Yuan, *Chem. Sci.*, 2025, **16**, 1528–1559.
46 Y. Zhou, R. Duan, H. Li, M. Zhao, C. Ding and C. Li, *ACS Catal.*, 2023, **13**, 10846–10854.
47 Y. Wei, J. Huang, H. Chen, S.-J. Zheng, R.-W. Huang, X.-Y. Dong, L.-K. Li, A. Cao, J. Cai and S.-Q. Zang, *Adv. Mater.*, 2024, **36**, 2404774.
48 S. Lu, G. Lin, H. Yan, Y. Li, T. Qi, Y. Li, S. Liang and L. Jiang, *ACS Catal.*, 2024, **14**, 14887–14894.
49 Y. Xu, K. Ren, T. Ren, M. Wang, Z. Wang, X. Li, L. Wang and H. Wang, *Appl. Catal., B*, 2022, **306**, 121094.
50 X. Zhang, G. Ma, L. Shui, G. Zhou and X. Wang, *Chem. Eng. J.*, 2022, **430**, 132666.
51 J. Wei, H. Lin, Y. Li, Y. Guo, S. Liu, M. Sun and Y.-Y. Li, *J. Hazard. Mater.*, 2025, **493**, 138264.
52 W. Gao, K. Xie, J. Xie, X. Wang, H. Zhang, S. Chen, H. Wang, Z. Li and C. Li, *Adv. Mater.*, 2023, **35**, 2202952.
53 D. Zhao, S. Wu, Y. Zhang, D. Cao, R. Li, Y. Long and G. Fan, *Chem. Eng. J.*, 2025, **513**, 163044.
54 H. Wang, B. Yang, R. L. Smith Jr, Y. Su and X. Qi, *Adv. Funct. Mater.*, 2025, **35**, 2425333.
55 R. Yuan, X.-H. Wang, S.-B. Yin, X. Ai, Y.-C. Yin, Y. Chen and S.-N. Li, *ACS Mater. Lett.*, 2025, **7**, 2310–2318.
56 Y. Xiong, Y. Wang, J. Zhou, F. Liu, F. Hao and Z. Fan, *Adv. Mater.*, 2023, **36**, 2304021.
57 H. Xu, Y. Ma, J. Chen, W.-X. Zhang and J. Yang, *Chem. Soc. Rev.*, 2022, **51**, 2710–2758.
58 M. Liu, Z. Lu, L. Yang, R. Gao, X. Zhang, Y. Wang and Y. Wang, *J. Environ. Chem. Eng.*, 2023, **11**, 109718.
59 H. Niu, Z. Zhang, X. Wang, X. Wan, C. Shao and Y. Guo, *Adv. Funct. Mater.*, 2021, **31**, 2008533.
60 Z. Yu, M. Gu, Y. Wang, H. Li, Y. Chen and L. Wei, *Adv. Energy Sustainability Res.*, 2024, **5**, 2300284.
61 A. C. A. de Vooys, G. L. Beltramo, B. van Riet, J. A. R. van Veen and M. T. M. Koper, *Electrochim. Acta*, 2004, **49**, 1307–1314.

62 C. Yang, T. Wei, C. Wang, F. Yue, X. Li, H. Pang, X. Zheng, Y. Zhang and F. Fu, *Mater. Horiz.*, 2025, **12**, 877–885.
63 A. Ma, J. Gui, Y. Huang and Y. Yu, *Nano Res.*, 2024, **17**, 7824–7829.
64 C. Lim, H. Jo and K. Yong, *ChemElectroChem*, 2025, **12**, e202400605.
65 H. Zhang, H. Wang, X. Cao, M. Chen, Y. Liu, Y. Zhou, M. Huang, L. Xia, Y. Wang, T. Li, D. Zheng, Y. Luo, S. Sun, X. Zhao and X. Sun, *Adv. Mater.*, 2024, **36**, 2312746.
66 Y. Ren, C. Yu, L. Wang, X. Tan, Z. Wang, Q. Wei, Y. Zhang and J. Qiu, *J. Am. Chem. Soc.*, 2022, **144**, 10193–10200.
67 J.-L. Fan, S.-B. Liu, M.-L. Chen, Z. Wu, S.-P. Sun and Y.-Y. Lou, *J. Mater. Chem. A*, 2024, **12**, 20077–20087.
68 W. Zheng, L. Zhu, Z. Yan, Z. Lin, Z. Lei, Y. Zhang, H. Xu, Z. Dang, C. Wei and C. Feng, *Environ. Sci. Technol.*, 2021, **55**, 13231–13243.
69 L. Liu, S.-J. Zheng, H. Chen, J. Cai and S.-Q. Zang, *Angew. Chem., Int. Ed.*, 2024, **63**, e202316910.
70 M. T. Tang, J. Halldin Stenlid, J. Guo, E. Corson, W. Tarpeh and F. Abild-Pedersen, *ACS Catal.*, 2025, **15**, 4489–4498.
71 W. Sun, Y. Xu, L. Yang, W. Wen, H. Zhang and X.-Y. Yu, *Small*, 2025, **21**, 2411215.
72 W. Liu, Y. Lv, H. Ou, J. Zhang, Y. Ren, M. Xia, Y. Li, H. Li, X. Ren, H. Hu and G. Yang, *Nat. Commun.*, 2025, **16**, 5716.
73 M. Li, Y. Wen, Y. Fang and B. Shan, *Angew. Chem., Int. Ed.*, 2024, **63**, e202405746.
74 J. Shi, L. Tang, Z. Shen and L. Ding, *Sep. Purif. Technol.*, 2025, **367**, 132954.
75 F. Du, J. Li, C. Wang, J. Yao, Z. Tan, Z. Yao, C. Li and C. Guo, *Chem. Eng. J.*, 2022, **434**, 134641.
76 L. Zhang, Y. Cai, Y. Li, C. Sun, Y. Xiao, Y. Yang, D. Chen, D. Xiao, C.-F. Lee, Y. Wang, S. Feng, H.-T. Wang, Y.-C. Shao, T.-S. Chan, H. Ishii, N. Hiraoka, X. Wang, J. Luo and L. Han, *Energy Environ. Sci.*, 2025, **18**, 2804–2816.
77 W. Ye, Y. Yao, X. Wei, M. Xu, S. Zhao, W. Wang, G. Jia, F. Dai, P. Gao, X. Lu, X. Li, B. Xi, N. Wang and S. Xiong, *Angew. Chem., Int. Ed.*, 2025, **64**, e202509303.
78 W. He, S. Chandra, T. Quast, S. Varhade, S. Dieckhöfer, J. R. C. Junqueira, H. Gao, S. Seisel and W. Schuhmann, *Adv. Mater.*, 2023, **35**, 2303050.
79 C. Wang, Y. Yang, Y. Yuan, Q. Lv, L. Zhou, L. Wang, X. Zheng, J. Liu, H. Wu, D. Pang and J. Zheng, *Mater. Horiz.*, 2025, **12**, 2840–2877.
80 F. M. Yap, G. Z. S. Ling, B. J. Su, J. Y. Loh and W.-J. Ong, *Nano Res. Energy*, 2024, **3**, 1–51.
81 F. M. Yap, J. Y. Loh, S. Yuan, X. Zeng and W.-J. Ong, *Adv. Funct. Mater.*, 2025, **35**, 2407605.
82 J. J. Foo, Z.-J. Chiah, S.-F. Ng and W.-J. Ong, *InfoScience*, 2024, **1**, e12023.
83 C. Wang, Q. Zhang, B. Yan, B. You, J. Zheng, L. Feng, C. Zhang, S. Jiang, W. Chen and S. He, *Nano-Micro Lett.*, 2023, **15**, 52.
84 Y. Fu, S. Wang, Y. Wang, P. Wei, J. Shao, T. Liu, G. Wang and X. Bao, *Angew. Chem., Int. Ed.*, 2023, **62**, e202303327.
85 T. J. Siang, P. Zhang, B. Chen and W.-J. Ong, *Chin. J. Catal.*, 2025, **69**, 84–98.
86 K. M. Lim, P. Zhang, S. H. W. Kok, V. Khoo, X. Zeng, L.-L. Tan, B. Chen and W.-J. Ong, *Adv. Funct. Mater.*, 2025, DOI: 10.1002/adfm.202508117.
87 A. Zhu, H. Liu, S. Bu, K. Liu, C. Luan, D. Lin, G. Gan, Y. Zhou, T. Zhang, K. Liu, G. Hong, H. Li and W. Zhang, *ACS Nano*, 2024, **18**, 22344–22355.
88 J. Wang, C. Cai, Y. Wang, X. Yang, D. Wu, Y. Zhu, M. Li, M. Gu and M. Shao, *ACS Catal.*, 2021, **11**, 15135–15140.
89 C. Liu, S. Yang, Y. Xiang, L. Wang, Q. Tang and D. Zhu, *Chem. Commun.*, 2025, **61**, 11025–11028.
90 S. Ye, Z. Chen, G. Zhang, W. Chen, C. Peng, X. Yang, L. Zheng, Y. Li, X. Ren, H. Cao, D. Xue, J. Qiu, Q. Zhang and J. Liu, *Energy Environ. Sci.*, 2022, **15**, 760–770.
91 K. Fan, W. Xie, J. Li, Y. Sun, P. Xu, Y. Tang, Z. Li and M. Shao, *Nat. Commun.*, 2022, **13**, 7958.
92 K.-H. Kim, H. Lee, X. Huang, J. H. Choi, C. Chen, J. K. Kang and D. O'Hare, *Energy Environ. Sci.*, 2023, **16**, 663–672.
93 W. Wang, J. Chen and E. C. M. Tse, *J. Am. Chem. Soc.*, 2023, **145**, 26678–26687.
94 M.-K. Wong, N. Saafie, S. Yuan, J. Y. Loh, F. M. Yap, X. Zeng and W.-J. Ong, *Small Methods*, 2025, DOI: 10.1002/smtd.202500261.
95 M.-K. Wong, J. Y. Loh, F. M. Yap and W.-J. Ong, *InfoMat*, 2025, **7**, e12639.
96 J. Y. Loh, F. M. Yap, T. J. Siang, X. Zeng and W.-J. Ong, *Small*, 2025, **21**, 2570187.
97 A. Yoon, L. Bai, F. Yang, F. Franco, C. Zhan, M. Rüscher, J. Timoshenko, C. Pratsch, S. Werner, H. S. Jeon, M. C. d O. Monteiro, S. W. Chee and B. Roldan Cuenya, *Nat. Mater.*, 2025, **24**, 762–769.
98 N. Zhou, Z. Wang, N. Zhang, D. Bao, H. Zhong and X. Zhang, *ACS Catal.*, 2023, **13**, 7529–7537.
99 Z. Li, M. Zheng, C. Yan, D. Yang, R. Yang, C. Zhang, H. Liu, P. Song, C. Yin, Z. Qi, D. Liu, X. Zhou, L. Song, C. Lv and G. Yu, *Nat. Commun.*, 2025, **16**, 8940.
100 H. Feng, Z. Xu, L. Ren, C. Liu, J. Zhuang, Z. Hu, X. Xu, J. Chen, J. Wang, W. Hao, Y. Du and S. X. Dou, *ACS Catal.*, 2018, **8**, 4288–4293.
101 C. Xie, D. Yan, H. Li, S. Du, W. Chen, Y. Wang, Y. Zou, R. Chen and S. Wang, *ACS Catal.*, 2020, **10**, 11082–11098.
102 Y. Zhang, Y. Zhang, H. Zhang, L. Bai, L. Hao, T. Ma and H. Huang, *Coord. Chem. Rev.*, 2021, **448**, 214147.
103 R. Jia, Y. Wang, C. Wang, Y. Ling, Y. Yu and B. Zhang, *ACS Catal.*, 2020, **10**, 3533–3540.
104 Z. Gong, W. Zhong, Z. He, Q. Liu, H. Chen, D. Zhou, N. Zhang, X. Kang and Y. Chen, *Appl. Catal., B*, 2022, **305**, 121021.
105 R. Daiyan, T. Tran-Phu, P. Kumar, K. Iputera, Z. Tong, J. Leverett, M. H. A. Khan, A. Asghar Esmailpour, A. Jalili, M. Lim, A. Tricoli, R.-S. Liu, X. Lu, E. Lovell and R. Amal, *Energy Environ. Sci.*, 2021, **14**, 3588–3598.
106 W. Zhong, Z. Gong, Z. He, N. Zhang, X. Kang, X. Mao and Y. Chen, *J. Energy Chem.*, 2023, **78**, 211–221.
107 L. Fang, S. Lu, S. Wang, X. Yang, C. Song, F. Yin and H. Liu, *Chem. – Eur. J.*, 2024, **30**, e202303249.
108 W. Tao, P. Wang, H. Li, R. Huang and G. Zhou, *Appl. Catal., B*, 2023, **324**, 122193.

109 H. Li, X. Xu, X. Lin, S. Chen, M. He, F. Peng and F. Gao, *J. Mater. Chem. A*, 2023, **11**, 2014–2022.
110 V. Khoo, Z.-J. Chiah, J. J. Foo, P. Zhang, Y. S. Ng, K. M. Lim, X. Zeng, B. Chen, C.-Y. Haw and W.-J. Ong, *Appl. Catal., B*, 2025, **372**, 125294.
111 S. Zhang, X. Yi, G. Hu, M. Chen, H. Shen, B. Li, L. Yang, W. Dai, J. Zou and S. Luo, *Coord. Chem. Rev.*, 2023, **478**, 214970.
112 A. Zhang, Y. Liang, H. Zhang, Z. Geng and J. Zeng, *Chem. Soc. Rev.*, 2021, **50**, 9817–9844.
113 V. Khoo, J. J. Foo, B. J. Su, K. M. Lim, C.-Y. Haw and W.-J. Ong, *Int. J. Hydrogen Energy*, 2025, **101**, 636–649.
114 R. Zhang, Y. Guo, S. Zhang, D. Chen, Y. Zhao, Z. Huang, L. Ma, P. Li, Q. Yang, G. Liang and C. Zhi, *Adv. Energy Mater.*, 2022, **12**, 2103872.
115 Z. Niu, S. Fan, X. Li, Z. Liu, J. Wang, J. Duan, M. O. Tadé and S. Liu, *ACS Appl. Mater. Interfaces*, 2022, **14**, 35477–35484.
116 J. Wang, Y. Wang, C. Cai, Y. Liu, D. Wu, M. Wang, M. Li, X. Wei, M. Shao and M. Gu, *Nano Lett.*, 2023, **23**, 1897–1903.
117 Y. Wan, M. Pei, Y. Tang, Y. Liu, W. Yan, J. Zhang and R. Lv, *Adv. Mater.*, 2025, **37**, 2417696.
118 B. Li, P. Xue, M. Qiao, Y. Tang and D. Zhu, *Chem. Commun.*, 2023, **59**, 13611–13614.
119 B. Yang, Y. Zhou, Z. Huang, B. Mei, Q. Kang, G. Chen, X. Liu, Z. Jiang, M. Liu and N. Zhang, *Nano Energy*, 2023, **117**, 108901.
120 Q. Wu, X. Fan, K. Liu, X. Quan and Y. Liu, *Appl. Catal., B*, 2025, **361**, 124597.
121 Y. Luo, K. Chen, P. Shen, X. Li, X. Li, Y. Li and K. Chu, *J. Colloid Interface Sci.*, 2023, **629**, 950–957.
122 J. Gao, B. Jiang, C. Ni, Y. Qi and X. Bi, *Chem. Eng. J.*, 2020, **382**, 123034.
123 S. Garcia-Segura, M. Lanzarini-Lopes, K. Hristovski and P. Westerhoff, *Appl. Catal., B*, 2018, **236**, 546–568.
124 X. Liu, C. Liu, X. He, Z. Cai, K. Dong, J. Li, X. Fan, T. Xie, X. Yang, Y. Luo, D. Zheng, S. Sun, S. Alfaifi, F. Gong and X. Sun, *Nano Res.*, 2024, **17**, 2276–2282.
125 X. Liang, N. Fu, S. Yao, Z. Li and Y. Li, *J. Am. Chem. Soc.*, 2022, **144**, 18155–18174.
126 Z. Lu, J. Zhang, Y. Wang, Y. Yu and L. Kong, *Mater. Horiz.*, 2025, **12**, 3286–3300.
127 X. Cheng, W. Shang, Y. Li, J. Hu, J. Guo, D. Cao, N. Zhang, S. Zhang, S. Song, T. Liu, W. Liu and Y. Shi, *Nano Res.*, 2024, **17**, 6826–6832.
128 X.-F. Cheng, J.-H. He, H.-Q. Ji, H.-Y. Zhang, Q. Cao, W.-J. Sun, C.-L. Yan and J.-M. Lu, *Adv. Mater.*, 2022, **34**, 2205767.
129 P. Li, R. Li, Y. Liu, M. Xie, Z. Jin and G. Yu, *J. Am. Chem. Soc.*, 2023, **145**, 6471–6479.
130 J. Y. Loh, J. J. Foo, F. M. Yap, H. Liang and W.-J. Ong, *Chin. J. Catal.*, 2024, **58**, 37–85.
131 X. Zhao, Q. Geng, F. Dong, K. Zhao, S. Chen, H. Yu and X. Quan, *Chem. Eng. J.*, 2023, **466**, 143314.
132 T. Zhu, Q. Chen, P. Liao, W. Duan, S. Liang, Z. Yan and C. Feng, *Small*, 2020, **16**, 2004526.
133 J. Suh, H. Choi, Y. Kong and J. Oh, *Adv. Sci.*, 2024, **11**, 2407250.
134 N. F. Agesta, F. M. Yap, X. Zeng, T. J. Siang and W.-J. Ong, *Int. J. Hydrogen Energy*, 2025, **192**, 152216.
135 W. Mo, J. J. Foo and W.-J. Ong, *Electron*, 2024, **2**, e20.
136 J. Hong, L. Zhang, Q. Zhu, Z. Du, Y. Zhou, T. Wågberg and G. Hu, *Mater. Horiz.*, 2023, **10**, 5969–5982.
137 J.-Y. Fang, Q.-Z. Zheng, Y.-Y. Lou, K.-M. Zhao, S.-N. Hu, G. Li, O. Akdim, X.-Y. Huang and S.-G. Sun, *Nat. Commun.*, 2022, **13**, 7899.
138 P. Liu, J. Yan, H. Huang and W. Song, *Chem. Eng. J.*, 2023, **466**, 143134.
139 G. A. Cerrón-Calle, A. S. Fajardo, C. M. Sánchez-Sánchez and S. Garcia-Segura, *Appl. Catal., B*, 2022, **302**, 120844.
140 X. Ma, J. Zhong, W. Huang, R. Wang, S. Li, Z. Zhou and C. Li, *Chem. Eng. J.*, 2023, **474**, 145721.
141 Y. Wang, F. Hao, M. Sun, M.-T. Liu, J. Zhou, Y. Xiong, C. Ye, X. Wang, F. Liu, J. Wang, P. Lu, Y. Ma, J. Yin, H.-C. Chen, Q. Zhang, L. Gu, H. M. Chen, B. Huang and Z. Fan, *Adv. Mater.*, 2024, **36**, 2313548.
142 R. Jia, X. Zhang, L. Gan, M. Tahir, Z.-F. Huang, L. Pan, R. Gao, C. Shi, X. Zhang, G. Yang and J.-J. Zou, *J. Mater. Chem. A*, 2025, **13**, 5732–5743.
143 W. Yu, J. Yu, M. Huang, Y. Wang, Y. Wang, J. Li, H. Liu and W. Zhou, *Energy Environ. Sci.*, 2023, **16**, 2991–3001.
144 J. Cai, Y. Wei, A. Cao, J. Huang, Z. Jiang, S. Lu and S.-Q. Zang, *Appl. Catal., B*, 2022, **316**, 121683.
145 Y. Bu, C. Wang, W. Zhang, X. Yang, J. Ding and G. Gao, *Angew. Chem., Int. Ed.*, 2023, **62**, e202217337.
146 T. Ren, H. Wang, S. Xu, H. Yu, K. Deng, Z. Wang, H. Wang, L. Wang and Y. Xu, *J. Mater. Chem. A*, 2023, **11**, 24854–24860.
147 J. Li, H. Li, K. Fan, J. Y. Lee, W. Xie and M. Shao, *Chem Catal.*, 2023, **3**, 100638.
148 K. M. Lim, V. Khoo and W.-J. Ong, *Exploration*, 2025, DOI: 10.1002/EXP.20240344.
149 Y. X. Leiu, K. M. Lim, Z.-J. Chiah, E. S.-Z. Mah and W.-J. Ong, *EcoEnergy*, 2025, **3**, 217–253.
150 F. Chen, X. Zhou, H. Wang, X. Liu, Q. Yang, X. Chen, Q. Mu, J. Liu, X. Li, X. Liao, Z. Jiang, Z. Jin and M. Jiang, *Adv. Funct. Mater.*, 2025, **35**, 2421405.
151 X.-H. Wang, R. Yuan, S.-B. Yin, Q.-L. Hong, Q.-G. Zhai, Y.-C. Jiang, Y. Chen and S.-N. Li, *Adv. Funct. Mater.*, 2024, **34**, 2310288.
152 X. Wang, J. Ren and Z. Gao, *J. Colloid Interface Sci.*, 2025, **693**, 137575.
153 X. Chen, Y. He, G. Ding, Z. Feng, Q. Wei, C. Sui, Z. Wang and Q. Jiang, *Nano Lett.*, 2025, **25**, 9508–9515.
154 L. Zhang, P. Jin, Z. Wu, B. Zhou, J. Jiang, A. Deng, Q. Li, T. Hussain, Y. Zhang, H. Liu and S. Wang, *Energy Environ. Mater.*, 2024, **7**, e12725.
155 X. Li, G. Hai, D. H. C. Wan, Y. Liao, Z. Yao, F. Zhao, L. Huang, J. Zhou, G. Li, G.-F. Chen, F. R. Wang, M. K. H. Leung and H. Wang, *J. Am. Chem. Soc.*, 2025, **147**, 8587–8596.
156 K. C. Majhi, Z. Zhang, F. Chunhua, Y. Lei and J. C.-H. Lam, *Curr. Opin. Green Sustainable Chem.*, 2025, **51**, 100995.

157 C. Xu, X. Qin, F. Zhang, Z. Zhang, X. Liu and Y. Yang, *Sep. Purif. Technol.*, 2025, **354**, 129212.
158 Y. Liu, S. Niu, Y. Zou, S. Huang, Y. Shi, S. Gao and P. Tsiakaras, *Appl. Catal., B*, 2025, **363**, 124729.
159 W. Duan, Y. Chen, Y. Zhu, L. Tian, W. Zheng, H. Fu, J.-L. Chen, Y.-J. Lin, J. C.-H. Lam, Y. Lei and C. Feng, *Appl. Catal., B*, 2025, **363**, 124812.
160 S. Tian, R. Wu, H. Liu, C. Yan, Z. Qi, P. Song, W.-J. Chen, L. Song, Z. Wang and C. Lv, *Angew. Chem., Int. Ed.*, 2025, **64**, e202510665.
161 S. Niu, Y. Wu, J. Wang, J. Gu, X.-Z. Liu, J. Zhang, L. Chen, J. Z. Liu, W.-J. Jiang, J.-S. Hu and X. Wu, *Angew. Chem., Int. Ed.*, 2025, **64**, e202508227.
162 J. Ding, L. Zhang, Z. Wei, Z. Wang, Q. Liu, G. Hu, J. Luo and X. Liu, *Small*, 2025, **21**, 2411317.
163 C. Zhang, X. Wang, J. Jiang, J. Zhang, A. Liu and L. Ai, *Appl. Catal., B*, 2025, **365**, 124991.
164 Q. Wang and Y. Shen, *Small*, 2025, **21**, 2505948.
165 P. Marbaniang, S. Ingavale, W. Yoopensuk, W. Limphirat, H. Wu, W. Tolek, W. Yospanya, J. Panpranot, Q. Wang, S. Kheawhom and C. Pornrungroj, *ACS Appl. Mater. Interfaces*, 2025, **17**, 52010–52023.
166 X. Huang, K. Wu, F. Yang, R. Fu, Y. Ji, W. Kong, C. Su and B. Xiao, *Chem. Eng. J.*, 2025, **504**, 158995.
167 M. G. Kallitsakis, K. D. Nikopoulos and I. N. Lykakis, *ChemCatChem*, 2025, **17**, e202401927.
168 X. Ji, Y. Yu, A. Ma, Y. Guan, H. Li, J. Lai and L. Wang, *J. Alloys Compd.*, 2025, **1010**, 178265.
169 F. M. Yap, S. Yuan, J. Y. Loh, J. Wang, X. Zeng and W.-J. Ong, *Angew. Chem., Int. Ed.*, 2025, e202513840.
170 F. M. Yap, J. Y. Loh, S.-F. Ng and W.-J. Ong, *Adv. Energy Mater.*, 2024, **14**, 2303614.
171 Y. Zhang, L. Chen, X. Yan, W. Teng, H. Ou, H. Li, Q. Huang, H. Hu and G. Yang, *AIChE J.*, 2025, **71**, e18849.
172 P. Cao, Y. Liu, R. Yang, Y. Li, Y. Cheng, J. Yu, X. Zhang, P. Phiri, X. Yuan, Y. Yang, N. Liu, Y. Liu and H. Li, *Catalysts*, 2025, **15**, 422.
173 T. Wei, Y.-L. Fan, X. Wang, W.-T. Lu and G. Zhang, *New J. Chem.*, 2025, **49**, 18129–18138.
174 M. A. El-Ghobashy, M. M. Khamis, A. S. Elsherbiny and I. A. Salem, *Environ. Sci. Pollut. Res.*, 2023, **30**, 106822.
175 F. Gan, K. Wu, F. Ma, C. Wei and C. Du, *Heliyon*, 2022, **8**, e12423.
176 M. Cao, A. Hu, M. Gad, B. Adyari, D. Qin, L. Zhang, Q. Sun and C.-P. Yu, *Sci. Total Environ.*, 2022, **823**, 153680.
177 C. Lin, W. Li, H. Chen, J. Feng, M. Zhu, J. Shi, M. Li, B. Hou, Z. Wang, X. Chen, J. Liu and W. Yan, *Adv. Sci.*, 2025, **12**, 2502262.
178 L. Luo, H. Han, L. Chen, D. Feng, L. Li, T. Zhai, Z. Chen, R. Gao, H. Wu, S. Liu, W. Pei and Y. Li, *Int. J. Hydrogen Energy*, 2024, **90**, 885–917.

